Properties and modulation by nitric oxide of skin impulse propagation through the epithelium of amphibian tadpoles

A thesis submitted to the University of St. Andrews for the degree of master of philosophy

Michael Harris Alpert

School of Biology
Division of Biomedical Sciences
Bute Medical Buildings
University of St. Andrews
St. Andrews
Fife
K16 9TS

September 2006

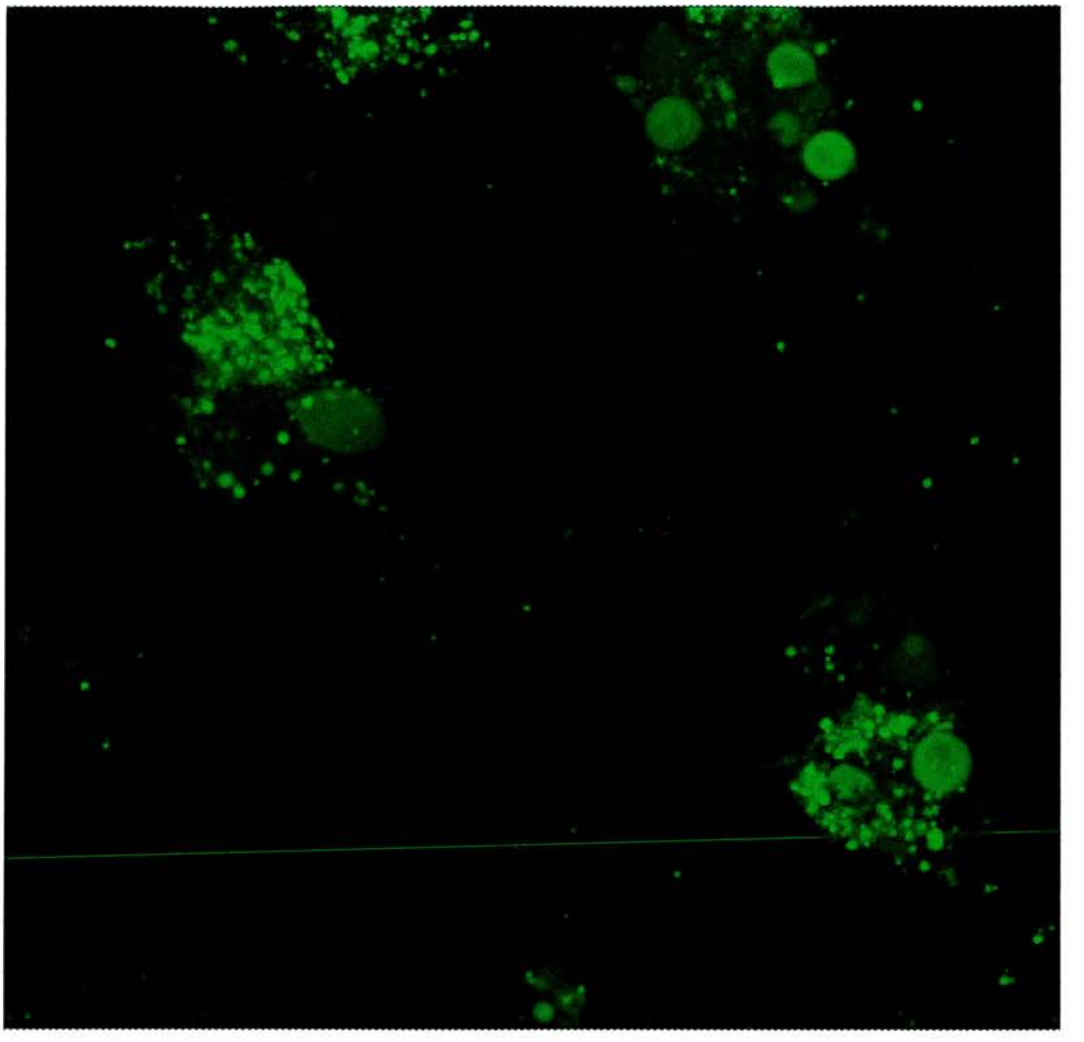

Sometimes the lights are shining on me
Other times I can barely see
Lately it's occurred to me
What a long, strange trip it's been

-The Grateful Dead

Declaration

I, Michael Harris Alpert, hereby certify that this thesis, which is approximately 35,000 words in length, has been written by me, that it is the record of work carried out by me and that it has not been submitted in any previous application for a higher degree.

Date 19/9/06 Signature of candidate

I was admitted as a research student under in October 2005 and as a candidate for the degree of Mater of philosophy in October 2005; the higher study for which this is a record was carried out in the University of St. Andrews between 2005 and 2006.

Date 19/9/06 Signature of candidate

I hereby certify that the candidate has fulfilled the conditions of the Resolution and Regulations appropriate for the degree of Master of philosophy in the University of St. Andrews and that the candidate is qualified to submit this thesis in application for that degree.

Date 19/9/06 Signature of supervisor

In submitting this thesis to the University of St. Andrews I understand that I am giving permission for it to be made available for use in accordance with the regulations of the University Library for the time being in force, subject to any copyright vested in the work not being affected thereby. I also understand that the title and abstract will be published, and that a copy of the work may be made and supplied to any bona fide library or research worker, that my thesis will be electronically accessible for personal or research use, and that the library has the continued access to the thesis. I have obtained any third-party copyright permissions that may be required in order to allow such access and migration.

Date 19/9/06 Signature of candidate

Acknowledgements

It was the middle of June 2005, and I was less than halfway between Atlanta and Anchorage, when I happened to stop for a few nights in Denver. At this point during my road trip, the emails had already started to pile up in my inbox. But sure enough, in the midst of it all, I received confirmation from *kts1* that I was to pack my bags, and catch a flight to Edinburgh in the fall. Now, nearly a year and a half and approximately 173 tadpoles later, I have made it through one of the most challenging years of my life as I tried to solve an epidermal puzzle. In hindsight, things are still hyperopic, and I might just have to accept certain shortcomings as a scientist in addition to begin to see the forest for the trees. I also never quite figured out how to both wait for good things to happen while simultaneously grabbing the proverbial "bull," and ended up with a love for *psy*trance and the overall homeostatic importance of the *wee buds*. The truth of it all is that the whole experience lies in quality. There is no doubt that this subjectivity is my pursuit in life, and I would be foolish not to see how much this year has brought me in an academic sense, which is never far from its straggling but prevalent counterpart: *development of self*. This year and this thesis were a trial, and will continue to act as a testament for my undying love of biology, even it is only just *neuroid*science. Needless to say, the completion of this thesis could not have been possible without several important people.

My editors

Keith I am here because of you. Not just here in St. Andrews, but here in the future. Looking back and thinking about all the electrodes and watchmaker's forceps I was breaking back in October, it is amazing to see the improvements I have made (aside from that minor SNAP-related incident), and you were there to guide my footsteps throughout this entire investigation. When I came here, I was very similar to one Plato's cavemen, chained to the wall; my knowledge of things to come would be unfathomable. To you I owe this opportunity that you have made possible, as you continue to lure in poor, helpless Emory undergraduates, and shape them into confident and competent scientists. I am very fortunate to make my *Australopithecine*-like imprint in the long legacy that is the Sillar Lab.

Victoria you continue to inspire me. Your breadth and depth of all aspects of life are insurmountable. I hope that as I continue to grow, I pick up on all the minutiae that are subject to the synaptic filters of our complex brain; using them to construct an immense web of understanding, just like you. Your interest in my studies and hobbies are endearing and what I consider to be the epitome of thoughtfulness and a genuine love for anything and everything that can fascinate. You are truly remarkable.

Psymic there are few words that can accurately describe our relationship, and suffice it to say that I will never be the same again. A year of spending nearly every waking minute with you is enough to drive a man to the realms of the *unsane*. Our ability to achieve symbiosis as flatmates, and as best friends is a rare quality, and I thank you for molding me into your little raver ever since that infamous night at *54 Boase*. You too have been through this whole experience, right by my side, and have been a witness to my growth as an individual. You emit such energy, lending me such a joy for life that I never knew possible. If anything, I hope that you have learned from me too, and will continue to develop your own skills as a scientist/anthropologist/Jr. mycologist/shamaness and as an individual. I love IBM (your).

My Foundation

JPI J.F.D.I., you never let me quit. All those long nights in the lab, and countless hours following, "Oh, I just have a quick question," seem far away now. You were always there for inquiries about anything science and non-science, but most importantly, as my friend. You have so much worldly knowledge and such profound skepticism that not even babies can make it

without being strip-searched. I could not have asked for a better lab partner and general consultant. Your advice was no less than invaluable in the progress of my research, as you were there to teach me all the JPI-patented tricks of the trade. I wish you the best of the luck in your research and holding on to those twins.

Bill The findings of this thesis would not have as much *significance* without your aid. Your time was so helpful and a necessary means to thinking critically about what I was trying to describe. You have an amazing ability to take on the problems of others and tackle them as if they were your own. Your kindness and patience are true virtues.

Hong-Yan and Bex The two of you continue to impress me with your organisation and pristine experimental results, never failing to have a clean desktop. Your advice and encouragement were more than I could ask for and I hope that you continue to make progress in your own work.

Isobel You are the life-giver. The *Xenopus* toad colony could never be what it is today without your ever-watchful eye. You facilitate the research in the lab in the most crucial way, especially with the constant influx of goodies from your kitchen. You are so kind and thoughtful that I cannot help but wonder what's in the water in Guardbridge. Its no surprise that the colony, both toad and human alike, fairs so well under your care.

Family A year felt much longer than it was, and I never thought I would be sad to be an ex-pat in this day and age. I must thank my grandparents, parents, step-parents, sisters, brothers, and step-brothers for ALL of their support in this past year. You all cannot imagine what a comfort it is to have such a large family, each one of you adding a different spice of inspiration.

Friends Never before have I lived and died by the message count in my inbox. More than any of you know is how much it meant to connect with others elsewhere when in the confines of a laboratory. It really expanded the walls, and drew my mind out of the bath whenever I needed a breather.

Muses Phish; the Grateful Dead; Medeski, Martin & Wood; Gov't Mule; Hallucinogen, Cosmosis, Broken Toy, the Mars Volta; Pearl Jam; the Red Hot Chili Peppers; the Slip; the Boom. Without the consistent support of music, I never would have made it through this thesis, or a single experiment with as much enjoyment.

*A special thanks to Dr. Tony Butler who supplied me with nearly all of the SNAP which was used to perform my experiments. My experiments could not have been completed without this crucial drug. Also, to Irvine Davidson for all those hours you spent taking pictures of amphibian skin with me and for all the coffee. The pictures are an invaluable aspect of my thesis. Lastly, thanks to the literature cited all-star, Dr. Dave McLean. Although we have never met, your Doctoral thesis proved to be an invaluable manual for the composition of this Masters.

Table of Contents

List of Figures

Chapter 1 – General Introduction

Chapter 3: Section 1 –Basic Properties

Chapter 3: Section 2 – Pharmacology

Chapter 3: Section 3 – Anatomy and Histology

Abbreviations

5-HT	5-Hydroxy tryptamine (serotonin)
8-Br-cGMP	8-bromo cyclic 3',5'-guanosine monophosphate
AC	adenylyl cyclase
ATP	adenosine triphosphate
$[Ca^{2+}]_i$	intracellular calcium
CaM	calmodulin
cAMP/cGMP	cyclic 3',5'-adenosine/guanosine monophosphate
Cx	connexin
CxHc	connexon hemichannel
C-PTIO	2-(4-carboxyphenyl)-4,4,5,5-tetramethylimidazoline-1-oxyl-3-oxide
DAF-2 DA (DAF)	4,5-diaminofluorescein diacetate
E_M	resting membrane potential
GJ	gap junction
GJC	gap junction channel
GJIC	gap junction intercellular communication
DA	dopamine
DMSO	dimethyl sulfoxide
GTP	guanosine triphosphate
$InsP_3$	inositol 1,4,5-trisphosphate
μm/M	micrometer/molar
ms/V	millisecond/volt
L-NAME	N^G-nitro-$_L$-arginine methyl esther
NADPHd	nicotinamide adenine dinucleotide phosphate diaphorase
NO	nitric oxide
e/i/nNOS	nitric oxide synthase ((e) epithelial, (i) inducibe, (n) neuronal)
ODQ	1H-[1,2,4]oxadiazolo[4,3-a]quinoxalin-1-one
PKA/C/G	protein kinase A/C/G
SEM	Scanning Electron Microscopy
S.E.M.	Standard error of the mean
sGC	soluble guanylyl cyclase
SNAP	*S*-nitroso-*n*-acetylpenicillamine
SP	substance P
V_T	voltage threshold for skin impulse activation

Abstract

1. I have examined the primary sensory system of the skin impulse and its potential modulation through endogenous neuroactive substances that are produced within the epithelial cells of the amphibian tadpole, *Xenopus laevis*.
2. Basic electrophysiological techniques including extracellular and intracellular recordings were used to monitor the skin impulse and corresponding activation of fictive swimming behaviour through the Rohon-Beard mechanosensory pathway in four different amphibian species at similar stages in development: *Xenopus laevis*, *Rana temporaria*, *Bufo bufo*, and *Triturus vulgaris*.
3. Scanning Electron Microscopy (SEM) was used to view the ultrastructural composition of the skin surface of these four different amphibian species at similar stages in development.
4. Pharmacological modulation of the impulse was investigated by applying several substances known to be found in or near the skin of *Xenopus* embryos: Serotonin (5-HT), Substance P (SP), and Nitric Oxide (NO). No consistent effects of either 5-HT or SP were found and thus no direct conclusions could be drawn on their possible role in skin impulse modulation. However, applications of an NO donor drug, SNAP, and the NO scavenger, C-PTIO, potently modulated the skin impulse.
5. NO modulated the cells of the skin by increasing: (1) the conduction delay of an impulse propagating across the epidermis, implying a possible uncoupling effect of gap junctional proteins between skin cells; (2) the duration of the waveform of the

skin impulse, suggesting that the conductance of voltage-gated ion channels were altered; (3) the resting membrane potential of skin cells.

6. Investigation into the cellular mechanism underlying NO was inconclusive. However, evidence negated the possibility that NO acts solely through the sGC/cGMP 2nd messenger cascade to uncouple gap junction channels.
7. Pharmacological findings prompted a search for an endogenous source for NO within the cells of the skin. A subpopulation of skin cells displayed widespread staining with the NADPHd technique, nNOS immunocytochemistry and DAF fluorescence. This indicated that NO is a sufficient and anatomically relevant candidate for skin impulse modulation in *Xenopus* embryos.

Chapter 1 – General Introduction

Electrical excitability is the cellular phenomenon in which a given change in resting membrane potential (E_M) leads to a positive feedback-induced, further change of membrane potential in the same direction. A cellular response can fall into two general categories: either graded, which depends upon the stimulus intensity, or all-or-none responses which are independent of stimulus intensity and basically uniform when the cell is excited over a given threshold determined by fundamental cellular properties. The classical conception of cell taxonomy holds that neurones and muscle fibers are the only cell types, which in complex organisms, display properties of electrical excitability and have the capacity for generating action potentials or impulses. However, the classical doctrine of cell excitability has been reformulated by experiments showing that synaptic transmission can occur independent of conducted impulses (Shepherd, 1981). Similarly, the work that has been conducted on non-nervous cell types which have the capacity to generate an impulse clearly demonstrates that excitability is a phenomenon shared by many non-neuronal cell types. Aside from muscle fibers, the non-neural cell types having this property have been investigated since the late 19th century, and include, but are not limited to, the fungus *Neurospora*, the polychaete annelid egg, cells in the stem of the pumpkin plant, the single-celled *Paramecium*, and mammalian cells as described in the rat pituitary and pancreas (Shepherd, 1981). Therefore, a variety of cells across the plant, animal and protistan phylogenetic boundaries display electrical excitability (Figure 1.1). Both vertebrate and invertebrate epithelial cells can display electrical excitability including the exumbrellar ectoderm of the coelenterate *Hydromedusae*, and cells within the epidermis of several species of amphibian tadpoles. Each of these cell types is

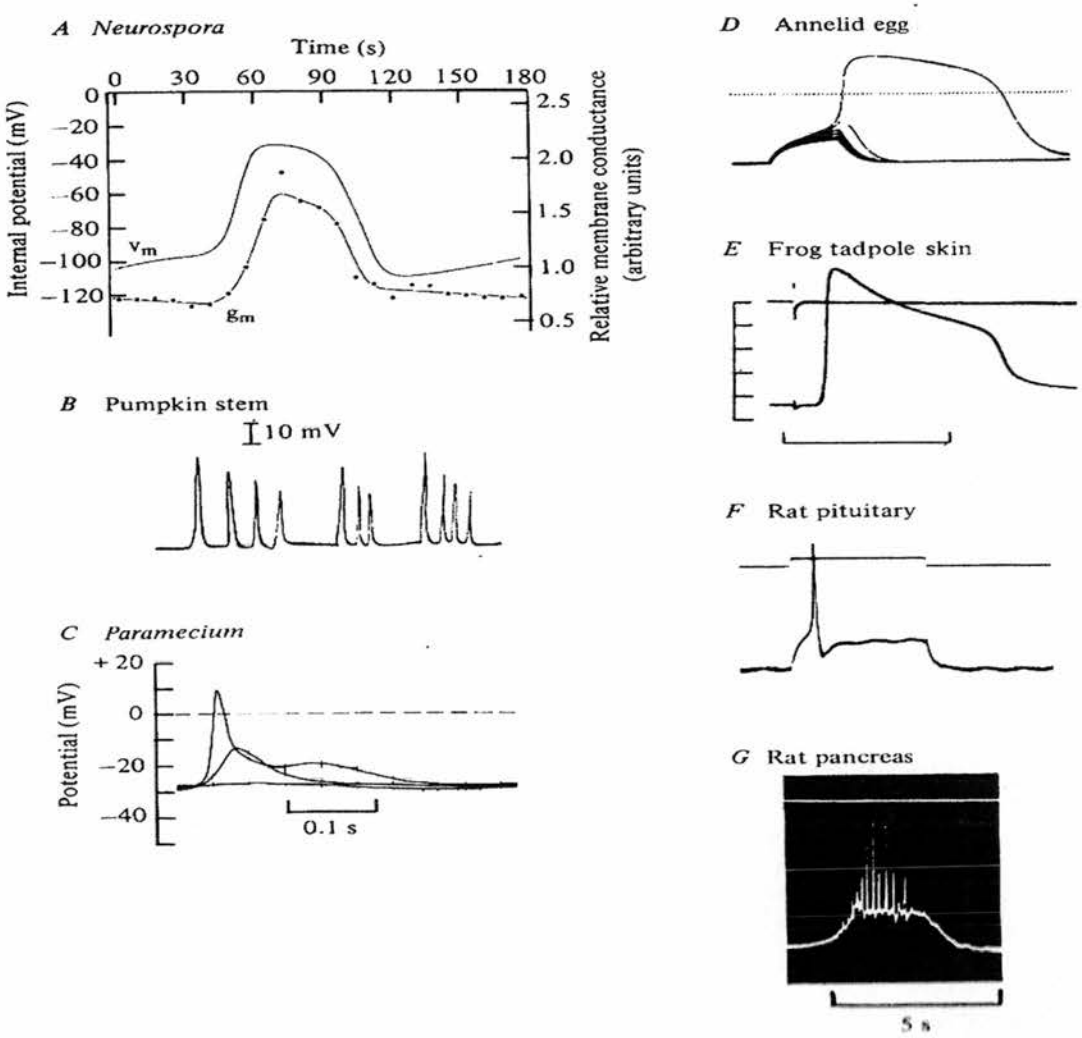

Figure 1. 1 Cross-species comparison of non-nervous impulses. (A) *Neurospora*, (B) pumpkin stem, (C) *Paramecium*, (D) Annelid egg, (E) Frog tadpole skin, scale bars show 20 mV divisions and 100 ms (F) Rat pituitary E_M= -58 mV and pancreas, E_M= -65 mV (G). Figure from (Shepherd, 1981).

well-known to exhibit an impulse which propagates from cell to cell through a two-dimensional syncytium. This form of conduction has been known as 'neuroid,' since G. H. Parker's work on sponges in the early 20th century (1919). Parker believed, although never proven, that in sponges, "[neuroid conduction] represents without a doubt that elemental property of protoplasmic transmission from which true nervous activity has

been evolved (Parker, 1919)." Furthermore, electrical excitability of non-neural tissue is thought to have evolved independently among disparate groups, as has its function in different cell types which controls behaviours from luminescence to sensory conduction (Mackie, 1970; Roberts, 1971). The present thesis is directed towards a further exploration of the properties, function, and potential modulation of the propagating 'skin impulse' found in amphibian tadpoles. At this point, however, a brief discussion of the evolution of conducting tissue will provide the context within which the implications of excitability in the epithelial cells of tadpole skin will be examined.

Evolutionary origins of electrical excitability

The phylogenetic origins of neuroid conduction are unclear, as this property may have evolved independently at several different times; its emergence is widespread (Mackie, 1970). Many species exhibit a form of neuroid conduction with similar implications for behavioural physiology. A variety of organisms are found to use neuroid conduction to trigger a locomotor response that is either protective or escape-generating in nature. In the *Hydromedusae*, transmission occurs between exumbrellar ectoderm and subumbrellar endodermal cell layers, exciting ectodermal smooth muscle to ultimately withdraw and enclose vulnerable areas in response to a noxious stimulus. Similarly, the siphonophore *Nanomia* can escape predation by conducting a neuroid signal in order to reverse the directionality of its ciliary beat. In addition to the previous examples of strictly locomotor behaviour, cells of the siphonophore, *Hippopodius*, can generate camouflage with either luminescence in the dark or 'blanching' in the light when invaded by an impulse. Of particular interest is the ciliary beating exhibited by the ctenophore

Pleurobrachia (a gelatinous aquatic animal), which is controlled by neuroid signals. These planktonic metazoans also have a nerve net which innervates their entire surface, running under the comb plates in which the cilia are arranged. The ciliary beating is inhibited when the comb plates become stimulated, which is thought to occur by activation of the underlying nerve net (Shepherd, 1981). Here is an example of the existence of a dual sensory system, both neuroid and neural, an organisation that also appears in *Xenopus* tadpoles.

The diverse functions of neuroid impulses across species correspond to the different cellular mechanisms of action. In general, when examining properties of conduction, the shape of a cell as well as its electrochemical gradient must be taken into account (Shepherd, 1981). For instance, in the both the alga *Nitella*, and the fungus *Neurospora*, Cl^- ion flux underlies the voltage changes observed across their cell membranes during morphogenesis. The *Paramecium* impulse, which mediates a sensory response and ciliary beating, is generated by movement of Ca^{2+}. In contrast, the annelid egg impulse is controlled by both Na^+ influx for a fast depolarisation and Ca^{2+} for a slower hyperpolarising current (Shepherd, 1981). In the former, the cell undergoes a unified depolarisation over its entire surface, as the signal is incapable of propagation due to the egg's spherical nature (Mackie, 1970). In exumbrellar ectoderm of Hydrozoa, like *Hydromedusae*, sensory signals and propagation are Na^+-dependent (Mackie and Passano, 1968). This reflects a principle in epithelial neuroid conduction as stated by Loewenstein (1966) whereby, "the entire connected cell system, rather than the single cell, constitutes the functional unit for propagation" (in Mackie, 1970). This theme of bridging cell populations into single functional units represents a trend in the evolution of

conducting tissues. Emphasis is diverted from the actions of an individual cell and directed towards the integration of an electrical signal within a multicellular tissue system.

Several general factors serve to define the conditions necessary for impulse conduction within a cell. Primarily, there is a need for an excitable membrane with an adequate distribution of voltage-gated ion channels. The membrane creates a separation of ions, establishing a dynamic polarisation between the lumen and extracellular space. The latter must be composed of a fluid medium of relatively low resistance. Within this cellular construct, the shape and core properties of the membrane will facilitate current flow, which is confined to designated regions of the cell (in Shepherd, 1981). The existence of variety within both the ions that are associated with the generation of impulses and the functions of neuroid conduction in several species support the contention that Mackie (1970) makes regarding the evolution of conducting tissues. Due to the differences between species, evolution is proposed to have occurred independently. However, the similarity in general organisation of conducting tissues (especially in epithelium), also suggests a similar method in the evolution of tissue morphology (i.e. from ectoderm to epidermis and neurones; discussed below; Figure 1.2). The multitude of biological systems which are capable of generating impulses in non-neural tissue suggests that the capacity to produce an impulse may be inherent to all biological membranes, given the appropriate environmental context (Slayman et al., 1976). However, Mackie (1970) argues that, "...probably most cells, both now and in the past, have been electrically inexcitable. Excitability would develop by the adjustment of the magnitudes and time courses of conductance to various monovalent and divalent ions."

Furthermore, Shepherd (1981) counters, that "in view of the fact that many nerve cells function without impulses, a more reasonable view is that the impulse in nervous tissue expresses general biological properties of excitability." Although much speculation can be made on the nature of excitability, the core cellular property responsible for the spread of excitation enabling cell to cell conduction is the type of junction which bridges neighbouring cells.

In a system where cells communicate via the release of chemical substances, the response latency could theoretically be decreased with more adapted cellular junctions. Assuming that the speed of transmission is an evolutionarily valuable asset for cellular performance, and if existing cell junctions could be incorporated to pass an electrical impulse, a parsimonious shift from chemical to electrical communication could improve cell functionality (Mackie, 1970). In fact, Mackie (1970) contends that "the evolution of conduction is inseparable from the evolution of junctional specialisation and that both are subject to the requirements of tissue homeostasis." In this light, a basic system built upon primordial conducting sheets, like the epithelium of *Hydromedusae*, can evolve into a system specialized with nervous and muscular units through junctional modification. Mackie's broad model proposes the method of transition by which individual cell conduction units undergo several basic changes to become both neural and neuroid in nature (Figure 1.2).

(A) Initially, electrically coupled tissue, described as the 'primordial myoepithelium,' begins to diverge into a distinct epithelium and myocytes, still expressing junctional coupling. (B-C) As myocytes move towards the interior of the animal, protoneurones evolve in order to facilitate electrical communication from the

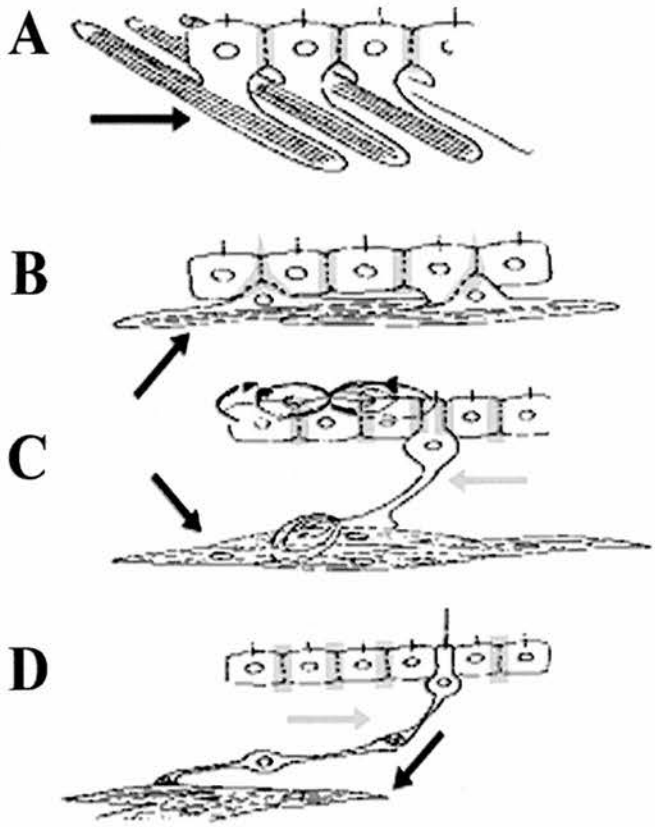

Figure 1. 2 Model of evolution from primordial epithelium to myocytes and neurones. (A) Shows primordial myoepithelium as a joint structure. (B) Shows divergence of myoctyes from the epithelial layer. (C) Shows the formation of protoneurones (grey arrow) and illustrates junctional communication (black ovular arrows). (D) Shows the morphology of the neuron (grey arrow) and its subsequent synapse onto a myocyte. Black arrow indicates myocytes; grey highlights indicate points of junctional coupling. Figure adapted from Mackie (1970).

exterior epithelium, establishing units capable of distal, directed conduction. (D) The final step arises when neurosensory cells and neurones become the effective conducting units through chemical transmission, even though the epithelium might still be capable of junctional flow, and hence neuroid conduction (Mackie, 1970).

In animals, electrotonic junctions are assumed to be the ancestral form of transmitting junctions. In an evolutionary divergence from electrical junctions, chemical junctions have prevailed for several reasons, amongst which are signal amplification, potential for inhibition, and in neurones, distal projection, directionality and gain control

(Mackie, 1970). The neurones can be viewed as a cell type concerned with information transfer, which sometimes takes the form of an impulse and is subject to modulation by other cells and structures such as a synapse (Shepherd, 1981). Mackie (1970) ventures that evolutionary transition to the use of nerve cells for information transfer involved the simultaneous loss of electrical propagation and the gain of a chemical basis for inducing depolarisation in effector cells through the use of biologically active substances native to the cell. While this idea remains unproven, the separate yet contemporaneous loss and gain could be the reason why retention of neuroid conduction is found within animals that have a functional nervous system. In an effort to both avoid redundancy and conserve structures and functions that perform adequate behaviours, evolution has allowed neuroid conduction to coexist with neural communication. This latter point directly relates to systems mentioned in *Pleurobrachia*, *Hydromedusae*, and for the remainder of this thesis, that which will be examined in *Xenopus*.

Phylogenetic and ontogenetic occurrence of neuroid conduction in epithelial cells

The epidermis of an organism is the main interface between the external environment and internal body structures, and as such represents a strategic point of defense. Typically, the epidermis is a passive structure which acts as a protective barrier, and lacks a means of direct communication between its constituent cells. In this respect, the epidermis of many amphibian tadpoles is highly unusual, and provides a clear example of unconventional use as a sensory system in its own right. In fact, for a brief period during late embryonic and early larval development, cells of the tadpole epidermis

exhibit properties of nervous tissue when presented with a noxious stimulus anywhere over their surface. This excitability takes the form of an impulse which superficially resembles those of cardiac cells (i.e. in duration and waveform) and which propagates from the point of origin throughout the epithelium via gap junctions (GJs) between neighbouring cells. This excitability is displayed by a range of anurans including the South African clawed frog, *Xenopus laevis*, the common frog, *Rana temporaria*, and the common toad *Bufo bufo*. The presumed function of the "skin impulse" in each species is to trigger escape responses and thereby avoid predation. In the case of *Xenopus*, there is substantial evidence that the skin impulse itself activates neural circuitry of the spinal cord, bypassing sensory neurons in the skin, to initiate trunk flexion in young embryos and rhythmic swimming movements in older embryos and larval animals after experiencing a strong stimulus (Roberts, 1996).

During vertebrate embryonic development, the cells of the ectoderm give rise to both the nervous tissue and the epidermis, which may be relevant to electrical properties found in the skin of *Xenopus* tadpoles. In cold-blooded vertebrates such as *Xenopus*, development of the embryo is highly temperature dependent, and the approximations of time after fertilisation are based on temperatures between 22-24°C. By stage 22 (Nieuwkoop and Faber, 1956), 24 hours after fertilisation, the initial structures of the epidermis have differentiated. It is at this stage when a skin impulse can first be recorded in the epithelium (Roberts, 1971). At stage 26, 5 ½ hours later, the impulse can be found over the entire epidermis. Then, by stage 29/30, 5 ½ hours after stage 26, the epidermis consists of two cell layers, and few significant structural changes take place until after the hatchling stage of 37/38, 53 ½ hours after fertilisation. Due to a thickening of the skin

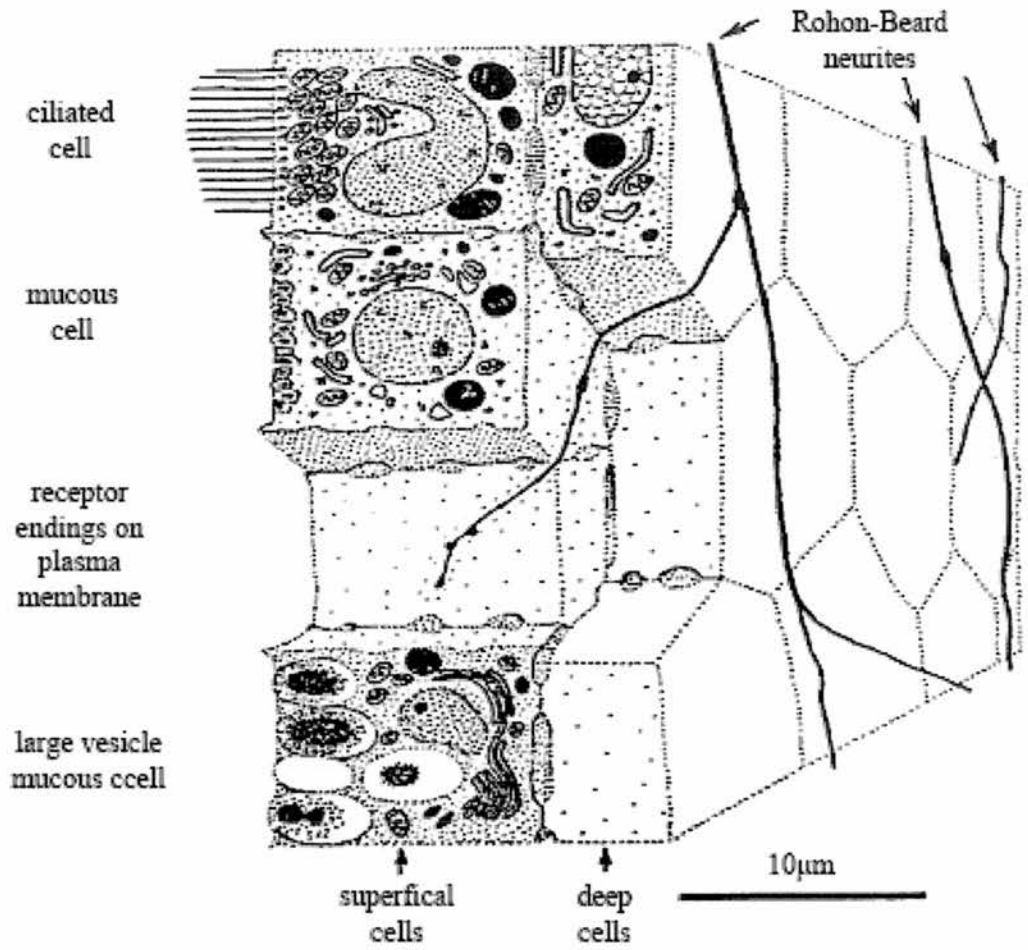

Figure 1. 3 Diagram of 2-layered structure of epidermis showing ciliated, mucous, large vesicle mucous cells, and the cutaneous innervations of primary sensory Rohon-Beard neurites. Figure adapted from Roberts (1998).

at the beginning of the larval period, cells become difficult to record from and skin impulses have not been found after stage 42, 3 days, 8 hrs. after fertilisation (Roberts, 1971).

The periderm, or outer epithelial layer, contains the pigment cells which disappear before metamorphosis. This layer is separate from the inner sensorial layer, or stratum germinativum, which is composed roughly of flattened epithelial cells (Roberts,

1998). These 'deep' cells are thinner than the outer, 'superficial' layer (Roberts, 1971). The deep cells are approximately 5 μm in depth, half the depth of the superficial cells, and form a homogenous layer of hexagonal-shaped cells. When examined under a scanning electron microscope (SEM), the epidermis appears as a heterogeneous mixture of ciliated 'hair' cells spread in a punctate manner, interspersed with 'cuboidal' cells (Roberts, 1971). Less apparent are the mucous cells, which contain large and small varicosities containing mucus, presumably secreted by the cells in order to coat the epidermis. Mucous cells can be identified by small pores on the outer surface of the cell. The composition of the superficial layer is non-uniform, each cell possibly combined with a mixture of varicosities, mitochondria, or cilia (Figure 1.3. A). By stage 39, 2 days, 8 ½ hours after fertilisation, mucous cells are termed 'goblet cells,' having surface dimensions of 16 x 12 μm, and are recognizable in the tail skin. These cells have a substantial lipid content and an elaborate rough endoplasmic reticulum. Mucous vesicles with a diameter up to 3 μm are reported to congregate along the cells' outer surfaces, which are exposed unless otherwise overlain by other flattened keratinized cells (Fox, 1988). The deep cell layer is situated upon a basal lamina, which separates the epidermis from other internal structures. As the tadpole develops, the cells of the epidermis continue to flatten and stretch to compensate for the increasing size of the tadpole.

In relation to impulse propagation, the connections between cells within each layer and their functional structure bear great importance. Upon anatomical examination of the skin in cross-section, two general patterns of contacts between cells of the epidermis arise (Figure 1.4; Roberts, 1971). First, the outer superficial cells form

contacts between adjacent cells and form the 'terminal bar,' a junctional complex visible in light microscopy studies. Second, superficial cells whose membranes do not compose

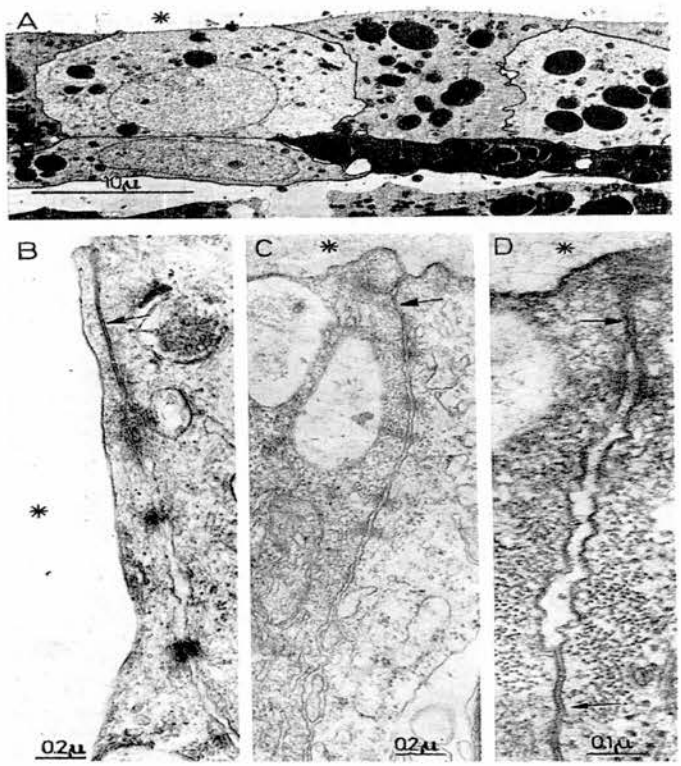

Figure 1. 4 Organisation of the skin and contacts in terminal bar region displayed with transmission electron microscopy (TEM). (A) Low power micrograph of belly skin from a stage 25 embryo. Intercellular boundaries have been inked over to clarify the cell layers. The outer surface is uppermost and shows the poorly developed vesicular structures at this stage. Dark blobs are pigment or yolk granules. (B-D) Higher power micrographs of the terminal bar region in a stage 32 embryo. Mucus is seen as a filamentous fuzz on the outer skin surface and in larger clear vesicles. Desmosomes are present and some areas of close membrane contact are indicated by arrows. Some 'simple apposition' is also present in (C). The only example of a close junction somewhat removed from the skin surface is shown in (D). Asterisks mark space outside animal. Figure from Roberts (1971).

the surface are also found to make contacts with each other. In addition they make contacts with underlying deep cells, which make contacts with other adjacent deep cells (Roberts, 1971). Distances between superficial cells range between 50 angstroms (Å) and several tenths of a micrometer (μm), and at times these cells are found to be occluded (Roberts, 1971). Between deep cells, intercellular space increases, and desmosomes

(adhesive intercellular junctions composed of polysaccharides; see Figure 1.5, 1.6) and hemidesmosomes are found. In both the terminal bar, and between a variety of cells deeper in the skin, short stretches of cell membranes are found to orient in a parallel manner with intercellular spaces ranging between 75 -150 Å, and are termed 'simple appositions (Roberts, 1971).' A parallel organisation of cell membranes amongst other highly convoluted regions suggests that these are sites of functional interactions (Furshpan and Potter, 1968). Close membrane spacing makes it difficult to recognize different appositions. However, with greater extracellular distances between cells, it becomes easier to distinguish between the various types of intercellular junctions found in these areas. Deeper to the skin, desmosomes have been documented, but 'tight' or 'gap' junctions have not been specifically located (Roberts, 1971). A tight junction can be defined as an intercellular junction (usually in the epithelium) where the plasma membranes of two adjacent cells are tightly linked, mainly for adhesive purposes. Gap junctions are fundamentally different in that they act as an intercellular link between two adjacent cells, allowing the passage of small molecules and ions between intracellular spaces. However, in the *Xenopus* embryo, several connexin proteins (subunits of connexon hemi-channels, discussed below) are known to provide a means of intercellular communication, particularly for dispersion of enzymes from the hatching gland (Levin and Mercola, 2000; Landesman et al., 2003). Evidence suggests that if gap junctions are present at earlier developmental stages, then their retention in embryonic life might provide a method for propagation of the skin impulse.

History of skin impulse – experiments in *Xenopus*

Reference to the skin impulse dates back to a publication by Wintrebert (1904). By performing a series of very simple experiments using the axolotl tadpole, Wintrebert concluded that the skin was excitable. It was shown that stimulation of the tail-end of the animal could produce flexion of the muscles in the rostral end even when spinalised and only connected by a small bridge of skin. If only the endoderm was left between the caudal and rostral end of the animal, then no flexion was found (Roberts, 1971). Wintrebert's findings were initially contested by Hooker (1911), Coghill (1924), and Dushane (1938), who all presented evidence against electrically coupled skin cells in amphibians. It was unclear if the properties of the skin were by action of the skin cells alone, or if another system (i.e. a nerve net) might be responsible for the effects observed following tactile stimulation of the skin. Any further speculation was halted when Roberts (1971) made intracellular recordings of the skin impulse, thus confirming Wintrebert's theory (Roberts, 1971). Roberts attempted to recreate the experiments performed by Wintrebert (1904) by cutting the skin in complex patterns (Figure 1.5).

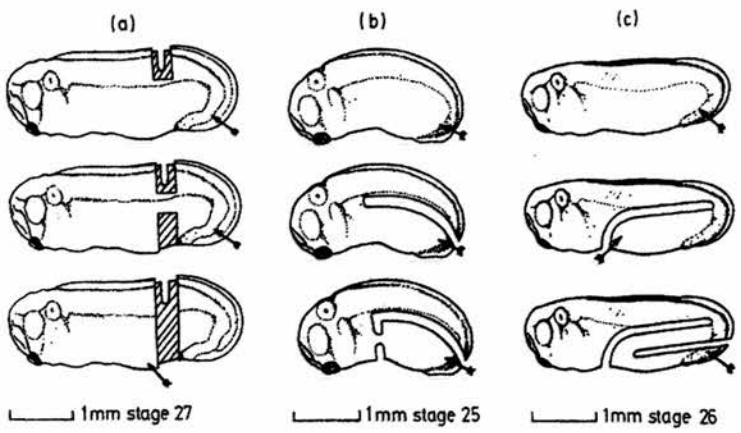

Figure 1. 5 Effects of spinal cord and skin cuts on responses of *Xenopus* embryos at stage 27 (a), stage 25 (b) and stage 26 (c). Arrows indicate locations where a pin-prick or electrical current pulse will evoke a response in rostral myotomes. Figure from (Roberts, 1971).

Using sharp glass microelectrodes, skin cells were penetrated, and one or two negative jumps in potential were recorded across the electrode. Two changes in recording potential were indicative of two layers of cells, as the electrode passed through the superficial into the deep layer. A 1ms extra- or intracellular current pulse anywhere to the epidermis would evoke an all-or-none, cardiac-like impulse across the membrane of both deep and superficial cells once the stimulation threshold was reached (see Figure 1.1). The response was not graded with stimulus intensity, and propagated without decrement through isolated sheets of tadpole skin. Resting potentials were variable in cells recorded from both intact animals and isolated skin preparations, ranging from -75 to -90 mV. Whenever a cell was found with a negative resting potential, it would exhibit an impulse upon appropriate stimulation. This suggests that most cells are capable of the depolarisation necessary for passing an impulse, but it is uncertain if all cells are capable of generating an impulse in response to the appropriate stimulus. Evoked impulses from sharp prods with a blunt pin confirmed that a similar nip from a predator would be an adequate stimulus.

Therefore, there are several pieces of evidence that point to a neuroid form of conduction in the skin of *Xenopus laevis* tadpoles (Roberts, 1971). It is established that impulses occur in peeled-off skin, eliminating the possibility of cells other than those of the skin being present. Additionally, in other experiments Roberts showed that cells removed from the developing ventral ectoderm (those destined to differentiate into epidermal cells; stage 17-19, see Figure 1.8) can be peeled off, cultured, and will develop with the same properties of excitability. Impulses exist in any skin cells where a negative resting potential is found, and are found in cells of the fin, where only skin cells reside.

Impulses can be found at stage 22, where Muntz (1964) showed via histological examination that neurones had yet to migrate far enough from the dorsal spinal cord to reach areas of the epidermis exhibiting excitability (reviewed in Roberts, 1971). Assuming these properties, Roberts (1971) suggested two possibilities for the structural basis of current dispersion: higher resistance layers at the inner and outer layers of the skin could act to funnel currents from cell to cell, or low resistance junctions between cells. Since the outer layer is rather impermeable, and does not experience rapid changes in impulse form like that of the inner layer, current funneling would not be possible with only one high resistance layer existing in the peeled-off skin. Studies of the skin with electron microscopy show the existence of close junctions, but cannot distinguish if they are tight or gap in nature (Figure 1.6). As mentioned earlier, close junctions outside the terminal bar region are not found, and simple appositions and desmosomes have only been found between inner and outer skin cells. GJs (see below) have not been specifically identified, but this may have resulted from tissue damage during the fixation process.

Role of the skin impulse: the dual touch system

After much confusion on the true nature of sensory pathways in the skin of amphibian tadpoles, Roberts (1974) proposed the existence of two sensory systems operating simultaneously in the epidermis of *Xenopus* tadpoles (reviewed in Roberts, 1974). In animals beginning at stage 27, recorded impulses in the skin almost always preceded a muscular response (Roberts, 1971) and the skin was excitable in areas of the surface of the animal that were not yet innervated by mechanosensory Rohon-Beard (R-B) cells. These are a subset of extra-ganglionic sensory neurones that were originally

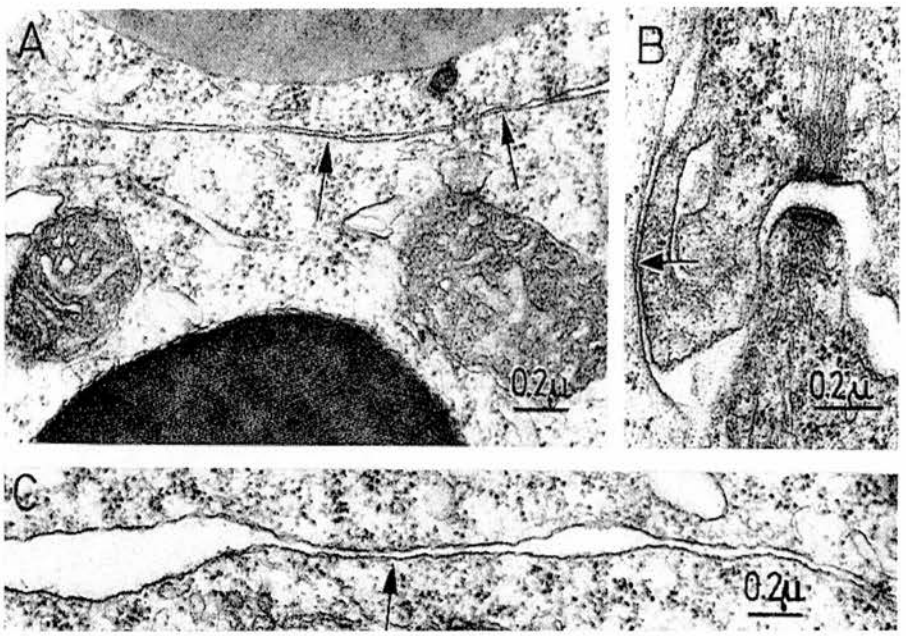

Figure 1. 6 TEM showing contacts between cells deeper in the skin. (A) Apposition (arrowed) between cells of a stage 25 embryo where extracellular space is small. (B) Apposition (arrowed) between a superficial cell and a deep cell with denser cytoplasm. The desmosome is between this cell and another deep cell. Skin of a stage 32 embryo. (C) Appositions (arrowed) in the skin of a stage 25 embryo with large extracellular space. Calibration line 0.2 μm. Figure from Roberts (1971).

discovered in several species of fish, and are now known to exist in amphibians, particularly *Xenopus* tadpoles (Nieuwkoop and Faber, 1956; Hughes, 1957). They first appear at stage 33/34, 1 day, 20 ½ hours after fertilisation, and continue to innervate the skin for much of the pre-metamorphic period.

Evidence for two types of sensory systems was revealed through various experiments testing the effects of tactile stimulation on the *Xenopus* tadpole at specified stages in development (Roberts, 1974). Beginning at stage 22, when skin impulses are first found, tadpoles were subjected to three types of mechanical stimuli: strokes from a mounted gerbil hair or baby hair, sharp prods with a blunt pin, or electrical shocks administered by a stimulating electrode (Roberts, 1974). Initially, poking the skin enough to dimple the surface caused flexion in the rostral trunk region, but it was often

non-specific to the side of the tadpole that was touched. Any area of the skin could be poked to evoke a twitch. To be certain that it was not simply a jarring of the tadpole from the one-directional prodding motion, fine forceps used to pinch the tail also produced the same flexion response. By stage 25, a muscular response can be evoked by a 1 ms current pulse. However, at stage 26, lighter touches performed by stroking the animal produced flexion on the opposite side of the body only when stroked with a hair over the myotomal region (the area of skin directly above the myotomes, slightly caudal to the head and ventral to the spinal cord). Furthermore, by stage 29/30, stroking sensitivity was seen to spread in a caudal manner to reach the tail bud, and by stage 31, the head, belly, dorsal and caudal fin, and ventral part of tail were all responsive to gentle stimulation. Up until this stage, only shocks and pokes had evoked muscular responses

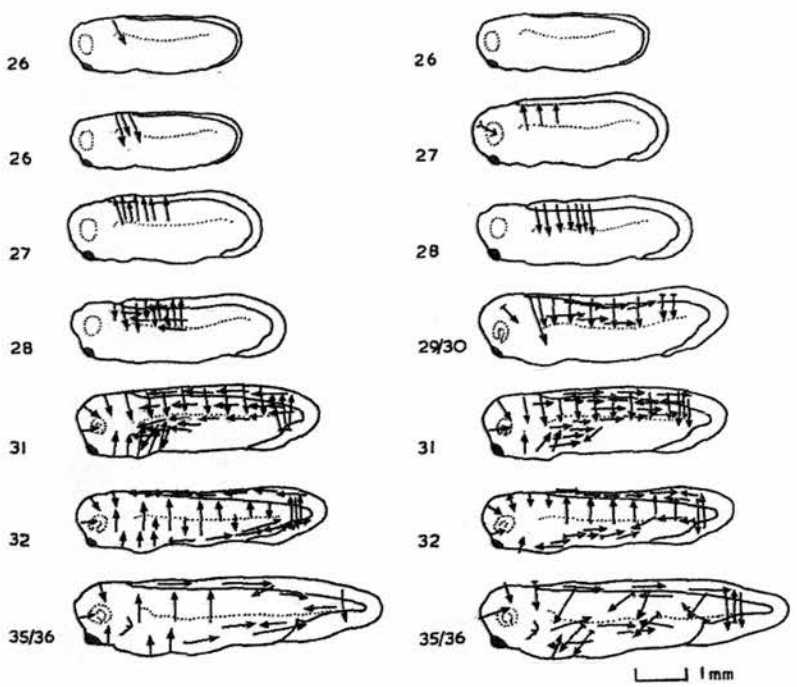

Figure 1. 7 Development of sensitivity to strokes in two embryos (left and right columns). The arrows indicate the extent and direction of strokes which evoked movements. Arrows with a line across the base evoked weak movements. Stage numbers are given to the left of each diagram. Figure from (Roberts and Smyth, 1974).

in those areas which had been unresponsive to light touch. Thus, the development of sensitivity to strokes or other non-invasive stimuli corresponds to innervation of the skin by R-B neurones (Figure 1.7).

Furthermore, lesion experiments performed on the developing tadpoles support the role of R-B cells in sensory reception. Since it is known that R-B neurones develop in the dorsal spinal cord, various transections were made at stage 17-19 (Roberts, 1974). In each case, when a portion of the developing dorsal neural crest was damaged, a corresponding area where R-B neurones were known to innervate the skin in stage 32 embryos became unresponsive to light touch stimulation (Figure 1.8). In this area, the skin did not demonstrate sensitivity to any orientation of stimulation. Yet, in the same area, and in the rest of the epidermis, responses were found from sharp pokes or shocks. Therefore, it was shown that R-B neurones are both sufficient and necessary to deliver mechanosensory signals eliciting response to light touch, directly to the central nervous system (CNS).

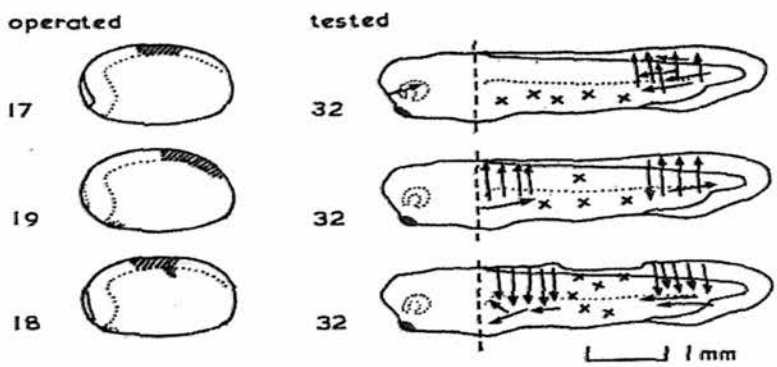

Figure 1. 8 The effect of neural crest lesions on subsequent skin sensitivity. Diagrams on the left show (cross hatched) areas where the neural crests were damaged. Diagrams on the right show the same embryo's sensitivity to pokes (crosses) and strokes (arrows) when tested later in development. The sensitivity of the head in front of the dashed line was not tested. Stage numbers are given on the left of each diagram. Figure from (Roberts and Smyth, 1974)

The second, generalized response to shocks and pokes acts as a precocious mechanism for predatory avoidance before a more complete innervation of the skin by neurones takes place during larval development (Roberts, 1998). It is these two pathways which act concurrently to deliver ascending mechanosensory information to the CNS.

Between these two pathways (i.e. neuroid and neural) there are three modalities of information that are received and propagated: touch, pressure, and noxious signals (Roberts, 1998). Both the touch and pressure modalities are coded in neural signals, the former via the neurones innervating the trunk of the tadpole, the latter via trigeminal neurones in the head. By the hatchling stage, 37/38 (Nieuwkoop and Faber, 1956), R-B neurites innervate the entire epidermis between the two layers, with projections terminating in between superficial cells (see Figure 1.3 B). In some instances, the nerve endings are found invaginated in the plasma membrane where they are wrapped by intracellular tonofilaments (structural cytoplasmic proteins, consisting of multiple tonofibrils found in epithelial cells; Roberts, 1998). These structures suggest a mechanical coupling between the skin cells and neurites, whereby the subsequent invasion of a skin impulse into such a cell could act to transduce the neuroid signal to a R-B neurite, activating a motor response. However, during the embryonic period, *Xenopus* tadpoles have been shown to exhibit two distinct, functional sensory pathways (Roberts, 1974). When the skin is presented with a light touch, the neural pathway is activated. In this manner, free nerve-endings act to relay afferent nerve impulses coding mechanoreceptive information directly to the CNS (Roberts, 1974). It is this pathway of R-B neurones that continues to develop until stage 50 when these neurones begin to degenerate, and are completely absent by stage 55. Beginning at stage 46, the dorsal root

ganglia start to develop, overlapping R-B innervation, and eventually supplying the skin with a more adult network of nerve innervation (Nieuwkoop and Faber, 1956).

The areas and patterns of sensitivity across the epidermis reflect the developmental onset of the two different pathways of sensory communication. In summary, development of sensitivity to light touch corresponds with nervous innervation of the skin by R-B neurites. Pokes were found to evoke impulses, whereas strokes never did. Additionally, pokes or shocks produced larger and persistent muscular responses, as opposed to short flexions from strokes made in all directions across the skin surface (Roberts, 1974). From these findings, it was deduced that the skin itself was excitable and responsible for the spikes seen from stronger pokes and shocks. This second pathway is thus neuroid and acts through direct communication between individual cells of the epidermis. Furthermore, two fundamentally different simultaneously acting pathways are apparent because stimulation to the skin at stages before it is innervated by neurones (stage 22) is coupled to a resulting muscular response. Even when neurones have grown laterally from the spinal cord and free nerve endings are found situated throughout the skin (stage 37/38), skin impulses can still be recorded from individual cells. Depending on the nature of the stimulus, and the age of the animal, a corresponding sensory response will follow. Organizing the sensory properties conceptually into a dual system allowed Roberts (1974) to account for the controversy over the nature of the skin impulse between earlier studies (e.g. that of Wintrebert, Coghill, Dushane, and Hooker). Due to different methods of tactile stimulation, Wintrebert and his challengers were only able to detect one modality, either neural or neuroid (Wintrebert, 1904; Hooker, 1911; Coghill, 1924; Dushane, 1938). It was not until Roberts' (1974) findings that both pathways could be

accounted for, and applied to understand the underlying peripheral sensory system of the *Xenopus* tadpole.

Generation of the skin impulse – ionic properties

As TEM images could not confirm the existence of either 'tight' or 'gap' junctions between the cells, it was then necessary to determine if these exhibited the physiological behaviour of electrically coupled cell (Roberts, 1971). In order to investigate the method by which the impulse could be propagated, cell to cell coupling was recorded by simultaneous penetration of two skin cells in close proximity. One microelectrode was used to generate a current, while the other recorded from a nearby cell. The cell being recorded hyperpolarised or depolarised in response to injected hyperpolarising or depolarising current in the former, respectively. Either response in the recording cell was abolished when the electrode was removed from the injection cell (Roberts, 1971). This cellular response suggests that the impulse in one cell triggers an identical impulse in surrounding cells by direct current flow through low resistance junctions. Impulse initiation involves fast sodium (Na^+) channels since a cell's impulse is reversibly abolished by tetrodotoxin (TTX, a voltage-gated sodium channel blocker) administered into the bathing solution (Roberts, 1971). Calcium (Ca^{2+}) currents were also thought to play an important role because of the resemblance of the skin impulse to a cardiac action potential. A cardiac impulse has a prolonged plateau influenced by the inward flux of Ca^{2+} into the cell (Silverthorn, 1998; Figure1.9). However, the addition of manganese (Mn^{2+}) ions to the bathing solution, which competitively inhibit Ca^{2+} channels, had little effect on the shape of the impulse (Roberts, 1971). Impulse duration

(i.e. the duration of time the cell is depolarised) was not seen to decrease as would be expected if the impulse were Ca^{2+}-dependent. In experiments designed to reduce the concentration of Na^{+} ions in the bathing solution, there were significant changes in the

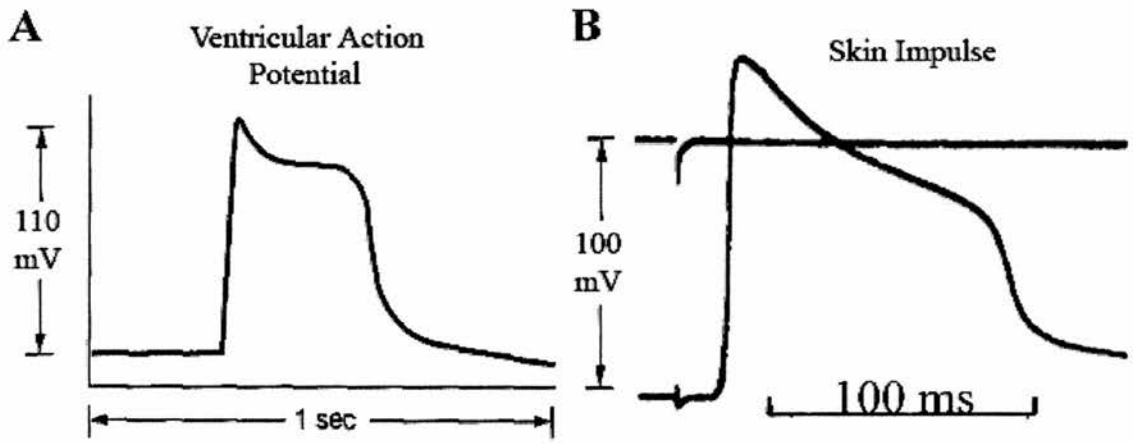

Figure 1. 9 (A) Intracellular recording of a ventricular action potential from a single cell of a vertebrate heart. (B) Intracellular recording of a skin impulse from a singe skin cell. The shape of the voltage trace between the two cell types suggests similar ionic mechanism of action. Figure from Silverthorn (1998) in (A) and Roberts (1971) in (B).

shape of the impulse only in preparations where the inner surface of the skin was exposed to the bath. This suggests that the outer surface is less likely to conduct current flow when the cell is invaded by an impulse, whereas the inner membranes of the cells can conduct impulses in a variety of external solutions (i.e. H_2O and solutions without Na^{+}). Due to the natural environment of the tadpole, it is suggested that the outer surface of the skin is less likely to be excitable in order to conserve the ions necessary for cell functionality (Roberts, 1971).

Access of the skin impulse by the CNS

Initially, it was speculated that as the impulse spreads, it eventually reaches a cell which is coupled to a R-B neurite, whereby the second sensory system can be activated (Roberts, 1974). Because neurites are found invaginated in the membranes of some skin cells, a mechanical coupling was thought to exist to transmit the neuroid signal of the skin to the ascending neural network of the R-B cells. However, through two main types of lesion experiments, the two pathways by which both soft and strong stimuli travel to the CNS were uncovered (as discussed above).

In a similar manner, the effects of other lesions were examined to determine the route of the skin impulse to the CNS. As it became clear that sharp prods were sufficient to generate a skin impulse which spreads across the entire epidermis, evoking a sustained muscular contraction in embryos, it followed that central nervous activity must be necessary to link the skin impulse to the muscular response (Roberts, 1974). It should then also follow, that if the impulse passes through the entire epidermis, and does not involve the activation of R-B neurites, then it must gain access into the CNS via another route. This was confirmed by experiments in which high spinalisation of the hatchling tadpole was carried out (Roberts, 1996). At the hatchling stage, the normal response to a 1ms current pulse to the tail is the generation of swimming activity. When an animal is immobilized in α-bungarotoxin (a nicotinic acetylcholine receptor antagonist), an electrode placed over the ventral root of the spinal cord can record the rhythmic burst of motor activity supplied by the CNS, which underlies swimming behaviour. However, in spinalised animals, fictive swimming was not observed after stimulation, even though an impulse could be recorded in the skin.

Due to the location of the lesion, several cranial nerves were suspected to provide skin impulse access to the CNS. In preparations where all but the 1st cranial nerve was cut, fictive swimming could still be produced by an electric shock to a denervated area of the skin (Roberts, 1996). If the 1st nerve is then cut, swimming is no longer produced, even though a skin impulse is still recorded. In similar preparations with the midbrain transected, and all but the 5th cranial nerves cut, swimming behaviour could be evoked until the latter was cut. It was also found that a single 5th nerve on one side was sufficient for the skin impulse to reach the CNS. Thus, the skin impulse propagates in an all-or-none manner in every direction with the trigeminal nerve (5th) and olfactory nerve (1st) each providing a pathway for the neuroid signals of the skin to induce neural motor signals within the CNS. However, the mechanism by which the skin impulse couples to these nerves is still unknown.

Propagation of the skin impulse - gap junction channels and regulation

In response to noxious stimuli, (i.e. sharp prod or electrical shock) a population of cells on the surface of the tadpole can depolarise, setting off a skin impulse which propagates from cell to cell throughout the epidermis. The impulse is thought to be triggered in each immediate surrounding cell in succession through direct current flow via available GJ channels (GJCs). GJs are the resultant conformation when two transmembrane, hexameric connexon hemichannels (CxHcs) between adjacent cells meet, forming a small pore through which the passage of small molecules and ions are permitted (reviewed in Evans et al., 2006). Each hemi-channel can be composed of multiple proteins from the connexin family, which are named according to molecular

weight, and arranged in a concentric manner around an inner pore. Since these pores directly couple the cytoplasm of neighbouring cells, such cellular processes as metabolism, signalling, secretion and in muscle fibers, contraction can be coordinated. CxHcs can exist in a cell membrane without docking head-to-head with another CxHc of a neighbouring cell, and are also found to exhibit different properties when isolated (reviewed in Evans et al., 2006). In addition, CxHcs are made of different oligomeric protein subtypes which are found to exhibit differing properties and responses to a variety of stimulators or modulators. Factors such as membrane potential, mechanical stress and intracellular Ca^{2+} ($[Ca^{2+}]_i$) concentration can readily affect the opening and closure properties of the individual CxHc and subsequent GJ pore.

As a result of the syncytial structure of the skin created by GJ pores, communication on an epidermal scale becomes possible. In the general model of GJ formation (Figure 1.10), membrane insertion begins with assembly in the rough endoplasmic reticulum (RER; reviewed in Evans et al., 2006). Single proteins are situated across the membrane of the RER with both an amino and carboxy terminus in the cytoplasm until joined by five other subunits. Oligomerisation occurs in mature endoplasmic reticulum, and the resulting protein is transported and sorted via the Golgi apparatus. When inserted into the plasma membrane, it is then a CxHc which can either be docked against an opposing CxHc in an adjacent cell to form a GJ, or can remain situated solely as an unopposed CxHc. Once docked, GJCs can congregate into assemblies called plaques which act to adhere neighbouring cells to one another (Figure 1.10).

GJCs are subject to regulation from a variety of signalling molecules including both paracrine and autocrine messengers (e.g. ATP and $[Ca^{2+}]_i$, respectively) which essentially act to gate the opening probability of the pores formed by connexin protein tubular formations. Recently, the properties of specific CxHc subtypes have been a target

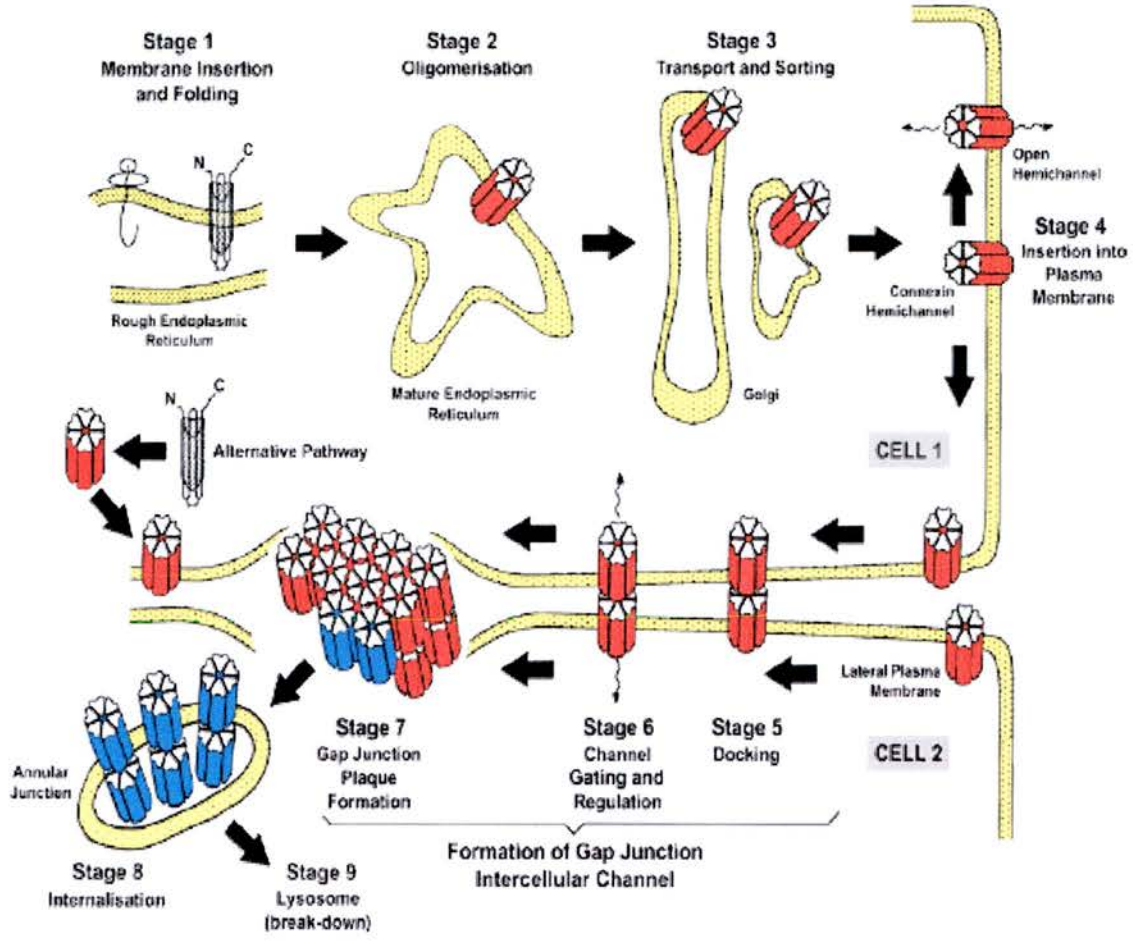

Figure 1.10 Diagram showing both CxHc and GJ step-wise assembly and membrane insertion. Figure from Evans et al. (2006).

of much investigation due to their various gating properties (reviewed in Evans et al., 2006). GJs are important structures for developing embryos, especially during pattern formation (Warner, 1985) and are specifically associated with hatching in the *Xenopus* embryo (Levin and Mercola, 2000). With the use of GJ antibodies during early

development, the importance of gap junction intracellular communication (GJIC) was established. GJ-specific antibodies bind directly to extracellular loop domains of connexin proteins composing the GJCs, decreasing the opening probability of the channel (Rozental et al., 1985). Channel blockage was found to disrupt developmental patterns and prevent structures from being transported to the correct location in developing embryos. Because GJ-permeable dyes were also found to be hindered in dispersion from seeded cells when the cells were treated with GJ-specific antibodies, closure of GJCs were thought to be the responsible for developmental defects (Warner, 1985).

Although GJs and CxHcs are similar in structure, the former being dodecameric and the latter being hexameric, their subsequent role in cell physiology can be quite different. GJs exhibit greater selectivity than CxHcs, allowing the passage of molecules in sizes ranging up to 1.5 kilodaltons (kDa), depending on the Cx subtype. Both GJs and CxHcs have subtypes with characteristic conductances for ion flux and are regulated by voltage, pH and phosphorylation. A major difference lies in the ability of GJs to be regulated by calmodulin (CaM), a Ca^{2+}-dependent protein. GJs are also regulated by Ca^{2+} released from internal stores, which can presumably interact with CaM present in the cytoplasm to directly close GJ pores. However, CxHcs can experience biphasic regulation whereby levels of Ca^{2+} above 500 μM will open connexins from within the cell, but levels below 30 μM will open most channels from the outside. Because GJCs are located in areas of close membrane apposition, channels are difficult to access specifically and are typically unaffected by changes occurring externally to the cell. However, unopposed CxHcs are directly open to external changes of molecules and ion concentrations, facilitating access due to the lack of steric effects. CxHcs are also found

to be sensitive to osmotic, mechanical, shear, and hypoxic stressors, along with direct mechanical sensitivity as opposed to GJCs which are not mechanosensitive. Further regulation of GJ and CxHcs in some models is achieved by activation of intracellular second messenger cascades involving G-protein coupled receptors. ATP can act upon nearby cells as a paracrine messenger, which can ultimately trigger a cascade of signals from cell to cell via GJs and CxHcs, such as the signal to release Ca^{2+} from internal stores (Figure 1.11; Evans et al., 2006). Other mechanisms involving aminergic and nitrergic modulation have been found in the retina of several animals (Piccolino et al., 1984; Blute et al., 1998). Many other systems are still under further exploration especially as the diffuse messenger, nitric oxide (NO), is proving to be an ideal candidate for short-range effects on surrounding cells.

Several connexin proteins are found in the developing *Xenopus* embryo. Connexin 30 (Cx30) is found in the developing hatching gland and pronephros (an early

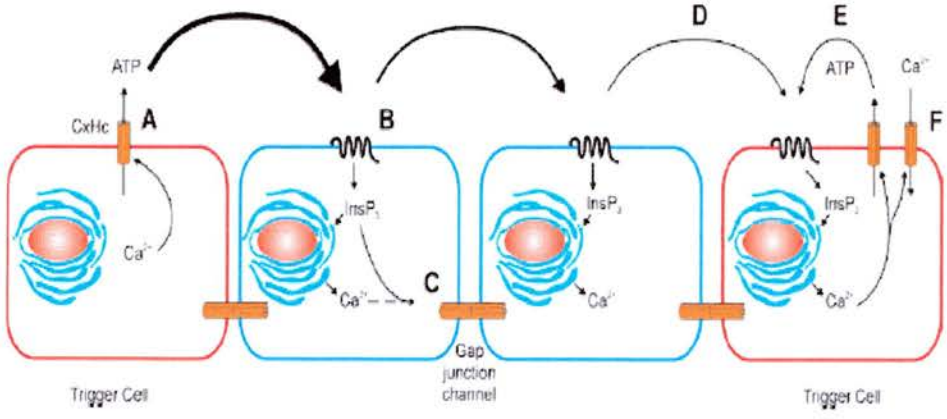

Figure 1. 11 CxHcs and Ca^{2+} signalling cascade. Ca^{2+} is released from intracellular stores (A), where it allows the release of ATP through CxHcs. ATP acts to activate G-protein coupled receptors and 2nd messenger cascades (B) which trigger GJC openings (C). Further downstream effects are seen in (D), where 2nd messenger cascades cause the release of ATP (E) as an autocrine messenger via CxHCs to trigger further release of Ca^{2+} via CxHCs (F). Figure from Evans et al. (2006).

stage of the developing kidney). At stage 22, animals treated with GJ blocking agents anandamide, 18α-glycyrrhetinic acid, or heptanol continued to develop normally, but were unable to hatch. This showed that Cx30 was involved in dispersion of a secreted metalloprotease from the hatching gland (Levin and Mercola, 2000). Depletion of the maternally expressed Cx38 causes paired oocytes *in vitro* to lose their property of electrotonic coupling. However, as embryogenesis ensues, blastomeres still establish GJIC, suggesting the involvement of other maternally expressed connexins. In addition, it was found that other maternally expressed connexins, namely Cx31 and Cx43.4 remain dormant in oocytes and their transcription is eventually found to increase in transcription as the embryo develops. Cx43 along with Cx31 and Cx43.4 are all found to increase during the period of neurulation, with the latter being the most abundant. Cx43.4 is found to be most prevalent in neural folds and thus plays a role in future dorsal structures (Levin and Mercola, 2000). Due to their location in the developing tissue expressing these connexins, these proteins could possibly lead to the formation of GJCs in future epidermal tissue. The developing ectoderm gives rise to the skin, and these cells may retain the connexins necessary to form GJ between neighbouring cells. This suggests that connexin expression and its important developmental role in the early embryo might be a potential area of regulation in the propagation of the skin impulse.

Scope of present study

In this thesis I have investigated basic properties of the skin impulse and how its propagation through the epithelium of *Xenopus* tadpoles is regulated. Signalling molecules such as 5-hydroxytryptamine (5-HT), substance P (SP), and nitric oxide (NO)

are found in the epidermis of the developing embryo and could potentially exert an effect on the excitability of the skin. Along with peptides like caerulein, and thyrotropin releasing hormone (TRH), 5-HT is found in developing granular glands in the skin (Seki et al., 1995). Although granular glands are mainly found in adult frogs, evidence for 5-HT immunoreactivity in the skin of *Xenopus* larvae has been reported in stage 42 animals (Figure 1.12; Blades, 1993).

In other systems like the retina, dopamine (DA) acts to directly gate GJCs through cyclic nucleotide-dependent mechanisms (reviewed in Katz, 1999). Since 5-HT is a monoamine like DA, it might have similar uncoupling effects in the skin of *Xenopus* tadpoles. Due to the localisation of 5-HT in the skin at early stages in development, it was then speculated that 5-HT might serve as potential modulator of the skin impulse. Blades (1993) showed effects with 5-HT on the initiation threshold for the skin impulse and a decrease in impulse propagation. However, it remains unclear if the effects seen

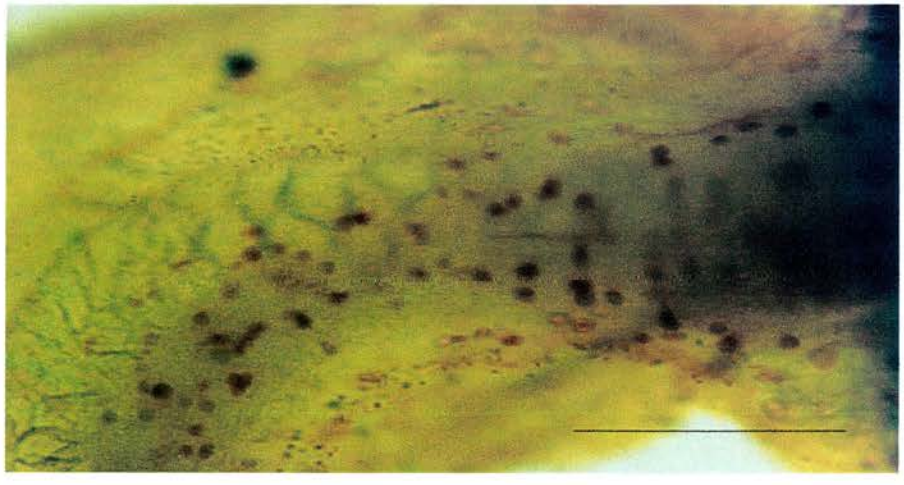

Figure 1. 12 5-HT immunoreactivity is displayed by skin cells (brown) in a punctate pattern. Scale bar shows 0.2 mm. Figure from Blades (1993).

were specifically related to GJ regulation, or an overall inhibition of the afferent sensory pathway which initiates swimming (Sillar and Simmers, 1994). Whereas effects of 5-HT on rhythmicity in the spinal motor system support a role for the release of 5-HT from central synapses (Sillar et al., 1992; Sillar and Simmers, 1994), it is unclear if peripheral release from 5-HT-producing skin cells exerts effects on the propagation of the skin impulse.

Even less is known about the effects of SP on tadpole embryos. In general, SP is known to have varying roles in different systems including nociception, inflammation, neurodegeneration, and neuroprotection (Satake and Kawada, 2006). In *Xenopus* tadpoles, exogenous addition of SP to an experimental preparation has been shown to increase the number of skin impulses following a single electrical shock. Where one shock usually produces one impulse, the production of multiple impulses suggests that skin experiences hypersensitivity when exposed to SP (Merrywest & Sillar, unpublished). SP-like immunoreactivity has been found in R-B neurons including peripheral neurites (Clarke et al., 1984; reviewed in Roberts, 1998), but the significance of its presence there is unclear, as glutamate is typically released from these neurones at central synapses (Sillar and Roberts, 1988). Other studies indicate an effect of SP on fictive swimming, whereby it has been shown to increase swim frequency (Lebofsky, 2002). This evidence suggests that SP does exert an effect on sensorimotor integration, but the exact mechanisms underlying its effect on skin sensory pathways remain unclear.

Research on the free radical gas, NO, continues to suggest widespread roles in cell physiology. Within the CNS of amphibian tadpoles, NO has been demonstrated to exert differing effects between species. In *Rana* embryos, application of an NO donor,

SNAP, was found to induce a ventral root motor pattern that is similar to a "lashing" behaviour, normally observed in response to dimmed lights (McLean et al., 2001). In addition, putative NOS (nitric oxide synthase; the enzyme which produces NO)-containing brainstem neurons were found to have possible reticulospinal projections to the spinal cord (McLean et al., 2001). The potential production of NO in both *Rana* and *Xenopus* tadpoles at embryological, larval, pre-metamorphic, and pro-metamorphic (i.e. for *Xenopus* only) stages has been well documented with the use of the NADPH diaphorase (NADPHd) technique (McLean et al., 2001; Ramanathan et al., 2006). Unlike other enzymes, NOS is resistant to formaldehyde fixation and possesses NADPH activity. Therefore, the localisation of NADPHd activity is generally a reliable marker for the presence of NOS. The developmental distribution of NADPHd staining proceeds similarly in both *Xenopus* and *Rana*, whereby three homologous nitrergic, NOS-positive neuronal clusters are established in the brainstem around the time of hatching (McLean and Sillar, 2000). However, the effect of exogenous NO on swimming in *Xenopus* is fundamentally different from *Rana* in that it reduces the swim frequency and the duration of fictive swim episodes, functioning much like a "brake" (McLean and Sillar, 2002). Also in *Xenopus*, the spatiotemporal distribution of NADPHd-positive neurons in the spinal cord suggests developmental roles for NO (McLean and Sillar, 2001). In keeping with this idea, plastic changes underlying the reconfiguration of spinal networks are thought to be influenced by NO production in areas of the spinal cord between the developing limb buds (Ramanathan et al., 2006). The patterning of expression which emerges during metamorphosis indicates that NOS -positive neurons are excluded from areas of the spinal cord which will eventually innervate the limbs. The location-specific

release of NO is thought to influence the subsequent transition of locomotor strategy from the undulatory swimming movements of the tadpole into the quadrupedal propulsion of the adult frog (Ramanathan et al., 2006). In relation to the present thesis, staining was also shown in cross-sections of skin at the hatchling stage, suggesting NO production in the cells of the epidermis in both *Xenopus* (Figure 1.13; McLean and Sillar, 2001) and *Rana* (McLean et al., 2001)

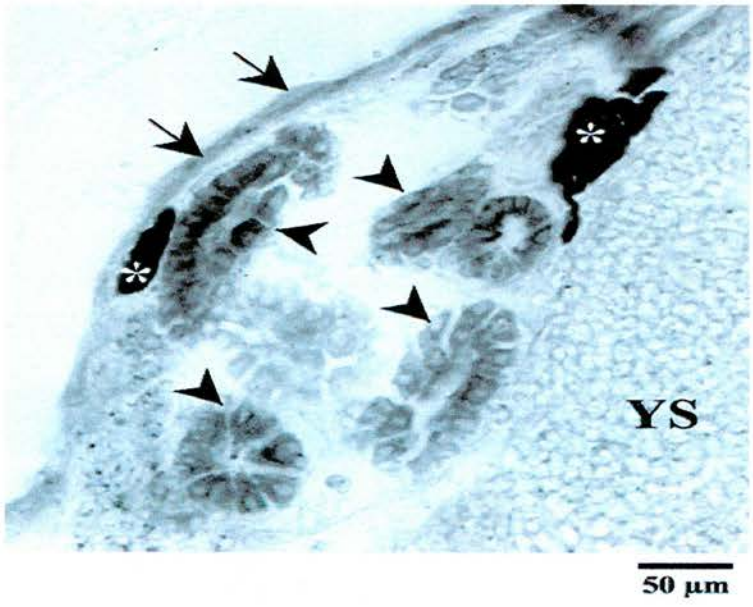

Figure 1. 13 Cross-section of stage 42 tadpole where arrows denote NADPHd staining in the epithelial cells of the skin. Arrow heads indicate staining in the endothelial cells of blood vessels White * indicates black pigmented melanophores. YS denotes the yolk sac. Figure from (McLean and Sillar, 2001)

In *Xenopus*, location-specific release could provide a link to the regulation of the skin impulse through modification of GJCs. This thesis has investigated the potential modulation of the skin impulse and its propagation by three neuroactive chemicals: 5-HT, SP, and NO. Their location in the developing embryo and their known effects in other systems, suggests these endogenously produced chemical messengers are candidates for the regulation of neuroid conduction in the epidermis of *Xenopus* tadpoles

Chapter 2 – Materials and Methods

Animals

Xenopus laevis embryos and larvae from stages 37/38-42 (Nieuwkoop and Faber, 1956) were obtained by weekly induced breeding from a laboratory colony of adults. *Triturus vulgaris* embryos were obtained by natural breeding from an adult colony. *Rana temporaria* and *Bufo bufo* spawn were collected from local ponds. All embryos were raised in dechlorinated tap water between 17 and 23°C to stagger their development. Some *Rana* and *Bufo* spawn was stored temporarily in a refrigerator at 4°C to delay development and maximize the use of a limited supply.

Electrophysiology

Extracellular

The majority of experiments were performed on stage 37/38 tadpole embryos (Nieuwkoop and Faber, 1956). Fine cuts were made using custom-made tungsten dissecting pins in the dorsal and ventral fins of the animal in order to facilitate immobilisation in 12.5 μM α-bungarotoxin (SIGMA). Animals were removed from the toxin when determined to be immobilized (c. 30-60 minutes). Animals were then transferred to a recording bath with circulating HEPES saline [composition (in mM): 115 NaCl, 2.5 KCl, 2.5 $NaHCO_3$, 10 HEPES, 1 $MgCl_2$ and 3 $CaCl_2$, pH 7.4 with NaOH]. Saline was gravity-fed from a 100 ml reservoir into a perspex chamber (c. 5 ml) containing a rotational platform with a Sylgard (Dow-Corning) surface. The solution was re-circulated with a flow rate of approximately 6-10 ml/min by a peristaltic pump back

into the reservoir. An identical reservoir containing 100 ml of saline was reserved for washing the preparation. All drugs were added directly to the reservoir.

Using fine custom-made tungsten pins, animals were pinned to the Sylgard through the notochord just above the otic capsule and at the end of the yolk sack. On the right side of the body, the flank skin between the pins was then removed using fine custom-made tungsten dissecting needles. Custom-made nonfilamented borosilicate glass (1.0 mm O.D., .58 mm I.D.; Harvard Apperatus, LTD.) suction electrodes (c. 50-70 μm) were used to measure extracellular recordings. Each electrode was filled with saline from the bath using a 1 ml plastic syringe (BD Plastipak™) connected via polythene tubing. In all preparations, one electrode was placed over the intermyotomal cleft to record ventral root impulses appropriate to drive swimming movements ("fictive swimming") and a second was placed on the epidermis, caudo-ventral to the eye, to record skin impulses. A custom-made glass stimulating suction electrode, wound with insulated copper wire (.05 mm, Goodfellow, Ltd.; Cambridge, UK) was placed on the tail skin. Fictive swimming behaviour and depolarisation of epidermal cells were achieved by delivering a 1 ms current pulse using a DS2A isolated stimulator (Digitimer, Welwyn Garden City, UK) at a determined threshold voltage sufficient to evoke fictive swimming and a skin impulse. All electrodes were positioned using Prior manipulators. Light was supplied to the bath by a highlight 2000 cold light source (Olympus Europe) fibre optic cable. Signals were amplified using differential AC amplifiers (A-M Systems Model 1700), displayed on a Gould digital Oscilloscope (20 Ms/sec 20 MHz (DSO) 1604), digitized using a CED micro 1401 and stored and processed on a Dell Dimension 2400 Desktop computer using Spike2 software (Cambridge Electronic Design v. 3.21).

Intracellular

For Intracellular recordings, microelectrodes were pulled from nonfilamented borosilicate glass (1.0 mm O.D., .58 mm I.D.; Harvard Apperatus, LTD.) using a P-2000 laser puller (Sutter Instruments Co.). Electrodes were then filled with 3M KCl and had resistances of 100-300 MΩ. Signals were supplied using a custom-built DC amplifier (courtesy of Dr. Steve Soffe, University of Bristol, UK) connected to a CED micro 1401 and Gould Oscilloscope as described above. Once in the saline, electrodes were balanced using a test function and dial, aligned on the oscilloscope, and lowered down towards the surface of the epidermis using the coarse adjustment of a micromanipulator (Goodfellow Technology, Cambridge). Using the fine control, the electrode was lowered onto the epidermis until a deflection in the recording trace from the oscilloscope was observed (c. 2 mV depolarisation). Penetration of skin cells was achieved by a brief capacity overcompensation used to deliver a high frequency vibration of the electrode sufficient to pierce the cell membrane, driving the electrode into the cell. Usually, a resting potential of c. -50 to -80 mV was immediately detected. Cells were recorded for as long as the penetration could be maintained, but in most cases recordings were stable for only a few minutes. If the membrane potential returned to 0 mV, an attempt to reenter the same cell was made by a slight upward and then downward movement with manipulator followed by an overcompensation. If the cell was unrecoverable, the manipulator was used to slightly withdraw the electrode to above the surface of the epidermis, moved a few tens of microns laterally, and then lowered again.

In some experiments a MASTER-8 (A.M.P.I) automatic stimulator was used to time both extracellular stimuli and a deliver high frequency trains of stimulations (c. 1-

2.5 Hz). A second, identical micromanipulator and amplifier, connected in the same manner as described above, was used to make simultaneous sharp, intracellular recordings. Paired recordings were made by penetrating cells in close proximity, approximately 50 to 100 μm apart. One microelectrode was used to inject either a depolarising or hyperpolarising current into one cell, and record the voltage response in the neighbouring cell. After injecting the desired current, the injection electrode was removed from the cell, and the same current injection was applied to check that there was no longer a voltage response that could be detected in the recording cell.

Pharmacology

Drugs were purchased from Sigma-Aldrich (serotonin creatinine sulfate complex (5-HT), 18-β Glycyrrhetinic acid (Fluka), $_N$-acetylpenicillamine (NAP)) and TOCRIS Bioscience (forskolin, substance P (SP), L-732-138, carboxy-PTIO (C-PTIO), spermine NONOate, ODQ, 8-Br-cGMP, L-NAME). *S*-nitroso-$_N$-acetylpenicillamine (SNAP) was either purchased from TOCRIS Bioscience or synthesized from NAP by the University of St. Andrews School of Chemistry. All drugs were made fresh daily whenever possible, diluted in a vehicle of distilled (Fistreem water purification, Leicestershire, England) H_2O (5-HT, SP, C-PTIO), dimethyl sulfoxide (DMSO; ANALAR®) (forskolin, SNAP, ODQ) or ethanol (L-732,138), to achieve the desired stock concentration using a Gilson pipette and stored in plastic 500 μL or 2 mL Eppendorf tubes (Axygen Scientific) either in a freezer at -30°C or in a refrigerator at 4°C. When necessary, light-sensitive substances (i.e. 5-HT and SNAP) were made into aliquots and wrapped individually in pieces of tin foil. Drugs using DMSO and ethanol as a vehicle were aliquoted so as not to exceed a

final bath concentration of .5% and 1%, respectively. All drugs were weighed using a Sartorius Handy H 110 microbalance.

Scanning Electron Microscopy

Glutaraldehyde solution for electron microscopy (BDH Laboratory Supplies) was diluted in 0.1 M phosphate buffer (PB, pH 7.4) to achieve a stock concentration of 2.5% (v/v). *Xenopus laevis* embryos and larvae from stages 37/38-42 (Nieuwkoop and Faber, 1956) were selected and fixed in 2.5 % glutaraldehyde in PB overnight in 10 mL glass vials. The same fixation process was used for *Rana temporaria* and *Bufo bufo* embryos from stages 18-22 (Gosner, 1960), and *Triturus vulgaris* embryos at the pre-hatching stage. Animals were removed from the fixing solution and placed in ascending concentrations of ethanol for 15 minutes each, beginning in 50%, then 70%, 96%, 100% and 100% again. After this dehydration process, the animals were stored in 100% ethanol until ready for critical point drying. Animals were placed in a Samdri-780 Critical Point Dryer. The critical point is reached at 1100 lb/in^2 and 32°C, after which infused liquid CO^2 is released as gas. Animals were then removed and carefully placed on double-sided tape using a fine paint brush. The tape was affixed to a 3 cm aluminium stub. Stubs were then placed inside an Emscope SC500 sputter coater for 3 minutes. Internal air was replaced by Argon (Ar) gas and held at -1 torr. A high voltage was supplied between the anode and cathode where the stub is situated. Ar atoms collide with the gold-plated anode, releasing gold atoms, which cover the specimen when attracted towards cathode. This created a gold coating on the exposed surface of the animal 15-20 nm thick.

All animals were viewed with a JEOL JSM-55 CF Scanning Microscope at an accelerating potential of 10 KV and a 65-70 μA. SemAfore (v. 5.0) "Digital slow scan recording system" software by Jeol was used to photograph the images. Images were either saved in .tiff or .jpeg file format and edited with Adobe Photoshop v. 7.0.1.

NADPH Diaphorase Histochemistry

Stage 37/38 *Xenopus* (wild-type and albino) and pre-hatching *Triturus* embryos were fixed in 4% paraformaldehyde (pH 7.4, 4°C) for 2 hours on a rocking agitator. The animals were then removed from the fixing solution and washed in PB (3 x 5 min). The animals were then placed in 10 ml glass vials containing either 10 % or 30 % sucrose in 0.1M PB solution and stored in the refrigerator until they sank (usually overnight). For wholemounts, animals were removed from sucrose solution and placed in a dish containing Sylgard (Dow-Corning) and filled with 0.1 M PB. The animal was pinned to the Sylgard through the notochord above the otic capsule and further along the tail past the anus. Cuts were made using fine, custom-made tungsten dissecting pins to prepare the skin for removal. First, a transverse cut was made under the surface just rostral to the pin above the otic capsule. Second, cuts were made along the dorsal fin and along the yolk sack and ventral fin. Using a pair of #5 watchmaker's forceps, the skin was gently pulled in a rostro-caudal direction and removed from the animal. The excised skin patch was pinned at each end into Sylgard. Using the same procedure, another skin patch was excised from the opposite side and then pinned next to the first. Using a razor blade, the Sylgard supporting the excised skin was carefully cut out of the petri dish.

The Sylgard block and pinned-out tissue was then placed in a 10 ml glass vial containing 5 ml of NADPH Diaphorase (NADPHd) staining solution (consisting of: 5 mg NADPH (Sigma N-1630), 4.95 ml 0.3% PB-TX, and 50 µl of nitroblue tetrazolium salt (NBT; Sigma N-6639) made up from 5mg NBT dissolved in 0.5ml PB-TX). Tissue was incubated at 37°C for 2 hours. In some preparations, the concentration of NBT was doubled. Tissue was incubated at 37°C for 2 hrs. The tissue was then removed and washed in 0.1 M PB and gently plated out onto on a slide. Tissue was either dehydrated in acetone or allowed to dry overnight. It was then cleared in a xylene series. Finally, the slides were mounted with DPX and sealed and coverslipped, ready for viewing.

A Zeiss Axiolab microscope (10x, 40x, and 100x magnification objectives) was used to view slides and a vertically mounted Olympus OM-2_N SLR 35 mm camera was used to photograph the specimens. All film was either ASA 200 or 400 35 mm (Fujifilm) stored in a refrigerator at 4°C prior to use. Immersion oil (Fluka) was applied to the cover slip when viewing at 100x magnification. All film processing was outsourced to Ian Joy Photography, St. Andrews, for colour processing and development. Images were digitally imported from film negatives onto CD, compressed as .jpegs, converted to Paint Shop Album Photos and edited with Adobe Photoshop software.

DAF-2 DA Fluorescent Labelling

For wholemount preparations, animals were placed in a 10 ml glass vial containing 1 µl/ml DAF-2 DA (4,5-diaminofluorescein diacetate, CALBIOCHEM) solution in HEPES saline [composition (in mM): 115 NaCl, 2.5 KCl, 2.5 $NaHCO_3$, 10 HEPES, 1 $MgCL_2$ and 3 $CaCl_2$, pH 7.4]. Vials were covered in tin foil and placed on a

rocking agitator for 15-30 minutes. The foil was removed from the vial and the staining solution was replaced with 4% paraformaldehyde in PB (pH 7.4, 4°C) for 2 hrs. After fixation, animals were then washed in 0.1M PB (3 x 5 min.). Specimens were mounted in a glass cavity slide, using Citifluor (glycerol solution, AF2, Citifluor, Ltd.), then coverslipped. Edges of the coverslip were affixed using nail polish. For excised skin patches, animals were anesthetized in tricaine methanesulphonate (MS-222) (0.1-1%; Sigma,-RBI, Poole, UK) for approximately 1-2 min, then placed in a glass petri dish with a Sylgard base, containing HEPES saline (for composition see above). Animals were then dissected as described above. The resulting Sylgard block and pinned skin was placed in a 10 ml glass vial containing 5 µl DAF-2DA in 5 ml HEPES saline (for composition see above). The vial was covered in tin foil and placed on a rocking agitator for 15-30 minutes. The foil was removed and the staining solution was replaced with 4% paraformaldehyde, (pH 7.4, 4°C) for 2 hrs. After fixation, the specimens were washed in 0.1M PB (3 x 5 min.). The tissue was unpinned and carefully transferred onto a glass slide using forceps and a fine paint brush, then mounted and coverslipped with citifluor. Edges of the coverslip were affixed using clear nail varnish, ready for viewing.

nNOS Fluorescent Labelling

For excised skin patches, animals were fixed in a 10 ml glass vial containing 4% paraformaldehyde (pH 7.4 for 2 hrs at room temperature on a rocker (Grant-Bio PMR-30). The fixing solution was removed using a plastic 2.5 ml pipette and the animals washed in 0.1 M PB (3 x 5 min.) Blocks of Sylgard with pinned excised skin patches were placed in a 10 ml glass vial containing 5 ml of blocking serum and primary

antibody (solution consisting of: 5% NGS (Normal Goat Serum, Jackson Immuno: 005-000-121), 3% BSA (Bovine Serum Albumin) in PBS-TX, pH 7.4 (0.9% PBS (NaCl in PB) and 0.3% Triton X) containing primary antibody at 1:100 (v/v) NOS-1 (R-20):sc-648, rabbit polyclonal antibody; Santa Cruz Biotechnology, Inc.). The tissue was incubated at 37°C for 24 hrs. After incubation with the primary antibody, the samples were washed in 0.1M PBS (3 x 10 min). 5 ml of blocking serum containing secondary antibody (1:100; pH 7.4; Cy™3-conjugated-red label AffiniPure Goat Anti-Rabbit IgG (H+L), Jackson Immuno, 111-165-144) was added to the vial, which was covered in tin foil and agitated on a rocker at room temperature for 24 hrs. The specimen was then washed in 0.9% PBS, for 24 hours, whilst covered with tinfoil and on the rocker. The block supporting the excised skin was then removed from the glass vial, and the tissue was carefully unpinned, mounted and coverslipped with Citifluor as above.

Confocal Microscopy

All prepared slides were viewed with a confocal microscope (Leica DM IRE2). The nNOS secondary antibody is known to fluoresce in the TRITC range (550-700 nm). DAF is known to fluoresce when excited at 492 nm, a wavelength which lies in the FITC range. Specimens were imaged either as optical sections with a thickness of 10 μm or as a z-stack at x10, x20, x40 or x63 magnification. Non-fluorescent immersion oil was used at x40 and x63. Images were recorded with Leica confocal software (v. 2.61 Build 1537).

Data Analysis

Electrophysiological data was analysed using Dataview software (v 4.7c, courtesy of Dr. W. J. Heitler)

Extracellular

Extracellular recordings were used to measure both motor bursts from the ventral root of the spinal cord during fictive swimming, and the depolarisation associated with the skin impulse from a population of epidermal cells. In some experiments, swimming, cycle period and episode duration were measured as a positive control to determine if applied drug were exhibiting effects on the central nervous system. Measurements of cycle period were taken by examining 30 bursts from 3 episodes in each control, drug, and wash period, beginning approximately 1 s after the stimulus artefact. Within Dataview, 'events' spanning the duration of each swim cycle were created by clicking the mouse at the beginning of each burst. The 'on time' of each event is recorded and imported into an Excel spreadsheet (Microsoft Corporation), where cycle period is computed by subtracting each event 'on time' from the 'on time' of the previous event (the first event being ignored). Episode durations were measured from the beginning of the first burst to the end of the last burst to create an event. The duration of the event is equivalent to the swim episode duration. Skin impulse delay was calculated in a similar manner whereby events were measured from the stimulus artefact until the greatest positive depolarisation of the burst. This was chosen in order to be consistent, as it was assumed to be the response of the cells directly below the recording electrode opening. The duration of the event is equivalent to the delay from stimulus to response as the skin impulse travels across the epidermis.

Intracellular

In all experiments, two parameters were measured from the resulting waveform of the skin impulse. First, the delay was measured from the stimulus artefact to the onset of the skin impulse. Second, the duration of the skin impulse was measured as the interval between the initial rapid depolarisation to the point where the membrane potential was judged to have returned to rest.

Microsoft Excel

All raw data consisted of measurements from multiple skin cells and was imported into Excel spreadsheets where data from each period (i.e. control, drug, and wash) were averaged for duration and resting potential (E_M). For delay, data from each period were fitted to a linear regression line. Measurements during an experiment were subject to a skin cell being penetrated, and were thus made at irregular intervals. All bar graphs were made from average values from each period, and error bars displayed ± standard error of the mean (S.E.M.)

MINITAB™ Statistical Software (MINITAB release 13.32)

The General Linear Model is a category of statistical tests which includes the analysis of variance (ANOVA). This test was performed to determine if there was a statistically significant difference between periods of a given test. All data was pooled from multiple skin cells from each period and averaged; either the average value for duration and membrane potential, or the average slope for delay. Tukey's *post hoc* test was used to determine statistical significance of the average slope of the delay, average duration, and average resting potential between control, drug, and wash periods; this indicated which periods were statistically different from one another.

Chapter 3 – Results

Section 1 – Electrical properties and propagation of the skin impulse in *Xenopus laevis* and other anuran amphibians

The basic electrophysiological properties of the skin impulse of *Xenopus laevis* embryos were recorded either extracellularly or intracellularly, or both, at hatchling stage 37/38, including conduction delay, impulse duration and waveform. Impulses were generated using an extracellular stimulating electrode positioned as close to the caudal end of the tail, such that sufficient contact was made, but without sucking the tail inside the pipette (Figure 3.1.1). This stimulation and recording configuration allowed the various parameters of the skin impulse to be measured under different experimental conditions such as varying the frequency of stimulation (discussed below) and in the presence of various pharmacological modulators (Results, Section 2). In addition, fictive swimming was monitored by placing glass suction electrodes over an intermyotomal cleft wherein lie the axons of motorneurons. Once electrodes were in place, beginning from 0 volts (V), the stimulus (1 ms duration) was increased in strength in 1 V intervals until the stimulus artefact was followed by a skin impulse (Figure 3.2.1 B). The stimulus intensity was then gradually reduced in order to better identify the stimulus threshold for the skin impulse. Skin impulse initiation thresholds (V_T) were often found to begin at a higher value at the start of preparations, but would eventually decrease over 5-10 minutes to a stable level. Usually, V_T ranged between 1 and 10 V in different animals. The thresholds for the skin impulse and for the initiation of fictive swimming were often similar but sometimes swimming could be initiated by the R-B pathway before the skin impulse

threshold was reached. The R-B pathway was also presumed to have been active when the first burst of swimming occurred prior to the recording of the skin impulse.

Conduction delay for the skin impulse can be defined as the duration of time it takes the skin impulse to propagate from the point of initiation to the point at which it is recorded. It can be measured by both extracellular and intracellular electrodes. Because the propagation of the impulse across the epithelium of the skin is presumed to involve transmission across gap junctions, delay measurements ought to serve as a marker for fluctuations in gap junctional coupling between cells. Because the distance between stimulating and recording electrodes remained constant, changes in delay can be attributed to modification of the coupling between the cells of the epidermis. From this, conduction velocity could theoretically be calculated. Roberts (1971) reported conduction velocities with an average of 7.7 cm/sec. However, because delay was seen to change during experiments, even with the electrodes at fixed distances, this proved to be an inaccurate measure for the velocity of the impulse (addressed below).

Extracellular recordings

Extracellular recordings of the skin impulse are made from the population of skin cells located beneath the electrode tip (c. 50 μm in diameter). The duration of the extracellular impulse will be affected by the diameter of the electrode tip, but responses are generally consistent between successive stimuli as long as a constant amount of suction on the skin is maintained. Because extracellular recordings are made using an AC amplifier, low frequency filters are set to remove extraneous electrical noise and consequently only the fast initial depolarisation of skin impulses produced by cells

beneath the tip are recorded. This causes the impulse to appear as a relatively brief, multiphasic spike (c. 15 ms) in the extracellular trace (see Figure 3.1.1 C). Extracellular recordings of the skin impulse provide less accurate measurements of delay than intracellular recordings. Thus, in all experiments where the conduction delay was investigated, intracellular recordings were used. Extracellular recordings provided a simple and useful way to monitor spontaneous impulses (i.e. impulses that occurred without prior electrical stimulation), to determine the initiation threshold and to monitor fictive swimming.

Fictive Swimming

Measurements of various parameters of fictive swimming (e.g. cycle period and episode duration) were used to asses whether the applied dugs (i.e. 5-HT and NO) were exerting an effect on the CNS. Their time course of action on swimming could then be compared to recordings of the skin impulse to determine if an effect was occurring simultaneously in the skin. Since the effects of various modulators on swimming are known for 5-HT (Sillar and Simmers, 1994) and NO (McLean and Sillar, 2002), they served as a control for drug efficacy. Changes in the motor patterns of fictive swimming are a useful indicator of changes in the epidermis since electric shocks above the initiation threshold are inextricably linked to a skin impulse which produces swimming behaviour in stage 37/38 embryos. Often, the initiation threshold for the skin impulse (V_T) and fictive swimming are identical, where a single shock will evoke a skin impulse which precedes the onset of the first burst in a swim episode (see Figure 3.1.1 B)

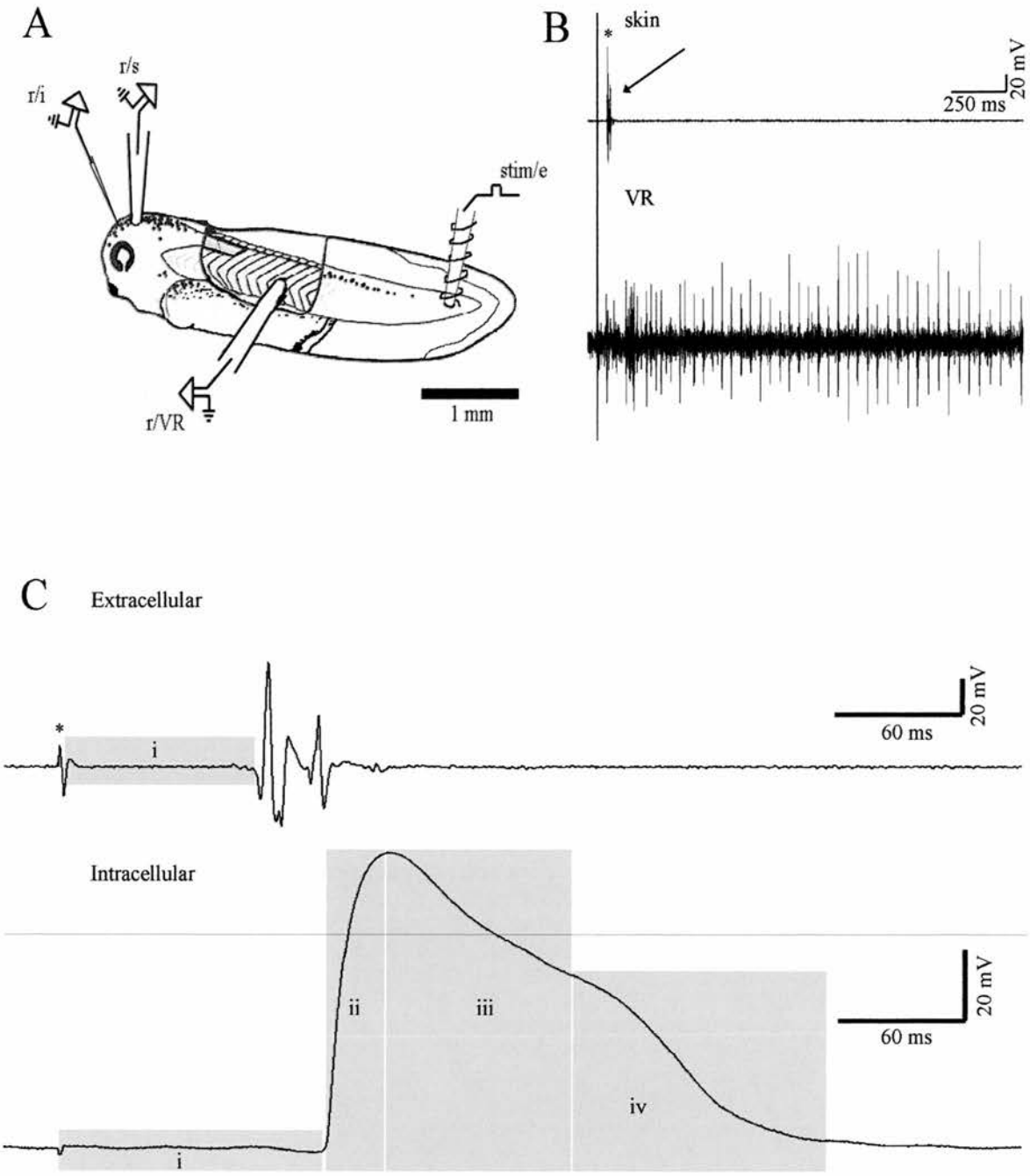

Figure 3.1. 1(A) Schematic diagram of the preparation used to initiate and monitor skin impulses in stage 37/38 *Xenopus* embryos. r/i, intracellular recording electrode; r/s, extracellular recording electrode on skin; stim/e, extracellular stimulating electrode on tail; r/VR, extracellular recording electrode on ventral root. Scale bar = 1 mm. (B) Extracellular recordings from r/s (top trace) showing skin impulse (arrow) and r/VR (bottom trace) showing swimming. * = stimulus artefact. Scale bars show 250 ms and 20 mV. (C) r/s from (B, top) and r/i (bottom) showing 4 phases of the skin impulse. (i, top and bottom) conduction delay; (ii) fast depolarisation; (iii) plateau; (iv) repolarisation. Phases ii-iv constitute impulse duration. Left side of grey box (i) indicates stimulus artefact. Grey horizontal line shows 0 mV. Scale bars = 60 ms and 20 mV.

Intracellular recordings

Intracellular recordings were used primarily to measure the waveform of the skin impulse and changes in both delay and duration. The intracellular preparation is identical to the extracellular one, but with an additional sharp, intracellular electrode that records the changes in voltage in an individual skin cell (see Figure 3.1.1 C).

Alterations in the waveform of the impulse may be indicative of changes in the underlying ionic mechanisms which govern the subsequent transmembrane voltage responses. Compared to conduction delay, impulse duration is a more variable parameter, exhibiting greater changes during the course of an experiment. Impulse duration can be defined as the length of time that a skin cell is depolarised from its negative resting potential when propagating an impulse. Values of both delay and duration were found to vary within experiments and between animals (discussed below). However, where delay would typically begin at 60 ms, and could be seen to double or more within the course of the experiment (1-3 hours), duration would initially measure 150 ms, potentially increasing to 500 ms. The falling phase of the impulse is biphasic, consisting of a plateau phase followed by a repolarisation back to E_M. While the duration of the impulse is quite variable during a given preparation, the repolarisation phase is usually greater than twice the plateau phase (see Figure 3.1.1 C). However, it should be noted that the accuracy in duration measurements was greatly affected by the quality of the penetration of the skin cell. Only penetrations which exhibited a resting potential in the range of -40 to -90 mV were used.

Effect of stimulus frequency on skin the skin impulse

Stimulation frequency affects conduction delay and skin impulse duration. Once V_T was determined, impulses were recorded intracellulary to assess the relationship between stimulus frequency and conduction delay. Tadpoles were stimulated at frequencies ranging from 0.05 Hz to 2 Hz (Figure. 3.1.2). At frequencies above 0.1 Hz, conduction delay was found to increase with successive stimuli (Figure. 3.1.2 Ai). Based on this finding, stimulation frequencies greater than 0.05 Hz were not used in subsequent pharmacological experiments to be certain that stimulus frequency was not in itself changing the conduction delay.

In addition to the effects on delay, there was a very marked decrease in impulse duration. (Figure 3.1.2 Aii). These effects on delay and duration are readily noticeable at stimulation frequencies of 1 Hz or above. Delay responded to successive stimuli by following a hyperbolic-like trend, whereas duration was found to make an immediate, nearly step-wise decrease after the initial impulse. A further decrease in delay is observed in the remainder of the train, but not nearly as large or as consistent in direction, since further stimuli produced responses that could fluctuate about the depressed level. The impulse will fail when the stimulation interval is shorter than the refractory period. If an increase in the stimulus intensity overcomes the failure, then the relative refractory period has been reached. However, if increasing the stimulus strength does not overcome the failure, then this demonstrates that the absolute refractory period has been reached. For example, in one experiment, a train of 30 impulses was completed with a 30:21 ratio of stimulus to impulse response at a V_T of 15 V and a stimulation frequency of 0.67 Hz. When V_T was increased to 20 V, a 1:1 ratio was observed, demonstrating that the relative

refractory period had been overcome (Figure 3.1.3). Failure ensued when a new relative refractory period was reached at a frequency of 1 Hz at 20 V. Here, a 30:27 ratio was observed, but became 1:1 when the voltage was increased to 30 V. Once trains ended, both delay and duration would return to initial values. The former appeared to follow a gradual decay from heightened values as it recovered to baseline in the 20 seconds following the last impulse in the train. However, further stimuli during this period counteracted the natural decay, but were a necessary means to determine how this parameter was changing after the stimulation train. In contrast, the duration recovered much faster, returning to initial levels in 3-5 seconds. The effects shown here to rapid stimulation display that delay and duration respond with different patterns and time courses of refractoriness, suggesting that modification in these parameters are mutually exclusive, and acting through different mechanisms (explored below in Results, Section 2).

Stimulus voltage

Conduction delay was found to markedly decrease with increased stimulus voltage (see Figure. 3.1.3). Within the preparation, a constant distance is maintained between the point of stimulation and the point of recording. Increasing stimulus voltage effectively decreases the distance over which the impulse propagates because the impulse is initiated at a greater distance as the current spreads from beneath the stimulating electrode. In order to accurately determine changes in delay across the skin surface, *Xenopus* embryos with high resting V_T values (e.g. >15 V) were discarded because the effective distance over which the impulse travelled would have been greatly reduced and

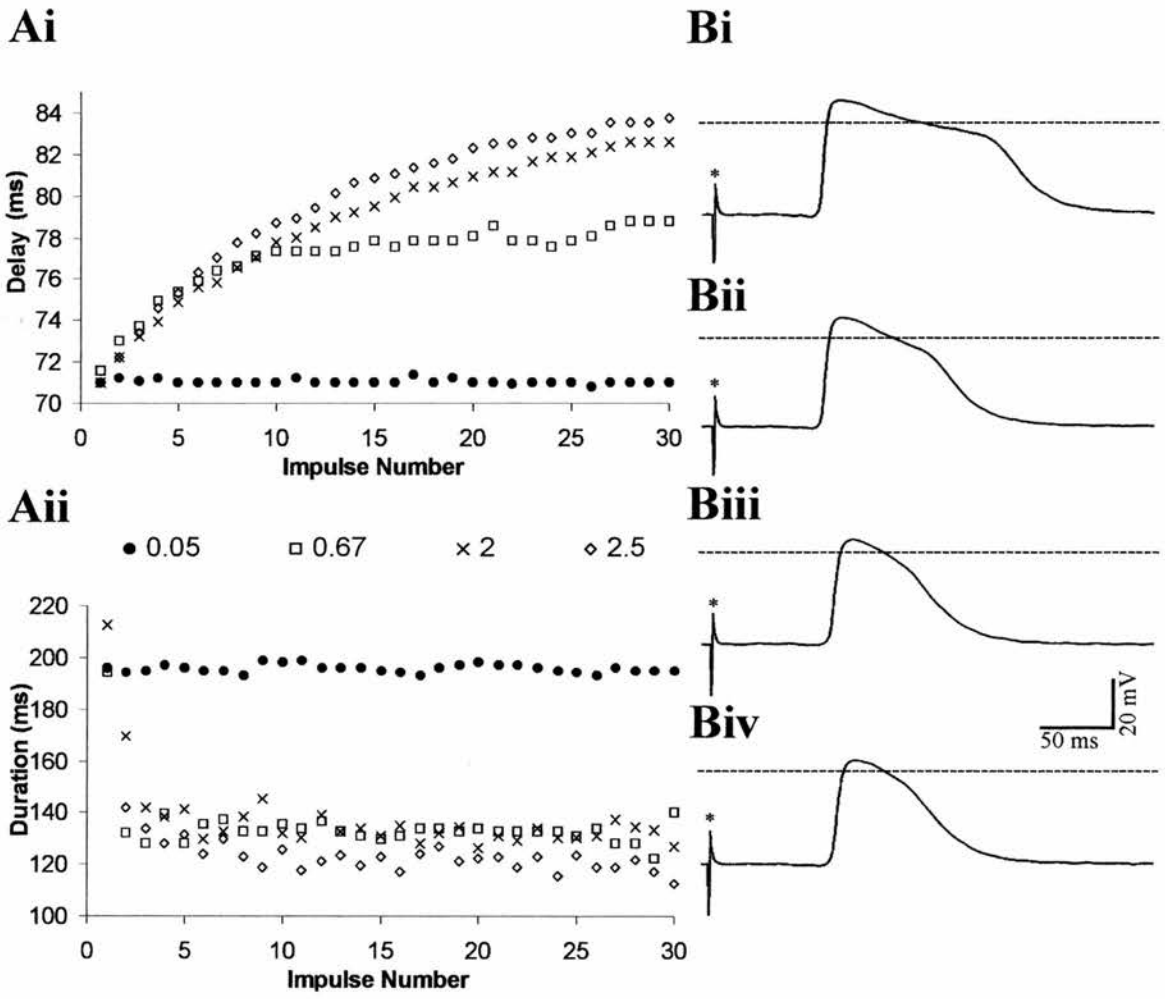

Figure 3.1. 2 (A) Effect of rapid stimulation on conduction delay (i) and impulse duration (ii) on stage 37/38 *Xenopus* embryos. Trains of 30 stimuli were conducted at 0.05, 0.67, 2, and 2.5 Hz, V_T = 30 V. Legend identifies stimulation frequency. (B) Intracellular recordings of 1st (i), 2nd (ii), 15th (iii), and 30th (iv) impulses from train at 0.67 Hz. Dashed line indicates 0 mV. Scales bars = 50 ms and 20 mV. * indicates stimulus artefact.

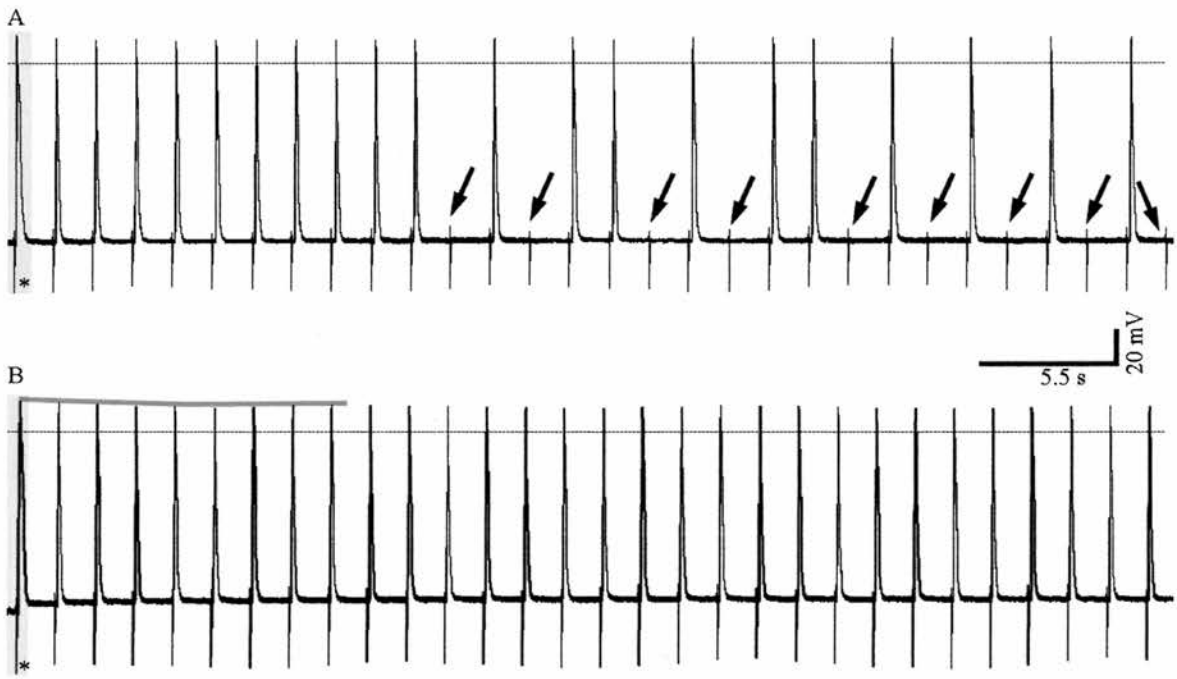

Figure 3.1. 3 Refractoriness of the skin impulse. (A-B) Two consecutive trains of 30 stimuli in the same cell of a stage 37/38 *Xenopus* embryo. (A) was conducted at 0.67 Hz, stimulating at the V_T of 15V. Arrows indicate stimuli which failed to produce a skin impulse. (B) was conducted at 0.67 Hz with a stimulus voltage of 20 V and sustained a 1:1 stimulus to impulse ratio. Horizontal grey bar shows a slight reduction in amplitude, most noticeable from the first 6 impulses the train. Vertical shaded area indicates the first impulse in each train. Dotted line marks 0 mV. * demarcates the first stimulus artefact in each train. Scale bar = 5.5s and 20 mV.

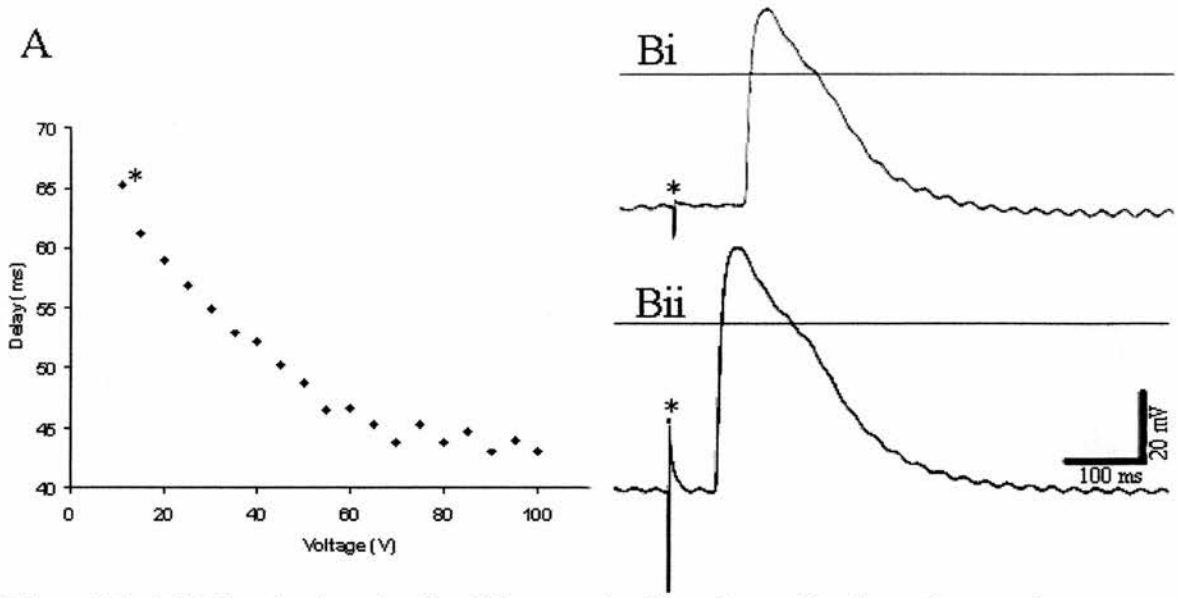

Figure 3.1. 4 (A) Graph of conduction delay vs. stimulus voltage, showing a decrease in conduction delay with increasing stimulus voltage and constant stimulus frequency (0.05 Hz). * indicates point at which V_T was reached. (Bi-Bii) First and last impulses from A, respectively. * indicates stimulus artefact. Horizontal line indicates 0 mV. Scale bars show 20 mV and 100 ms. Note the decreased resting membrane potential, larger stimulus artefact, longer duration and decreased delay in Bii.

masked smaller changes in conduction delay. Sudden changes in V_T greater than 5 V called for an examination of the preparation under the microscope, as this usually indicated that suction on the tail with the stimulating electrode had changed.

Time-dependent effects of skin impulse delay and duration

At the beginning of an experiment, the delay was found to vary considerably. Initially, some animals exhibited a decrease in delay, which would reach a steady state, then proceed to increase for the remainder of the experiment. In preparations recorded for more than 30 minutes, it was apparent that an upward trend occurred in relation to both delay and duration, often beginning about 20 minutes after the start of the experiment. In all control experiments (n=7), the trend was variable in its rate of increase, but was often linear (Figure 3.1.5). In experiments where a wash to fresh saline was conducted after 1 hour, no change in the apparent trend was observed. In preparations that lasted for 3 hours, there was no evidence that the changes in delay or duration had reached a maximum value or were likely to reverse in slope. Several possible explanations could account for this trend including changes in temperature or pH of the bathing solution. To reduce temperature output caused by fiber optic illuminator, the light was turned down to its lowest aperture during the experiment. Temperature was recorded, but did not rise more than 2°C over the course of 3 hours. pH was also checked and was found to be within the range of the desired value of 7.4. The entire flow system of the rig was washed thoroughly after each experiment with dH_2O, and tubing was changed regularly to avoid bacterial and fungal infection/growth. Despite these

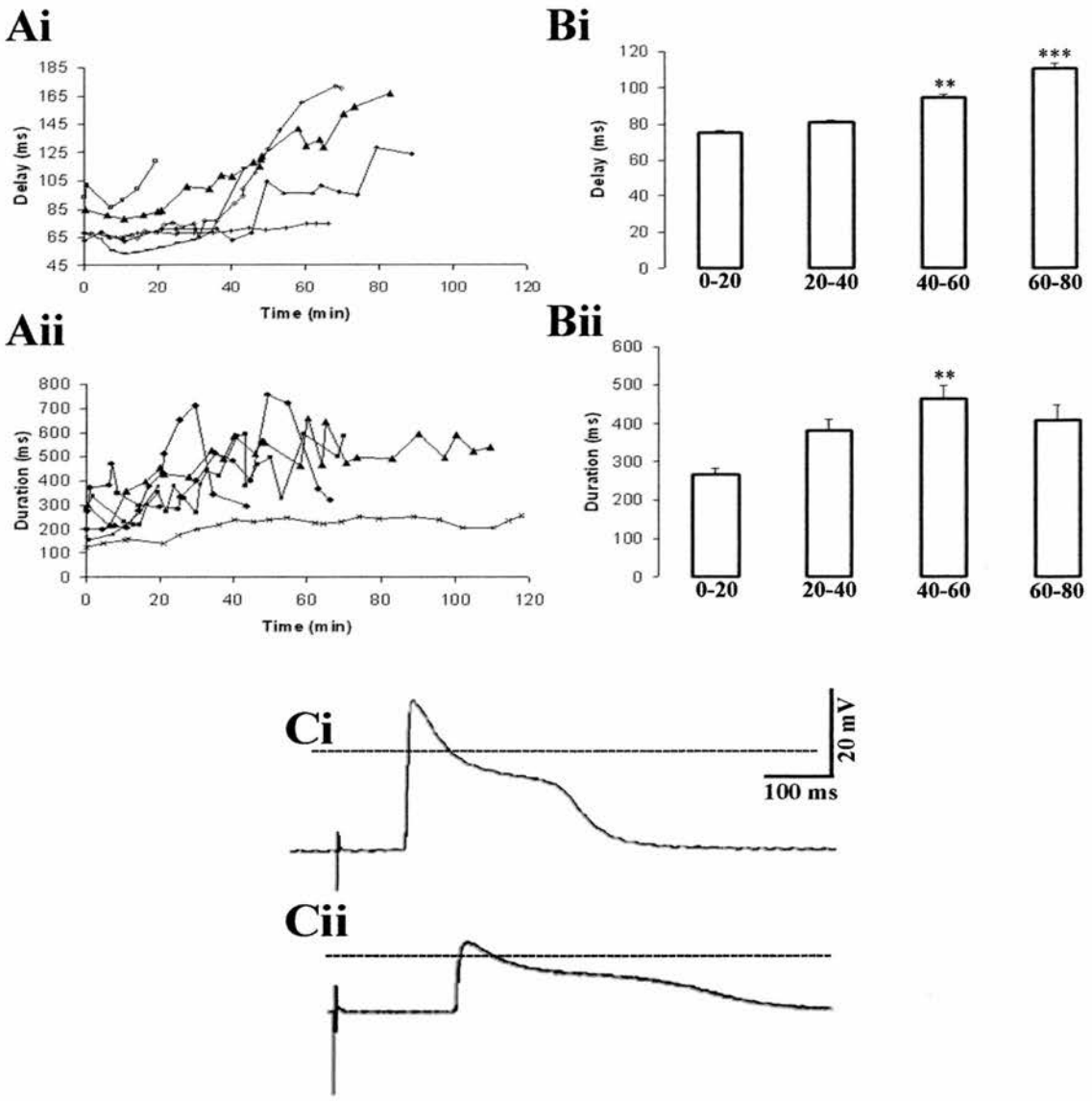

Figure 3.1. 5 (A) Time-dependent effects on conduction delay (i) and impulse duration (ii) in stage 37/38 *Xenopus* embryo. Graphs show progression of 6 animals with upward trends in both delay (i) and duration (ii). (B) Pooled data for delay (i, n=7) and duration (ii, n=4) taken at 20 minute intervals from the start of an experiment. Delay (i) in both the 40-60 (**, $p<0.05$) and 60-80 (***, $p<0.01$) minute periods are significant and highly significant from 0-20 minute, respectively. The 60-80 minute period is also significant and highly significant from the 20-40 (***, $p<0.01$) minute period and 40-60 (**, $p<0.05$), respectively. Duration (ii) during the 40-60 minute period is significantly different from control (**, $p<0.05$). (C) Intracellular recordings from Ai-ii showing an initial impulse (i) in one cell and the final impulse in a different cell (ii) from the start of a preparation. Dotted lines indicate 0 mV. *indicates stimulus artefact. Scale bar = 160 ms and 20 mV.

precautionary measures, general upward trends were still observed, indicating time-dependent changes in an unknown property of the preparation. The possibilities of wound healing, natural aging or the accumulation of an intrinsic modulation at this stage are discussed later (see Discussion).

In one experiment (Figure 3.1.6), an upward trend in delay commenced with a slope of 0.53 and a range of 67-89ms for 40 minutes when the stimulating electrode was adjusted due to excessive suction. After being repositioned further rostrally upon the tail (approximately 50 μm), a new upward trend emerged with a slope of 0.16, and a range of 77-87 ms. The actual value of the delay decreased initially from 87 ms to 81 ms, but this was attributed to the point of stimulation being closer to the point of recording on the head (see Figure 3.1.1 A). This observation suggested that gradual increase in conduction delay could correspond to excessive suction on the tail. As the skin is quite elastic at this stage, too much suction could patially draw the skin up the pipette and effectively increase the distance from stimulating to recording electrode. However, in all subsequent experiments from the present (n=105), closer attention was given to the amount of suction applied to the stimulating electrode, and any increases in delay were not associated with excessive suction from the stimulating electrode. Still, it is unclear if damage to the epidermis directly under the mouth of the stimulating electrode might account for upward trends in conduction delay. Furthermore, after the electrode was repositioned, the initial delay was greater than values at the onset of the experiment. This suggests that in addition to any effect caused by suction (i.e. skin damage), a change in the animal had taken place in the previous 40 minutes.

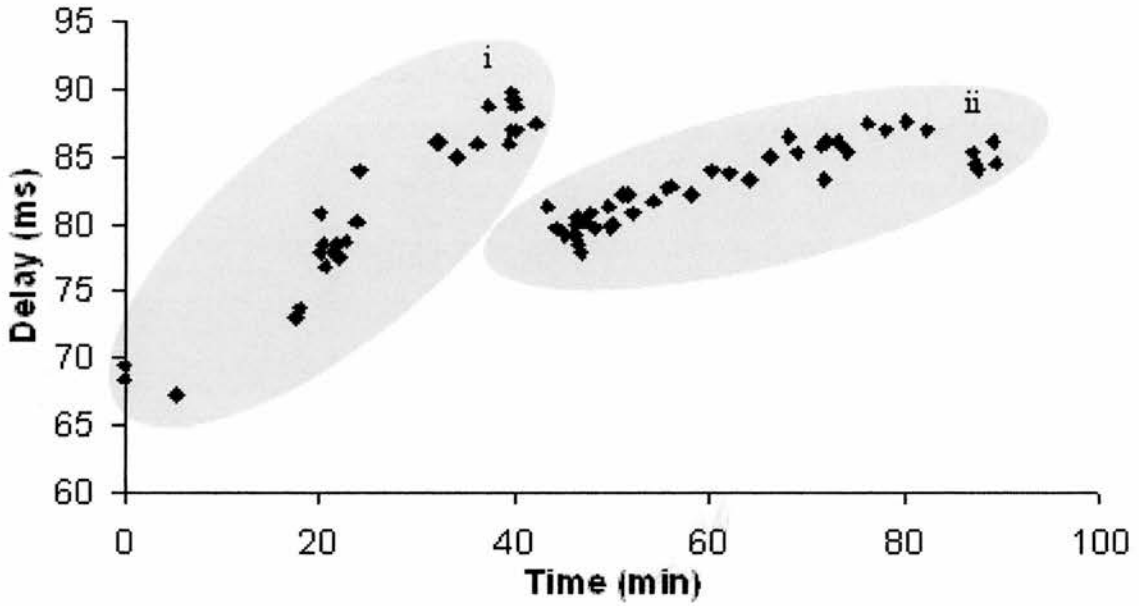

Figure 3.1. 6 Experiment displaying two different rates of delay increases in the same stage 37/38 *Xenopus* embryo. (i) shows initial trend of delay increase and (ii) shows a trend in delay with a decreased slope after the stimulating electrode has been positioned further rostrally along the tail, accounting for the sharp decrease in delay observed in (ii).

Effect of dissection on skin impulse delay and duration

To determine whether the increasing trends in delay and duration were a result of the large lesion created by removing the skin over the mytomes on one side (see Figure 3.1 A), animals were left intact, while skin impulses were generated and recorded intracellularly. In all preparations (n=6), both delay and duration were found to increase in a similar manner to lesioned animals (see Figure 3.1.5). In one experiment (Figure 3.1.7), delay decreases initially from 63 ms to 56 ms before making a stepwise increase back to 63 ms. Next, a slowly increasing trend is observed with a few fluctuations as delay approaches 68 ms before proceeding in a downward trend to 62 ms. From this point, delay commences a sharp, increasing trend, whereby the delay ranges from 66 to 83 ms in 20 min. Prior to this, delay ranged 56 to 68 ms in a 60 minute period. Duration underwent a more sustained increase with a few abrupt fluctuations, ultimately ranging from 120 to 330 ms over a 90 minutes period. This increasing trend suggests that the changes in lesioned animals are not due to the lesion itself, but possibly a result of endogenous changes to the properties of the skin. That is, changes in delay and duration are possibly indicative of an intrinsic property of the tadpole in this specific preparation. Additionally, wounds caused by the pinning technique, causing large lesions to various tissue layers throughout the embryo could be responsible for these observed changes (see Materials and Methods, Chapter 2). However, changes in delay and duration were not measured without pinning the animal through the notochord.

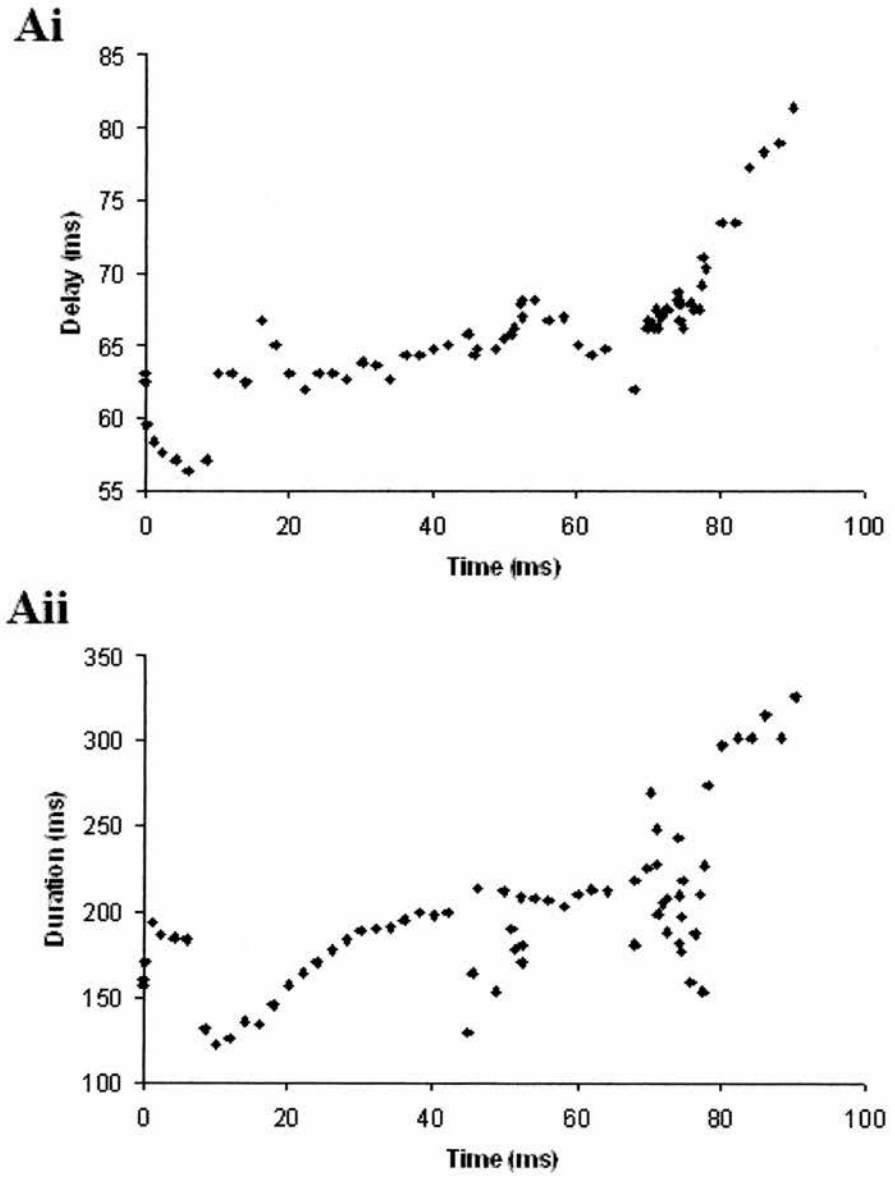

Figure 3.1. 7 (A) Graphs displaying delay (i) and duration (ii) vs. time in an non-lesioned stage 37/38 *Xenopus* embryo. Delay (i) and duration (ii) follow an increasing trend despite the skin being intact.

Evidence for different properties between deep and superficial layers of skin

While measuring the skin impulse intracellularly, three important differences were often seen between successive penetrations of different skin cells: (1) conduction delay often appeared to make step-wise changes in value, c. 15-20 ms, (2) impulses displayed various different resting potentials (-40 to -90 mV) and (3) had different waveforms. At first, this was attributed to large variability between different skin cells. Then, cells were then grouped according to several factors: (1) resting potential, (2) different waveforms, including slope of initial rise, and duration, and (3) delay. After grouping cells by these parameters, two parallel trends were observed in delay and duration vs. time. Cells either had (i) a low resting potential (-40 to -60 mV), slower rise (Figure 3.1.9 C, right impulse), shorter duration and longer delay, or (ii) a higher resting potential (-60 – 90 mV), faster rise (Figure 3.1.9 C, left impulse), longer duration and shorter delay. Cells in group (i) usually displayed a high initial delay, which decreased to a stable value before commencing an increasing trend. Often, the shape of the impulse began as small and rounded, eventually becoming more defined to resemble that of a cardiac action potential. Cells in group (ii) usually began displaying increasing trends in delay and duration from the start of an experiment. As delay and duration varied during experiments, so did their range. However, delay usually differed between 10 and 15 ms, and duration could differ by 100 ms, with the difference increasing throughout the experiment as the type (ii) impulse duration exhibited a greater degree of change.

In order to determine if the differences between groups (i) and (ii) could be attributed the two different cell layers in the skin (as described by Roberts (1971), see Introduction, Chapter 1) the sharp electrode was lowered down to the skin, and a cell was

penetrated as usual by overcompensation to drive the electrode into the cell. Once in a cell, the animal was stimulated once to produce a skin impulse. The electrode was then lowered several microns (μm) until the membrane potential began to decrease and then overcompensated to pierce into the second layer of skin cells. This was usually followed by a decrease in the resting membrane potential (c. -30 mV). The animal was then stimulated again to produce an impulse, this time larger than the preceding impulse before the second overcompensation (Figure 3.8). Impulses in group (i) typically appeared as the initial impulse recorded, whereas cells in group (ii) appeared as the second, deeper impulse.

To further investigate the existence of distinctly different impulses between skin layers, simultaneous, paired intracellular recordings were performed. In these preparations, one electrode was used to penetrate a skin cell in the superficial layer of skin (first layer entered upon lowering the electrode and overcompensating), while the other was used to penetrate a presumed deep skin cell with the method described above. When stable cells were maintained by both electrodes, the animal was stimulated to generate an impulse. In the presumed superficial layer, an impulse was of smaller magnitude, shorter duration, and longer delay compared to an impulse in the presumed deep layer (n=18; Figure 3.1.9). Again, the cells described above in group (i) are characteristic of impulses found after the first penetration (presumed superficial) and cells from group (ii) are characteristic of cells found after a second penetration (presumed deep layer) of skin cells (Figure 3.8). Because these two impulses can be recorded simultaneously, it shows that two different types of impulses may propagate concurrently through the skin, most probably through the inner and outer layers, respectively.

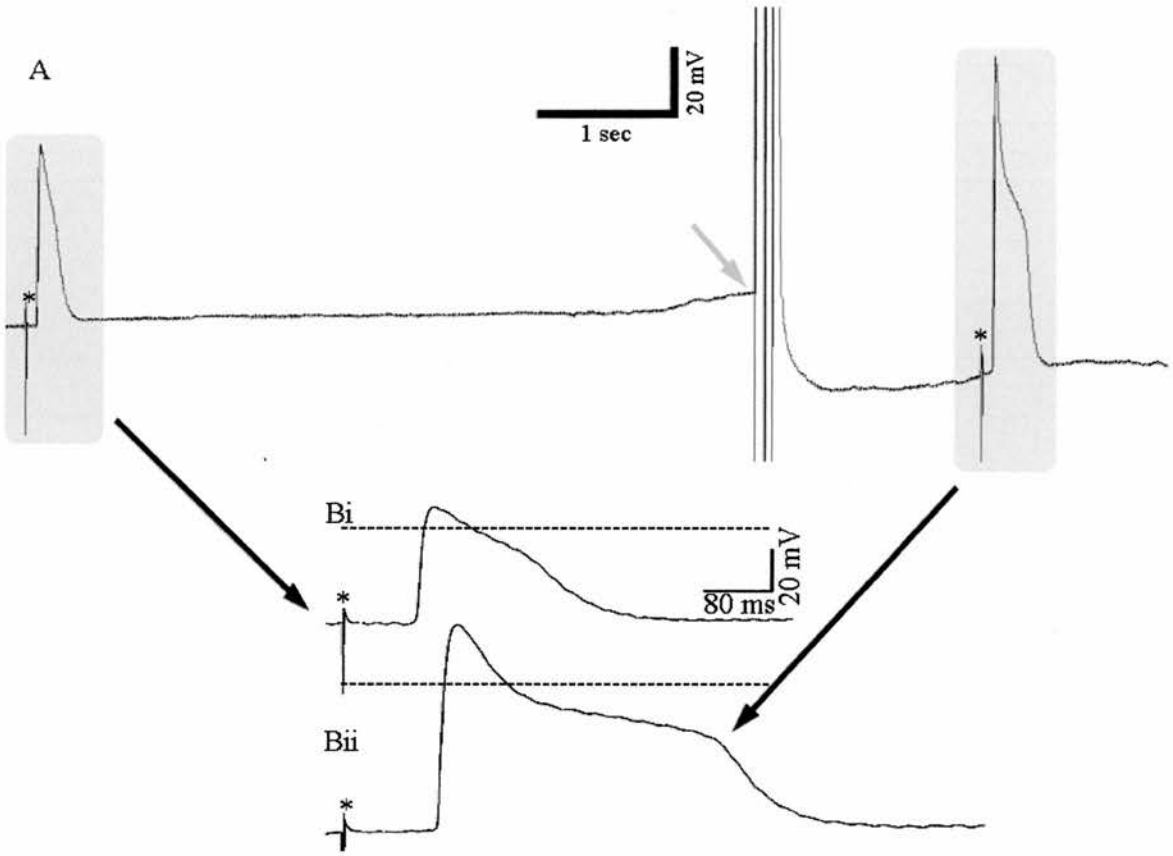

Figure 3.1. 8 (A-B) Intracellular recording of a skin cell from a stage 37/38 *Xenopus* embryo. (A) Grey arrow indicates when the overcompensation button was depressed while simultaneously lowering the micromanipulator. Grey area on the left indicates an impulse from a presumed superficial skin cell, while grey area on the right indicates an impulse from a presumed skin cell in the deep layer of skin. Note the lower resting membrane potential in the cell on the right. Scale bar shows 1 sec and 20 mV. (Bi-ii) Enlarged view of A, black arrows indicate respective impulses. Note the longer delay, larger amplitude and longer duration in Bii. Dotted line indicates 0 mV. * indicates stimulus artefact. Scale bars = 80 ms and 20 mV.

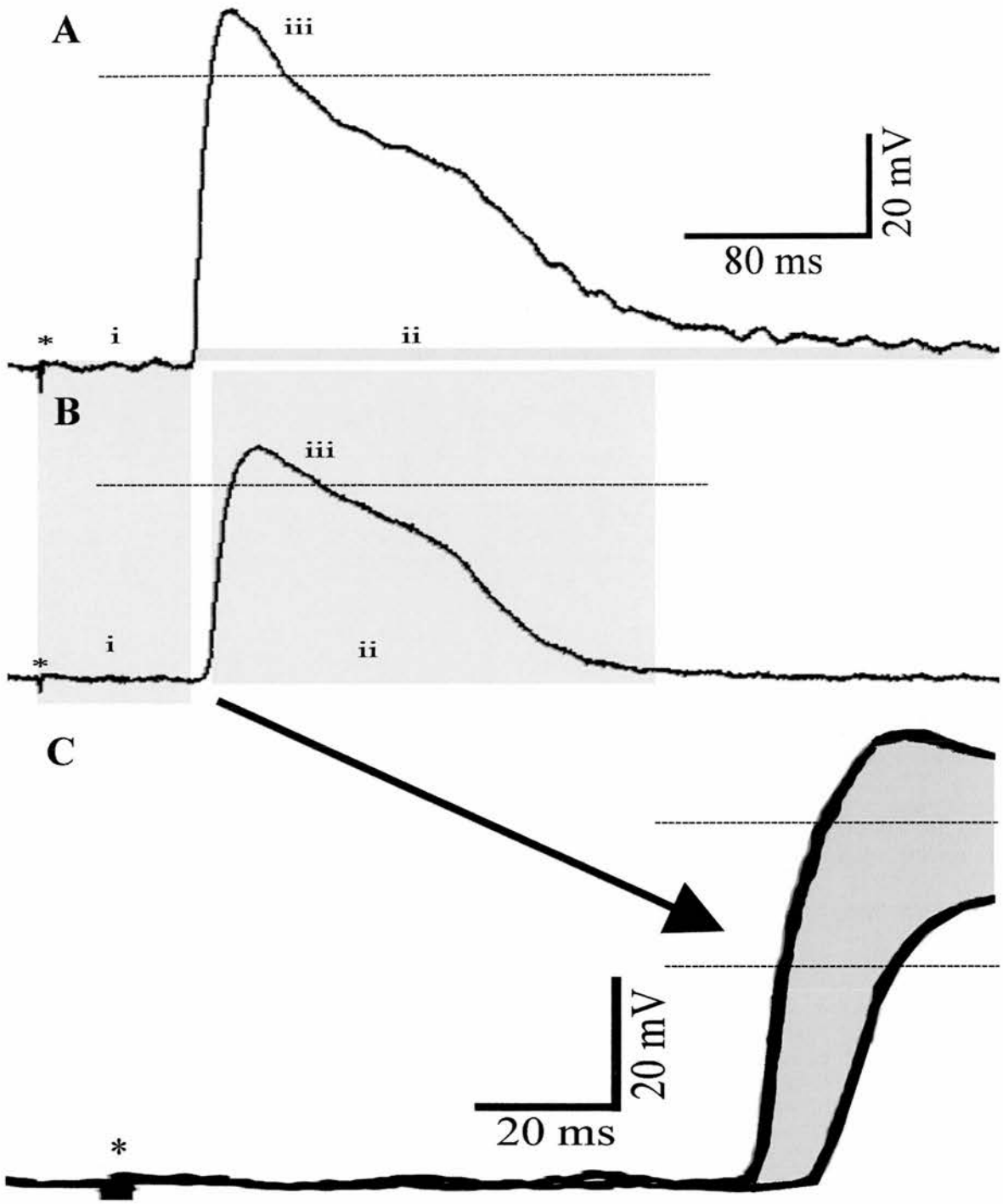

Figure 3.1. 9 (A-B) Simultaneous intracellular recording of two skin cells. Presumed deep cell (A) and presumed superficial cell (B). Note several differences between impulses: (i) delay, (ii) duration, (iii) absolute amplitude and pronounced peak. Superficial impulse returns to resting membrane potential long before the deep impulse (C) Overlay of A and B and enlarged and expanded to show difference in slope of rising phase and delay (grey area). Dotted lines indicate 0 mV. * indicates stimulus artefact. Scale bar = 80 ms (A-B), 20 ms (C) and 20 mV (A-C).

Electrophysiological evidence for coupling between skin cells in Xenopus

To investigate if current flows directly between skin cells via electrical synapses (GJCs), two skin cells were penetrated simultaneously using a similar preparation to that described above. Presumed deep cells were penetrated by both electrodes. Impulses from those cells after injecting the current suggest that both cells were in the same layer of skin cells due to the similarity in waveform (i.e. fast rise, long duration) and equivalence in delay. However, the cells had different resting membrane potentials and subsequently different absolute amplitudes (Figure 3.1.10). Once stable recordings were made from cells within approximately 50 μm of another, a current was injected into once cell and the resulting voltage deflection was observed in the other cell, and vice versa. The same was repeated with roles of injecting and recording being reversed (Figure 3.1.10). Increasing steps of current produce increasing steps in voltage deflection. In one experiment, cells were sufficiently far apart that a large hyperpolarising current (10 nA, 200 ms) was necessary to produce a 20 mV negative deflection in the recording cell for a corresponding length in time. The response of the recording cell was 0 mV after the electrode was removed and the same current injection was given, confirming cell to cell electrotonic coupling. Cells also responded to depolarising current injections with a corresponding positive deflection in the recording cell (not shown). These findings confirm those of Roberts (1971), further suggesting that the skin cells are electrically coupled as demonstrated by the relative ease with which current can pass between nearby cells.

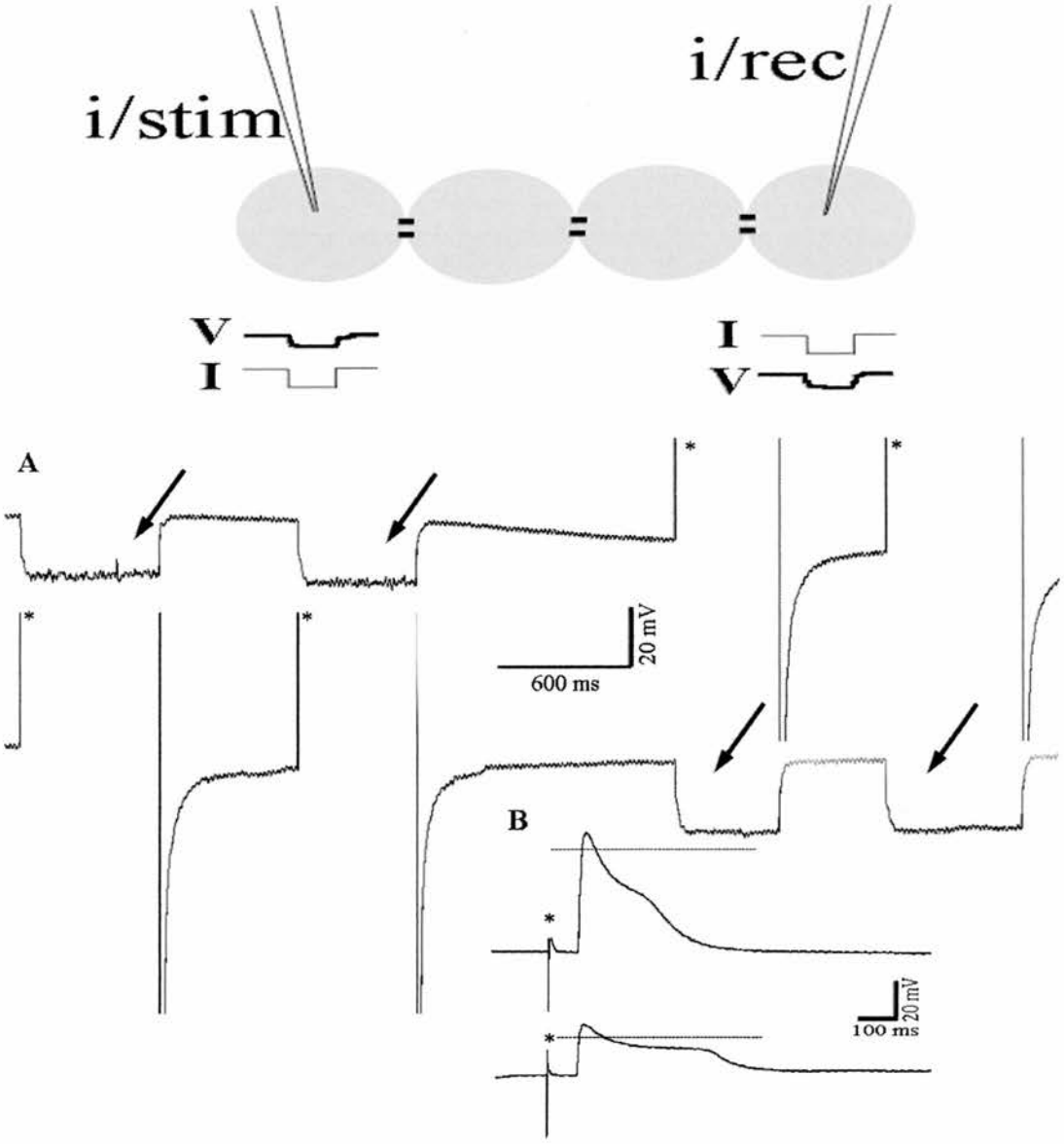

Figure 3.1. 10 Schematic drawing of paired recording preparation. Grey circles represent skin cells which are presumed to be coupled by gap junctions (black bars in parallel). Intracellular electrodes i/stim (stimulating) and i/rec (recording) are shown on outer cells, and are capable of performing both roles. (A) Paired intracellular recordings of two skin cells approximately 50 μm apart (top and bottom trace) in a stage 37/38 *Xenopus* embryo. * indicates hyperpolarising current injection of 10 nA in one cell and arrow indicates the simultaneous hyperpolarising voltage response in second cell in parallel. Note, due to a large size of current pulses used, the bridge is out of balance so voltage of stimulated cell is off trace. Scale bars show 600 ms and 20 mV. (B) Intracellular recording of skin impulse from the same two cells after current injection. Dotted line indicates 0 mV. * indicates stimulus artefact. Scale bars = 100 ms and 20 mV.

Comparative study on skin impulse properties in other embryos of amphibian species

The skin impulse in *Xenopus* was compared with three other, locally available amphibian species at equivalent stages in development. Impulses from at least 3 skin cells were examined in *Bufo bufo* (n=9), *Rana temporaria* (n=12) and *Triturus vulgaris* (n=3). In *Triturus*, skin cells exhibited a negative resting potential around -60 mV, but skin impulse were not found even after maximum stimulation capacity (100 V; n refers to number of animals; Figure 3.1.12). In all preparations, electrodes were placed approximately 6 mm apart. In *Bufo*, impulses appeared similar to presumed deep cells in *Xenopus* with broad plateau phases and a long duration, c. 200 ms. Conduction delay was also found to be in the same range of 60-80 ms (n=3). Skin cells were more difficult to penetrate and maintain than in *Xenopus*. In *Rana*, impulses were often similar to presumed superficial cells in *Xenopus*, but exhibiting a much longer conduction delay, ranging from 90-142 ms (n=6). Skin cells were also difficult to penetrate possibly due to thickness, and recordings were more difficult to maintain than in *Xenopus*. However, when a stable recording was achieved, skin impulses in *Rana* responded differently when stimulated repetitively at high frequencies (1 Hz -.67 Hz). Neither conduction delay nor impulse duration was observed to change in trains of 30 stimuli (n=3) with varying frequencies at the stimulus threshold (Figure 3.1.11). This suggest intrinsically different mechanisms underlying refractoriness in *Rana* compared to *Xenopus*.

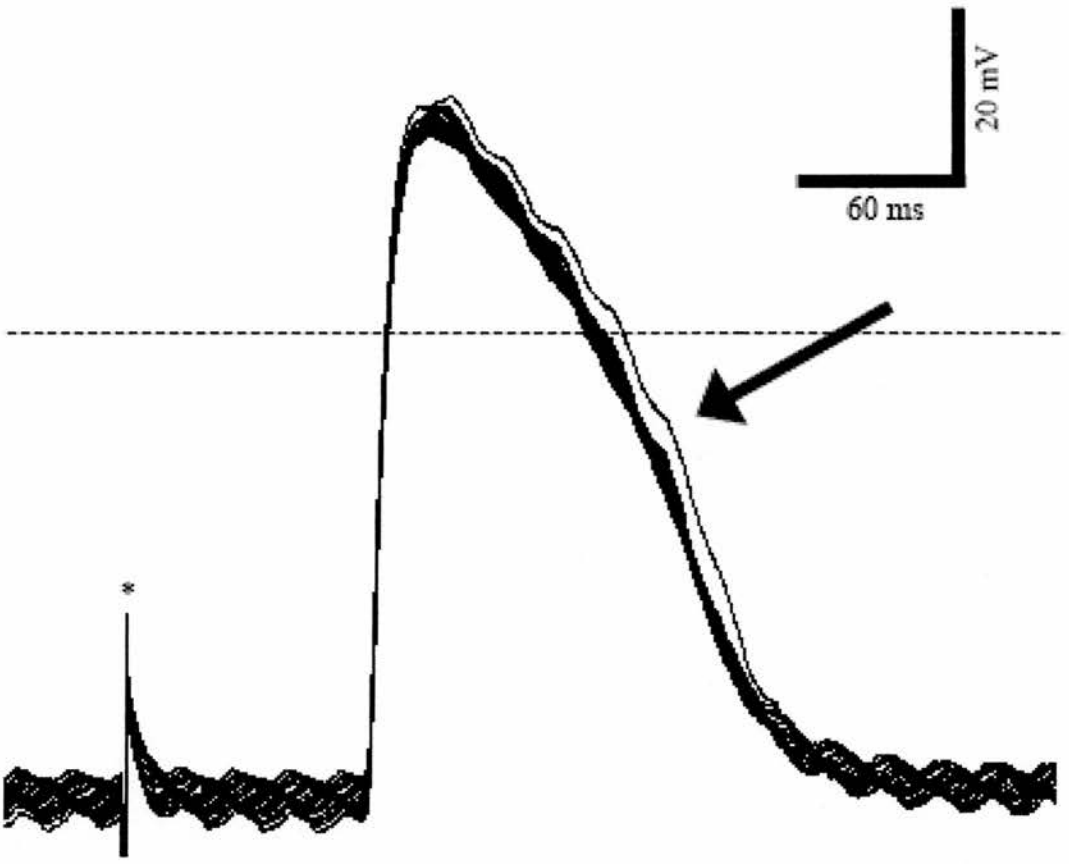

Figure 3.1. 11 Repetitive stimulation in a stage 21 *Rana* embryo. Successive overlays from a train of 30 impulses conducted at .67 Hz, $V_T = 32$ V. Skin impulse delay does not change in successive impulses. Skin impulse duration decreases by approximately 5 ms after the initial impulse (arrow), and remains relatively constant thereafter. *indicates stimulus artefact. Grey line indicates 0 mV. Scale bars = 60 ms and 20 mV.

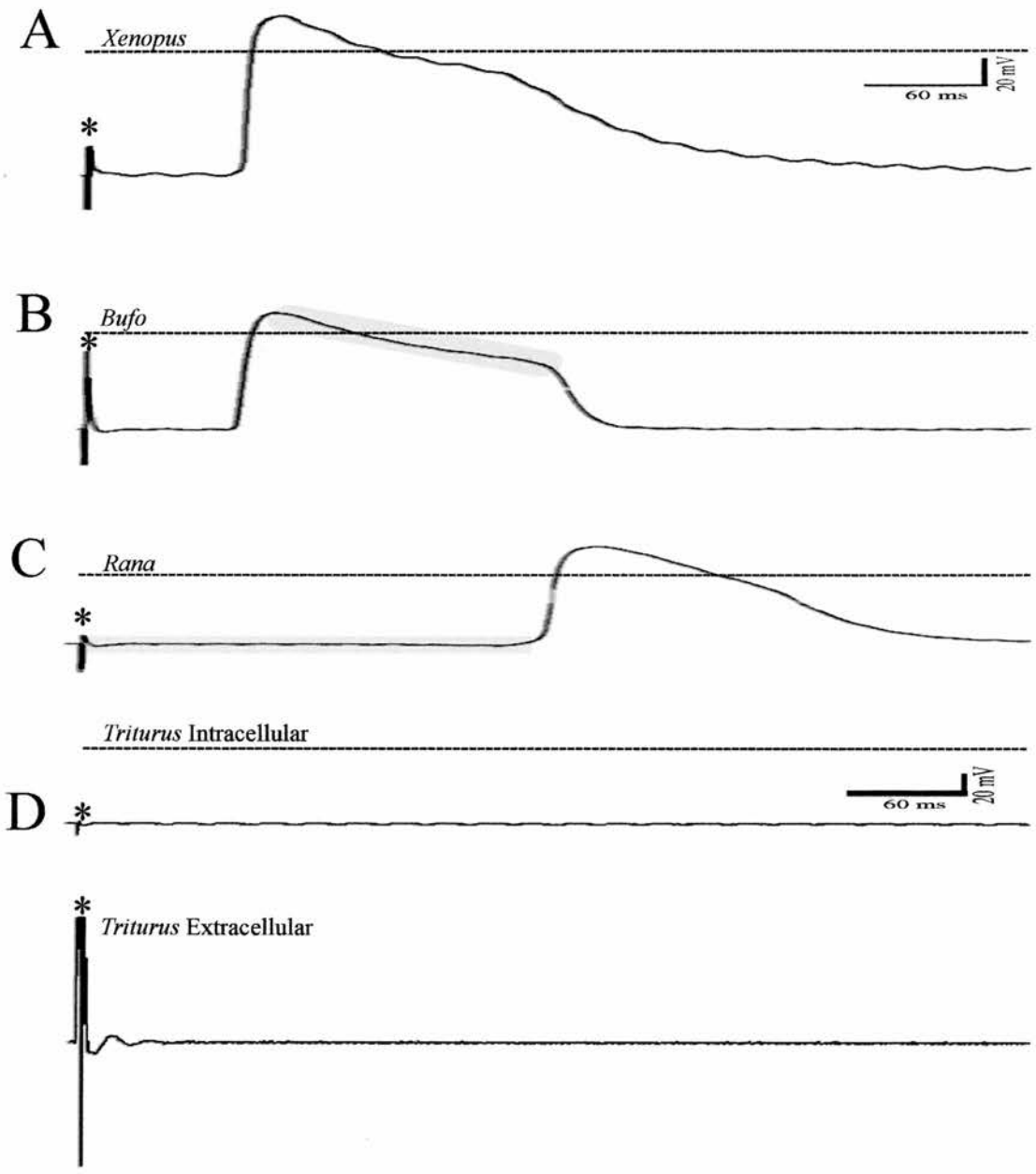

Figure 3.1. 12 Intracellular recordings of skin impulses from three different tadpole species of similar age: *Xenopus*, stage 37/38 (A), *Bufo* stage 21 (B), and *Rana* stage 21 (C). Note the varying durations and amplitude between species. A long shoulder in *Bufo* (grey area, ii) and the characteristically longer conduction delay in *Rana* (grey box, iii) are shown. (iv) Shows intracellular (top trace) and extracellular (bottom trace) recordings from a population of skin cells and a single cell, respectively, from a hatchling *Triturus* embryo. No skin impulse was produced from the stimulus. * indicates stimulus artefact. Dotted lines indicate 0 mV. Scale bars = 60 ms and 20 mV.

This investigation of the skin impulse in *Xenopus* at stage 37/38, has revealed several basic properties in accordance with previous published work (Roberts, 1971): (1) impulses were generated via a noxious electrical stimulus to the tail, (2) recorded both extracellulary and intracellularly from any cell on the epidermis, (3) could elicit fictive swimming behaviour, and (4) pass between two nearby cells via electrotonic junctions. Additionally, refractoriness was demonstrated by high frequency repetitive stimulation at V_T which produced marked changes in delay, duration, and impulse amplitude. Stimulus voltage was also shown to dramatically affect conduction delay. Most interestingly, evidence suggests two simultaneously propagated impulses in both layers of the skin. Cross-species comparison show similar impulses with only slight differences in waveform. Lastly, time-dependent effects for delay and duration were also shown, but it is still unclear as to the nature of this property, or if can be isolated and prevented. The remainder of the thesis seeks to address the possible modulation of this intrinsic rise in delay and duration of the skin impulse through the use of various exogenously applied neuroactive substances, which may be present in the skin.

Section 2 – Pharmacological modulation of the skin impulse in Xenopus

Several physiologically active substances have been reported in the epidermis of Xenopus, even at stage 37/38, including 5-HT (Blades, 1993), Substance P (SP; Clarke et al., 1984; Roberts, 1998), and NO (McLean and Sillar, 2001). Thus, an investigation into whether they might modulate the skin impulse began by exposing preparations to these substances. The pharmacological approach used in experiments can be divided into three main categories: (1) serotonergic, (2) peptidergic, and (3) nitrergic. Within each category, appropriate receptor agonists and antagonists (or donors and scavengers in the case of NO) as well as modulators of downstream targets were investigated. Only intracellular data is included and the parameters measured for all experiments include both conduction delay and impulse duration. In some experiments with the NO donor, SNAP, and the NO scavenger, C-PTIO, measurements were made in both presumed superficial and deep cell layers. The remainder of experiments are only indicative of changes to delay and duration in the presumed deep cell layer. Data from each individual experiment reflects measurements pooled from multiple skin cells, except when specified otherwise. For statistical analysis of the effect on delay, the change in the slope of trend lines fitted to the data were used instead of average values during each period. Because measurements were recorded at irregular intervals throughout an experiment, taking average values for a given period (i.e. control, drug, wash) was not indicative of the changes observed, nor did it act as an accurate indicator of the reversibility of any potential effects. However, since changes in duration occurred and washed off more quickly, statistical analysis was performed on average values during a given period.

Gap junction blocker

18-β-glycyrrhetinic acid

Initial experiments were conducted to determine how an uncoupling effect on GJ would manifest with regard to conduction delay and impulse duration. 18-β-glycyrrhetinic acid (18-β-GA; 75-100 μM), a known gap junction blocker, had no significant effect on conduction delay, and although average duration did increase irreversibly, this increase was not significantly different from control experiments ($p<0.01$; $n= 6$). As 18-β-GA is reported to require 40 or more minutes to take effect (H. Zhang, personal communication), this may be too slow a time course to display an effect in light of the already increasing trends found in control experiments. Additionally, at concentrations above 100 μM (n=3), the skin was found to degrade and shed heavily into the bath. Skin cells became difficult to record at this point, and the effect did not wash off. Thus, due to the irreversibility of 18-β-GA effects on GJ channels, it proved not to be a useful modulator of GJCs within this skin cell preparation.

Serotonergic modulation

5-HT

The effect of serotonin (5-HT) on the skin impulse was tested by bath-application of 100 μM 5-HT (c.f. Blades, 1993). In the presence of 5-HT, both delay and duration were highly variable. In pooled data (100 μM 5-HT) for the average delay slope (n=3) and duration (n=2), no consistent changes were found. On the basis of these data, it is impossible to conclude if any effects were caused by 5-HT for either delay or duration (see Discussion, Chapter 4). However, I detected no changes in the threshold for activation of swimming following skin stimulation as has been reported previously (Sillar and Simmers, 1994). This suggests that the stock of 5-HT used in these experiments may

have lost its efficacy. Alternatively, 5-HT may have been unable to effectively access sites within the skin.

Cyclic nucleotide-induced modulation

As effects on delay and duration in the presence of 5-HT were either absent or highly variable, the effects of one of the potential downstream second messengers of 5-HT, 3'-5'-cyclic adenosine monophosphate (cAMP, reviewed in Katz, 1999), were then investigated. cAMP is produced by the intracellular enzyme adenylyl cyclase (AC). forskolin, a cell-permeable activator of adenylyl cyclase, was used to artificially elevate levels of cAMP *in vivo*. Pooled data (n=6) revealed that bath application of 100 μM forskolin reversibly increases the trend in delay, and the wash showing a highly significant decrease in slope from forskolin ($p<0.01$; Figure 4.2.1 Bi). Although the increase in forskolin is not significant, a wash-off is indicative of a potential drug effect as it differs from the trend seen in control experiments. Average duration is also found to significantly ($p<0.01$) and irreversibly increase, the wash being significantly higher than forskolin ($p<0.05$; Figure 3.2.1 Bii). In all experiments, delay data show an increasing trend in the presence of forskolin (n=6), which either reverses (n=3), decreases (n=2), or increases in value (n=1).

In summary, 5-HT, showed inconsistent results possibly due to an inefficient method of access into the skin or due to the combating effects of 5-HT receptor sub-types (see Discussion, Chapter 4). However, the reversible increase in the slope of the delay in the presence of forskolin suggests a possible cAMP-dependent uncoupling effect on GJCs. Additionally, the irreversible change in duration during forskolin may reflect a drug effect as the increase is highly significant, as opposed to only significant as in control. This may reflect the time course of intracellular amplification and the subsequent delay in washing off a largely amplified effect.

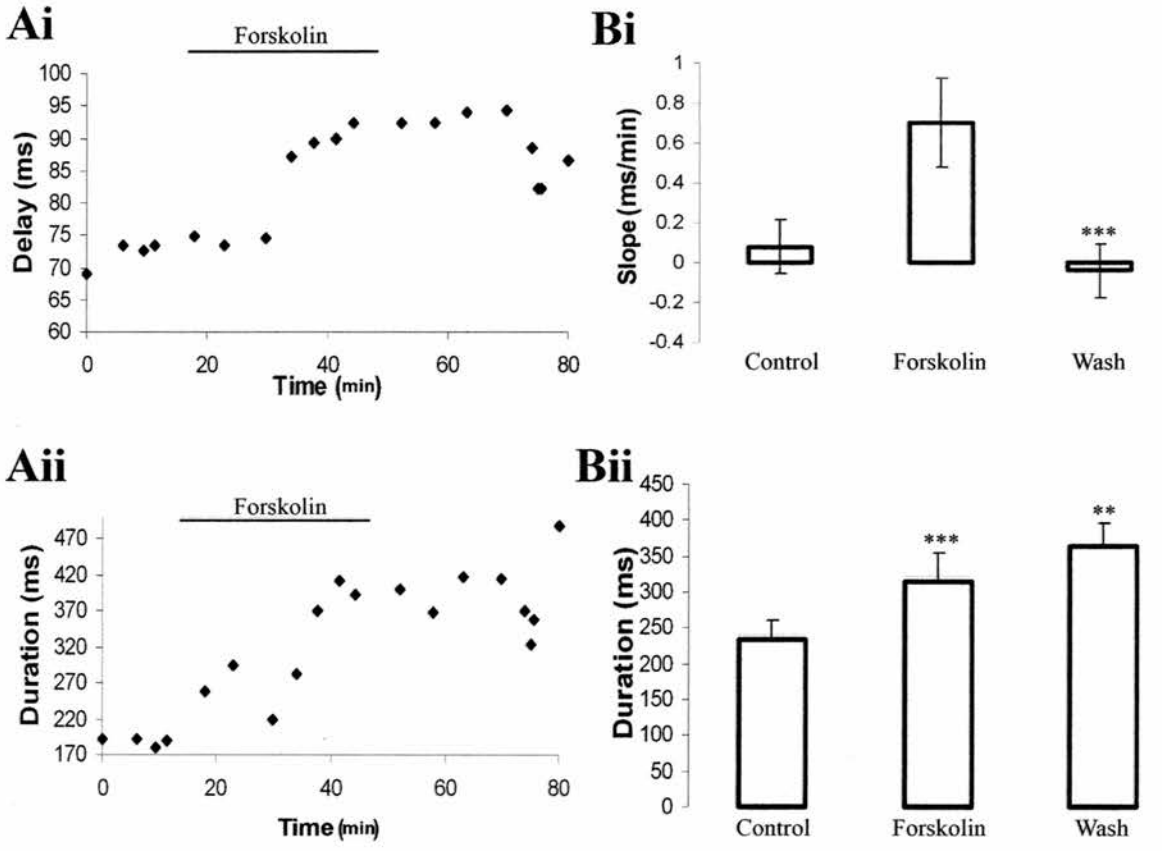

Figure 3.2. 1 Effect of 100 μM forskolin on conduction delay and impulse duration in a stage 37/38 *Xenopus* embryo. (Ai-ii) shows one experiment, where in the presence of forskolin (black bar), a reversible increase delay (i) and an irreversible increase in duration (ii) was observed. (Bi-ii) shows pooled data from 6 intracellular experiments showing a reversible increase in delay, with the wash being different from forskolin (i, ***$p<0.05$) and an irreversible increase duration (ii, ***$p<0.01$, ** $p<0.05$). Error bars reflect S.E.M.

Peptiderdic modulation

Substance P

When Substance P (SP; c.f. Lebofsky, 2002) was bath-applied to the preparation to artificially increase the concentration of this peptide *in vivo*, no significant changes ($p>0.05$) in delay or duration were observed (n=4). The slope of the trend in delay was either seen to increase (n=2), decrease (n=1), or reverse (n=1). In pooled data, these inconsistent changes in slope are reflected by a large S.E.M. (Figure 3.2.2 Bi). Based on these findings, it is impossible to determine if SP is exerting an effect on either delay or duration, as the trends are either too variable (delay) or consistently increased with no sign of a washing off (duration).

During SP experiments, fictive swimming was also recorded as SP has been reported to cause a decrease in cycle period (Lebofsky, 2002) and an increase in spontaneous skin impulse occurrence (K.T. Sillar, personal communication). However, any changes were inconsistent for both parameters. In addition, spontaneous swim episode frequency was monitored, showing evidence of an increase during SP-application, but was not significantly greater than control, suggesting naturally excitable animals. Thus, SP does not appear to have an effect on the skin impulse, but this may also be a result of drug access (see Discussion, Chapter 4).

NK_1-receptor antagonist

In order to investigate whether the increasing trend observed in both delay and duration during control experiments might be due to either the endogenous release of SP or from the exogenous addition of SP *in vivo*, an antagonist was applied. SP is the natural agonist at neurokinin-1 (NK_1) receptors, which can be inhibited by an NK_1 antagonist. Bath-application of NK_1 antagonist, L-732,138 (1 μM), was used to inhibit

both the action of endogenously released SP and any effects that exogenously added SP might be exerting on the skin impulse. In pooled data (n=3), the presence of L-732,138 had no significant change in the trend of delay, but it did have a highly significant and reversible decrease in the average duration ($p<0.01$).

The vehicle in which L-732,138 was supplied to the bath was 100 % ethanol. In order to reach the desired concentration of 1 μM L-732,138, the effective concentration of ethanol was subsequently brought to 1% (v/v). To determine if any vehicle-related effects had occurred in experiments using L-732,138, 1% (v/v) ethanol was bath-applied in one control experiment. No significant change was found in the average slope of the delay, whereas a highly significant ($p<0.01$) and reversible decrease in duration occurs (n=1). Thus, the decrease in duration following L-732,138 application can be attributed to a vehicle-related effect from the ethanol.

Bath-application of L-732,138 in the presence of Substance P showed identical effects to experiments performed with L-732,138 alone, whereby the slope of the delay did not change, and the average duration showed a highly significant and reversible decrease (n=5). Therefore, SP and its receptor antagonist, L-732,138, are both shown to have no apparent effects on the skin impulse delay or duration.

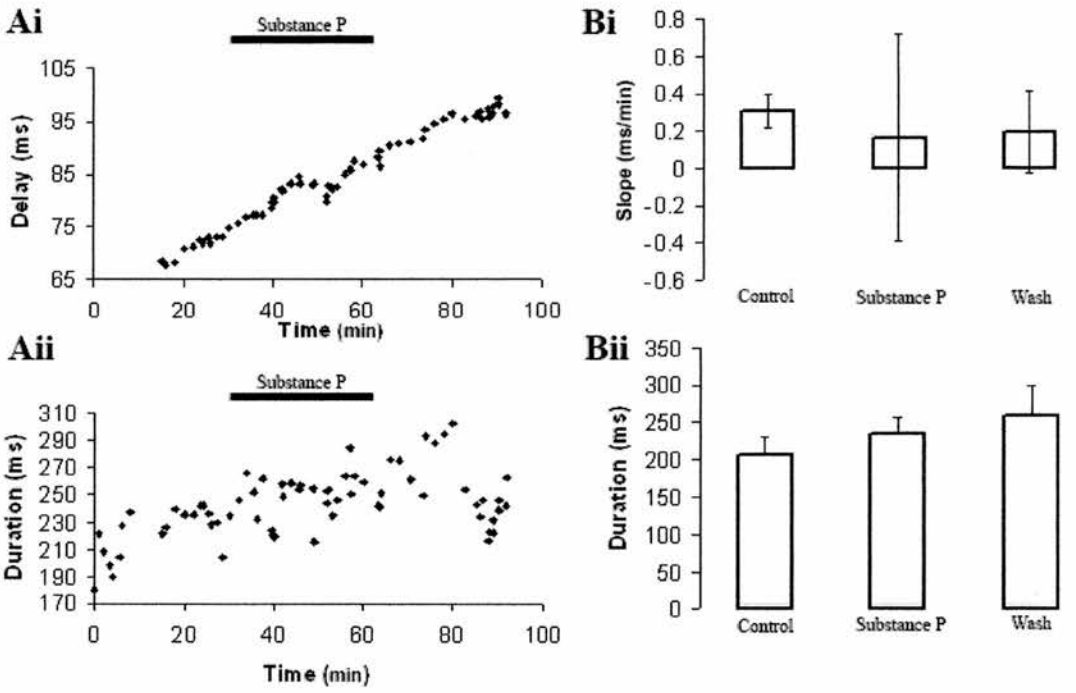

Figure 3.2. 2 Effect of 6 μM SP on skin impulse delay and duration in a stage 37/38 *Xenopus* embryo. (Ai-ii) Graphs displaying raw data points of delay (i) and duration (ii) vs. time from one preparation. In the presence of SP (black bar), no characteristic deviations from the initial trend are seen. (Bi-ii) Pooled data from 4 experiments showing the average slope (i) and duration (ii) for control, Substance P, and wash periods. Error bars reflect S.E.M.

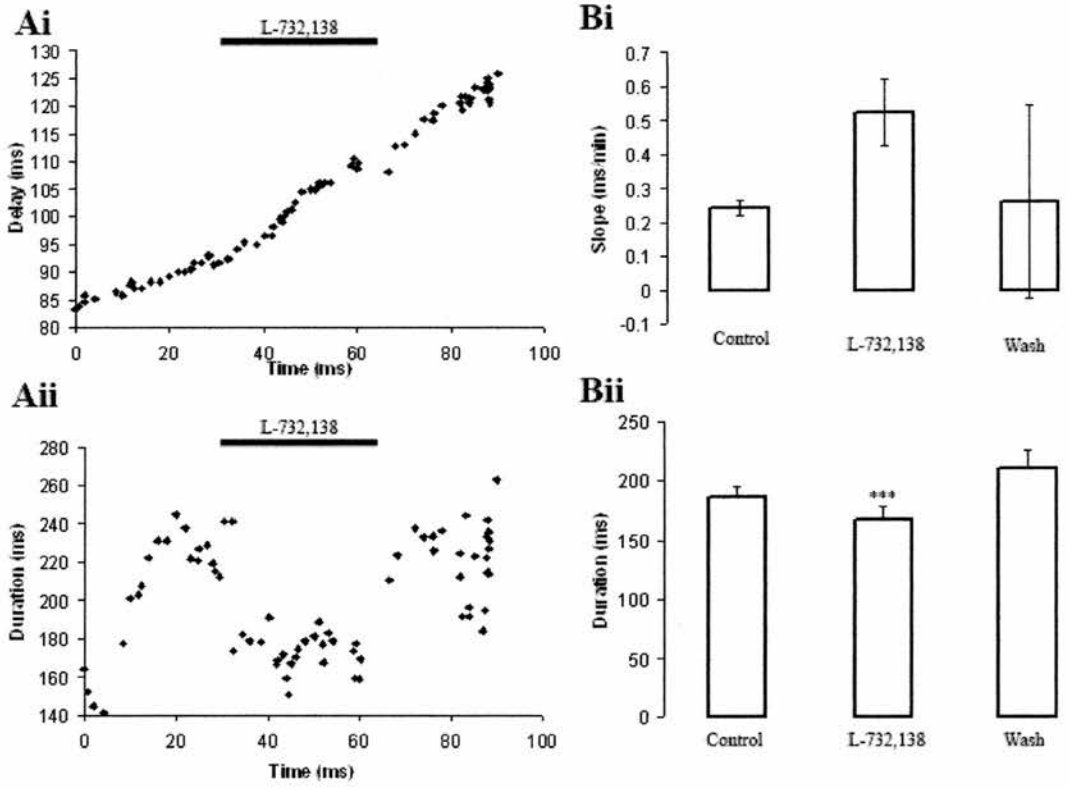

Figure 3.2. 3 Effect of 1 μM L-732,138 on skin impulse delay and duration in a stage 37/38 *Xenopus* embryo. (A) Graphs of raw data points showing delay (i) and duration (ii) vs. time for one preparation In the presence of L-732,138 (black bar), delay (i) maintains an increasing trend and duration (ii) reversibly decreases. (B) Pooled data from 3 intracellular experiments. L-732,138 shows no significant increase in the average slope (i) and a highly significant, reversible decrease in average duration (ii, ***, $p<0.01$). Error bars reflect S.E.M.

Nitrergic Modulation

NO donor

To investigate the potential modulatory effects of the free radical NO, bath-application of the NO donor, *S*-nitroso-*n*-acetylpenicillamine (SNAP; 500 μM, c.f. McLean and Siller (2002)) was used to exogenously raise levels of NO *in vivo*. The effect of SNAP was examined in both presumed superficial and deep cell layers.

Pooled data (Figure 3.2.4 B) for superficial cells showed that the slope of the trend in delay significantly and reversibly increases ($n=6$; $p<0.01$) in the presence of SNAP in addition to the average duration ($n=6$; $p<0.01$); wash periods in both are significantly different from SNAP ($p<0.01$). These data strongly suggest that SNAP has a reliable and consistent effect on delay and duration of superficial cells. Additionally, SNAP produced a markedly faster and more dramatic increase in the duration than in delay. Duration was found to increase within minutes of drug application, where as the delay trend accelerated upwards while in the presence of SNAP. Examples of presumed superficial impulses found in control, SNAP, and wash periods are illustrated in Figure 3.2.6 B.

In pooled data for presumed deep cells, the average slope of the delay and the average duration were also found to increase reversibly ($p<0.01$, $n=21$), reversing in slope ($p<0.01$) and returning to control values ($p<0.01$), respectively (Figure 3.2.5 B). Figure 3.2.5 A shows one experiment where both the delay and duration of presumed deep cells reversibly increases in the presence of SNAP. Also displayed are two characteristic patterns found in the presence of SNAP: (1) an initial decrease in the delay ($n=15$; arrowed in Figure 3.2.5 Ai), and (2) a rapid increase in the duration immediately after the application of SNAP. The former then assumes an increasing trend, whereas the latter reaches a peak. Examples of presumed deep impulses found in control, SNAP, and wash periods are illustrated in Figure 3.2.6 A.

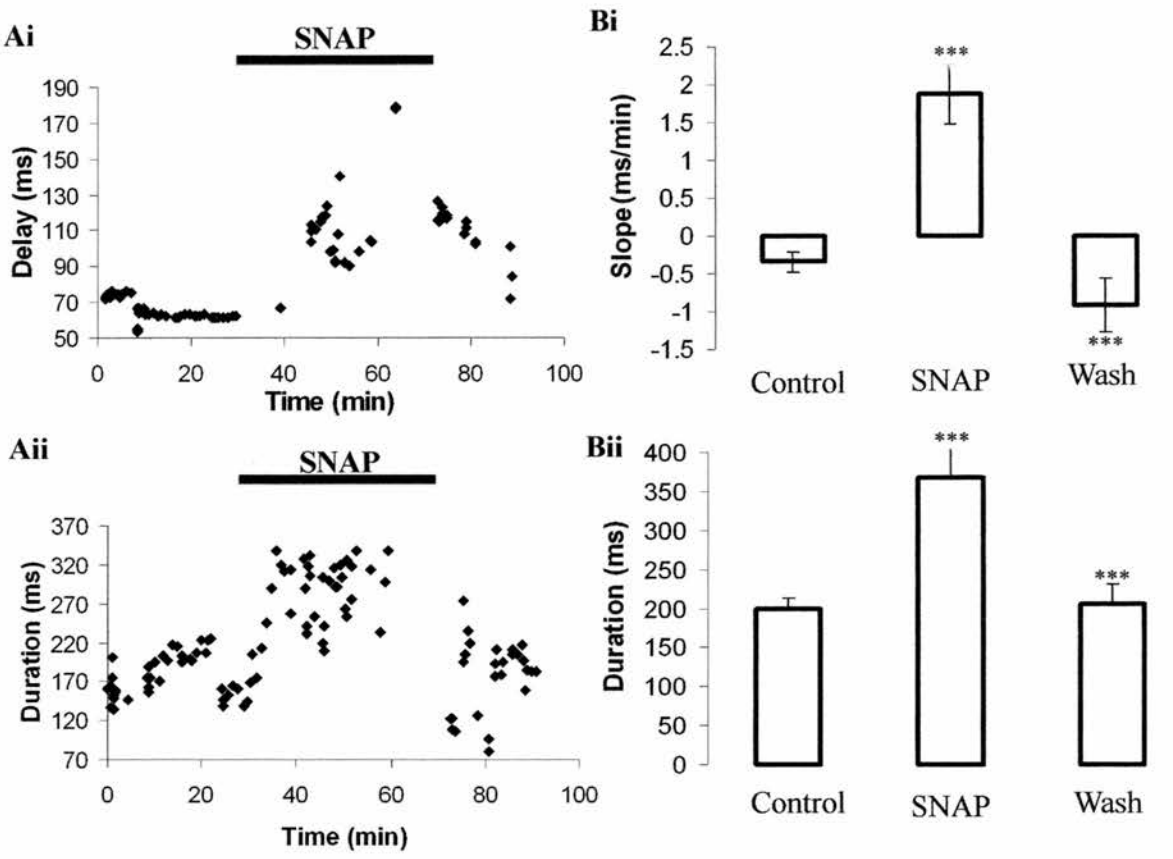

Figure 3.2. 4 Effect of 500 μM SNAP on conduction delay and skin impulse duration of superficial cells in a stage 37/38 *Xenopus* embryo. (Ai-ii) show the results of one intracellular experiment in terms of delay and duration vs. time, respectively. In the presence of SNAP (black bar), both delay (i) and duration (ii) reversibly increased. (Bi-ii) shows pooled data from 6 experiments for delay slope (i) and duration (ii), where SNAP is shown to reversibly increase the slope of delay changes (i, ***$p<0.01$) and reversibly increase duration (ii, ***$p<0.01$); the wash is highly significant from SNAP for both parameters (*** $p<0.01$). Error bars reflect S.E.M.

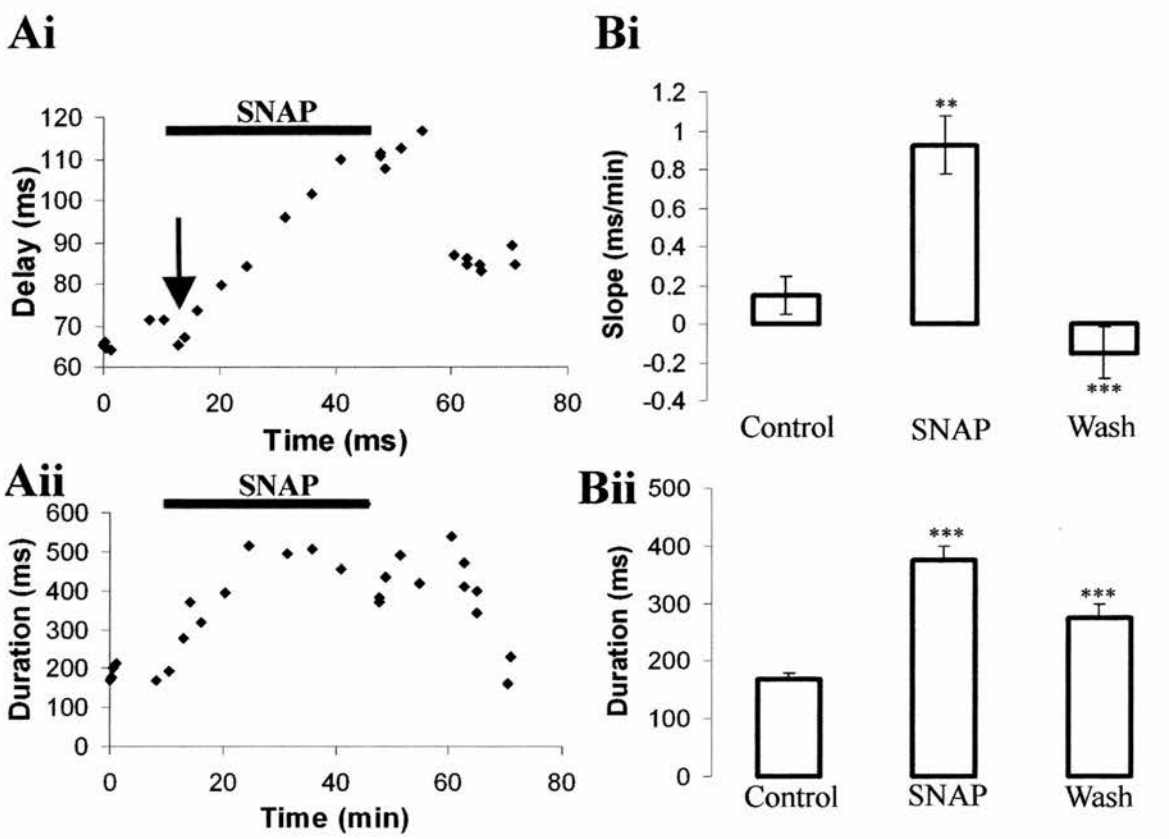

Figure 3.2. 5 Effect of 500 μM SNAP on conduction delay and skin impulse duration of deep cells in a stage 37/38 *Xenopus* embryo. In the presence of SNAP (black bar), both delay (i) and duration (ii) reversibly increased. (Ai) arrow indicates consistent pattern of an initial decrease before increasing in trend (Bi-ii) shows pooled data from 15 experiments for delay slope (i) and duration (ii), where the slope of delay and average duration are shown to increase reversibly (i, ii; ***$p<0.01$); the wash is highly significant from SNAP for both parameters (***$p<0.01$). Error bars reflect S.E.M.

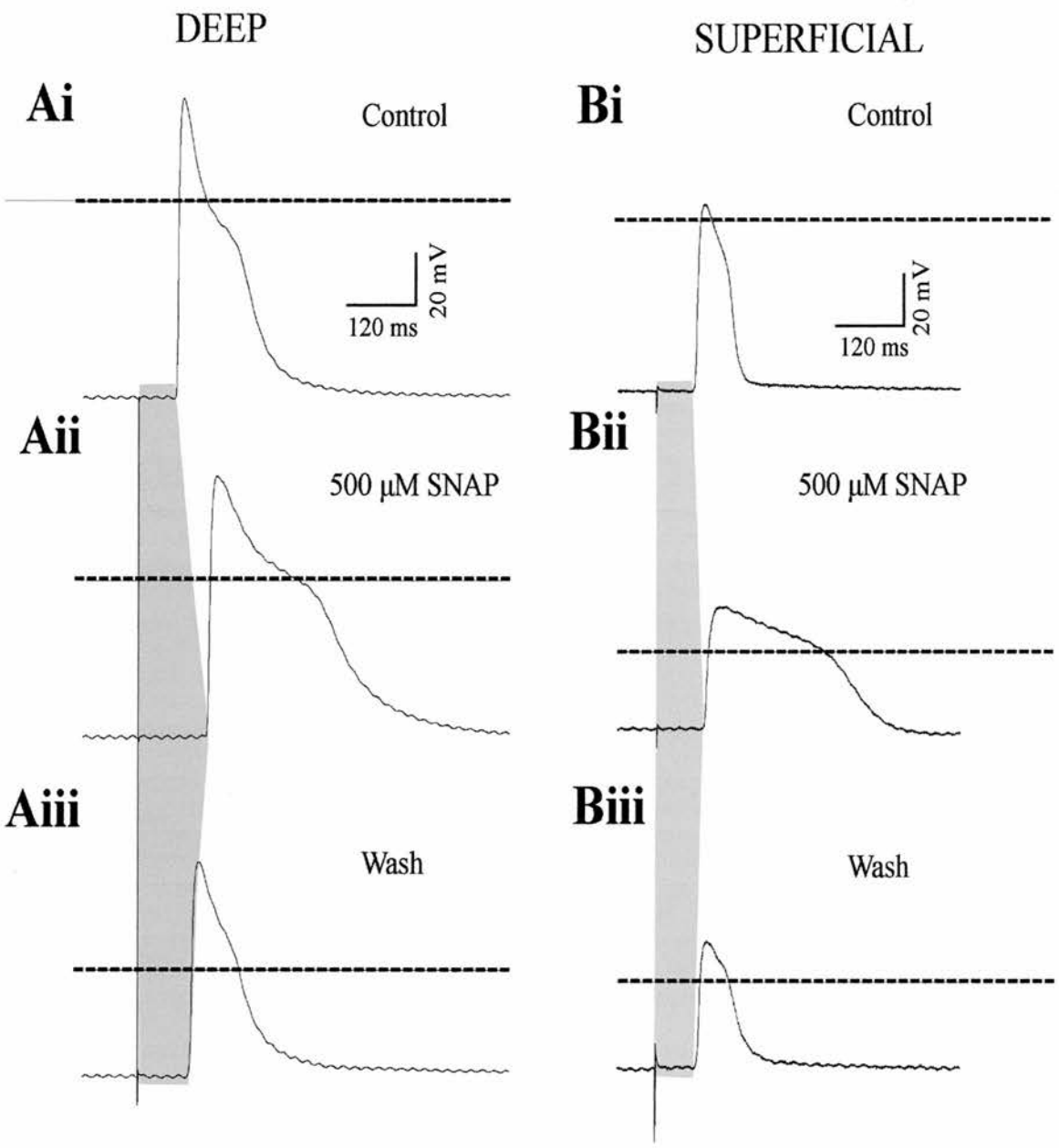

Figure 3.2. 6 Intracellular recordings of presumed deep (A) and superficial (B) impulses from two stage 37/38 *Xenopus* embryos. (Ai-iii) Deep impulses under control (i), 500 μM SNAP (ii) and Wash (iii) conditions. (Bi-iii) Superficial impulses under control (i), 500 μM SNAP (ii) and Wash (iii) conditions. The left boundary of grey area marks the stimulus artefact, and the right boundary displays the change in delay between each condition (A-B). Dotted line indicates 0 mV in each trace. Scale bars show 120 ms and 20 mV.

Vehicle effects

To assess if any vehicle-related effects were occurring in experiments with SNAP, control experiments were carried out in the presence of 0.5% dimethyl sulfoxide (DMSO). In pooled data for presumed superficial cells, no significant change was observed for either delay or duration (Figure 3.2.7 B). In pooled data from presumed deep cells, no change was observed in the average slope of the delay (n=3), whereas the average duration significantly and irreversibly increased ($p<0.05$; n=3). However, as this change is irreversible, it showed no characteristic difference from control conditions.

In summary, for both presumed deep and superficial cells, the average slope of the delay and the average duration reversibly increased in the presence of SNAP. Evidence suggests that this effect is not vehicle-related, even though a statistically significant increase occurred in duration. Therefore, it seems likely that SNAP triggers both a rapid and reversible increase in duration, and an accelerated increase and reversible increase in the trend of delay.

NO scavenger

C-PTIO, an NO scavenger, was used to counter the effects of SNAP-induced elevation of NO. Equimolar concentrations of C-PTIO (500 μM) were added in the presence of SNAP to test the hypothesis that the increased effect in skin impulse delay and duration in the presence of SNAP was due to the exogenously induced elevation of NO. In pooled data for presumed deep cells, the average slope of the delay was found to increase significantly in the presence of SNAP ($p<0.01$; n=9). Following the addition of C-PTIO, a highly significant reversal in the trend of SNAP was found ($p<0.01$; n=9), an effect which was partially reversible in the wash. In the presence of SNAP, the average skin impulse duration showed a highly significant increase ($p<0.01$; n=9). This effect was significantly reversed in the presence of C-PTIO ($p<0.01$; n=9), and continued to

decrease in the wash (Figure 3.2.8 B). In one experiment (Figure 3.2.8 A), delay is shown to rapidly increase from 60 to 120 ms within 25 minutes of the application of SNAP. The delay then decreased shortly after C-PTIO was added, approaching control values in the wash. The duration followed a similar pattern by rapidly increasing in the presence of SNAP from approximately 200 to 350 ms. After addition of C-PTIO, the delay decreased by approximately100 ms, and ultimately returned to control values in the wash.

In summary, the SNAP-induced changes in presumed deep cells are reversed by the NO scavenger, C-PTIO. This shows that the SNAP-induced effect is most likely do to the release of exogenous NO. Further exploration into the possible intracellular mechanisms underlying this change is examined below.

To investigate the potential modulation of endogenously released NO, C-PTIO was bath-applied to reduce NO levels *in vivo*. In pooled data from presumed superficial cells, no significant change was seen in either delay or duration (n=3; Figure 3.2.9 B). Similarly, in pooled data from presumed deep cells (n=3) no change was observed in either parameter (n=3). In one experiment (Figure 3.2.9 A), presumed superficial cells showed no increase in delay in the presence of C-PTIO, but instead maintained a decreasing trend that stabilized 10 minutes before the addition of the drug. Duration was found to decrease by 100 ms beginning immediately after application of C-PTIO. In presumed deep cells, delay began to decrease 20 minutes after application of C-PTIO, and began to increase in the wash. Duration followed a similar trend, as it showed a decreasing pattern in the presence of C-PTIO, and an increasing pattern in the wash. This experiment, along with pooled data for deep and superficial cells, strongly suggests that C-PTIO prevents the characteristic rise in delay and duration that is seen in control

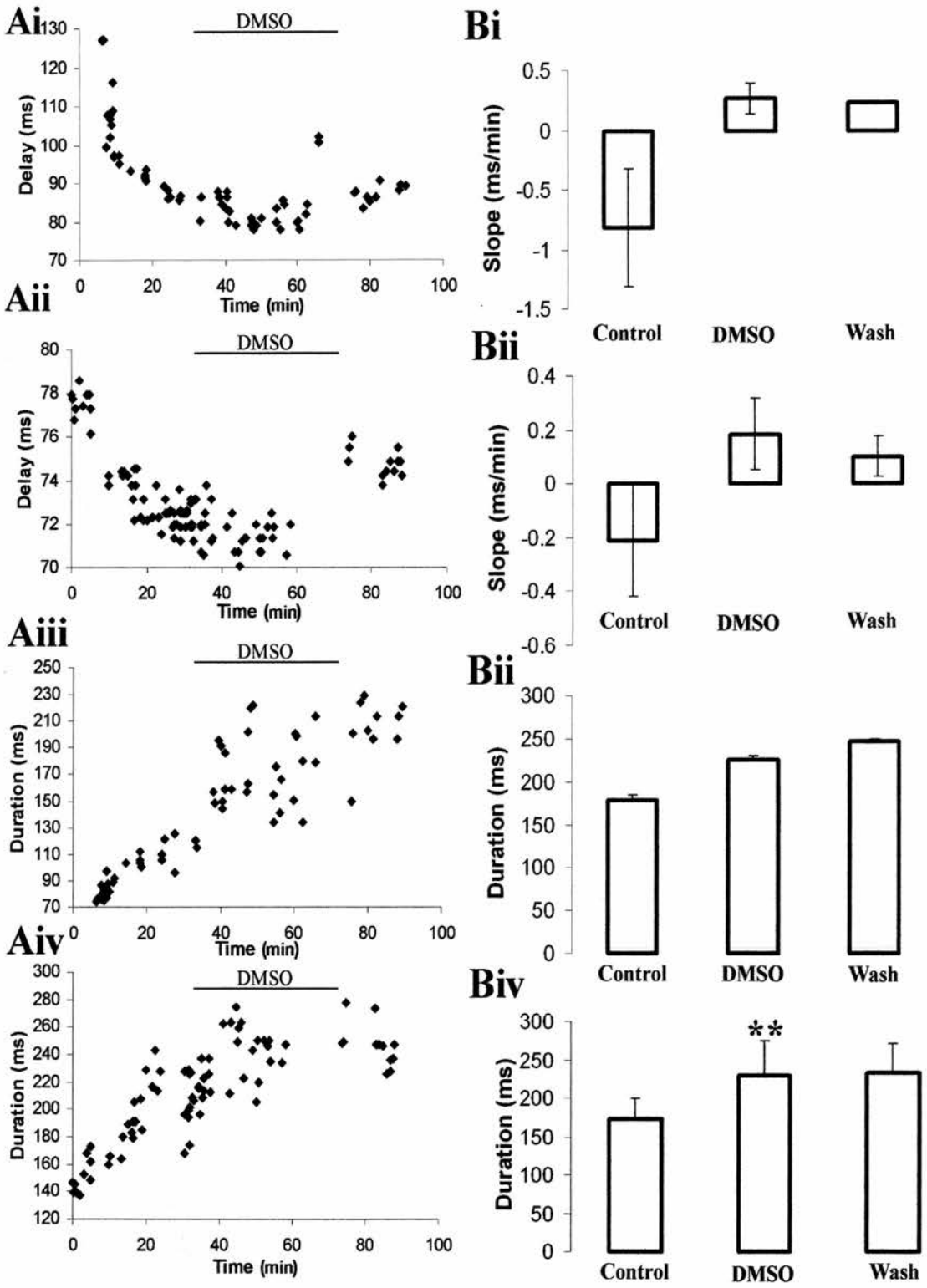

Figure 3.2. 7 Effect of 0.5% DMSO on conduction delay and impulse duration of both superficial and deep skin cells in a stage 37/38 *Xenopus* embryo. (Ai-iv) graphs displaying raw data points of superficial and deep delay (i-ii, respectively) and duration (iii-iv, respectively). (Bi-iv) graphs displaying pooled data from 3 experiments. (i-ii) show the average delay slope for superficial and deep, respectively and (iii-iv) show the average superficial and deep duration (iii-iv), respectively. The duration of deep cells was shown to irreversibly increase with high statistical significance (**P<0.05). Black bars indicate the period of drug application (Ai-iv). Error bars reflect S.E.M.

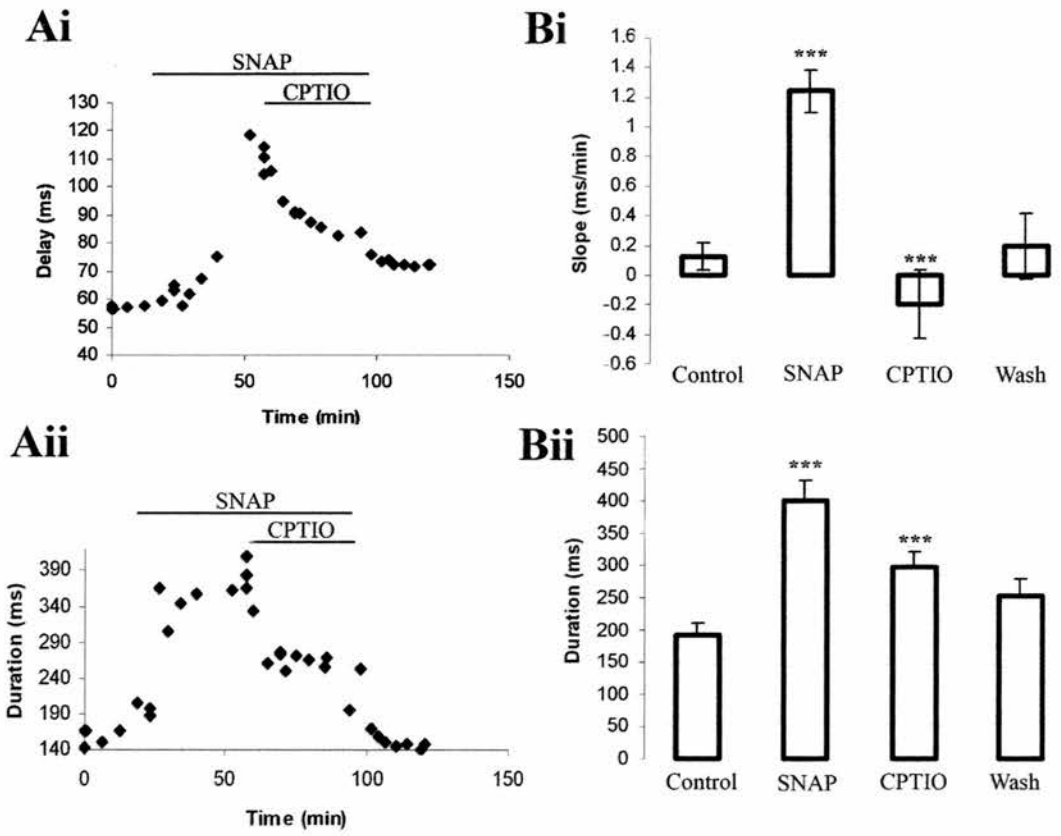

Figure 3.2. 8 Effect of 500 μM SNAP followed by 500 μM C-PTIO on skin impulse delay and duration for deep cells in a stage 37/38 *Xenopus* embryo. (Ai-ii) graphs showing raw data points for delay (i) and duration (ii) vs. time, respectively. In the presence of SNAP (black bar), delay (i) and duration (ii) increase, but decrease in the presence of C-PTIO (black bar) and SNAP. (Bi-ii) Pooled data from 9 experiments show that in the presence of SNAP, the slope of the trend in delay (i) and average duration (ii) significantly increases (***, $p<0.01$). In the presence of C-PTIO, the slope of the trend in delay (i) and average duration (ii) significantly decrease (***, $p<0.01$) from SNAP-induced changes. Error bars reflect S.E.M.

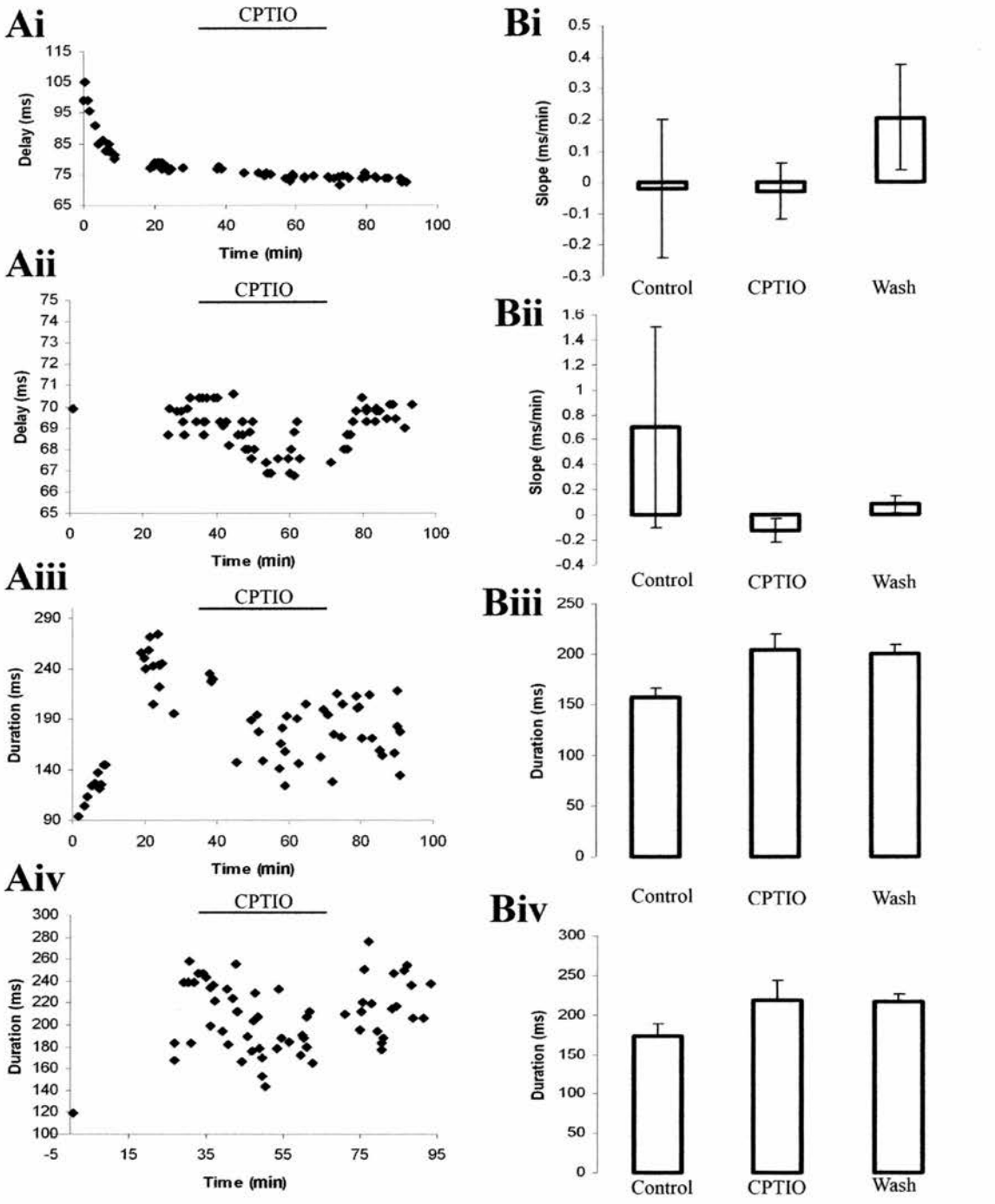

Figure 3.2. 9 Effect of 500 μM C-PTIO on conduction delay and impulse duration of both superficial and deep skin cells in a stage 37/38 *Xenopus* embryo. (Ai-iv) graphs displaying raw data points of superficial and deep delay (i-ii, respectively) and duration (iii-iv, respectively). In one animal, C-PTIO prevented the characteristic increase in delay for superficial cells (i), reversibly decreased the delay in deep cells (ii), decreased the duration in superficial cells (iii), and reversibly increased the duration in deep cells (iv). (Bi-iv) graphs displaying pooled data from 3 experiments. (i-ii) show the average delay slope for superficial and deep, respectively and (iii-iv) show the average superficial and deep duration (iii-iv), respectively. Black bars indicate the period of drug application (Ai-iv). Error bars reflect S.E.M.

experiments. This in turn suggests that an endogenous source of NO present in the tissue is responsible for this intrinsic increase of both parameters (explored below and in Results, section 3).

Effect of SNAP and C-PTIO on resting membrane potential

To begin to explore the cellular basis for the SNAP-induced effect on skin impulse delay and duration, the average resting membrane potential of multiple cells was compared before, during and after the application of SNAP followed by C-PTIO. In pooled data for SNAP (n=12), resting membrane potential significantly and reversibly depolarised in the presence of SNAP ($p<0.05$; Figure 3.2.10 B). However, following addition of C-PTIO (n=9), this change reversed and E_M returned towards control levels. In one representative experiment, E_M was found to depolarise in the presence of SNAP and decrease in the wash (Figure 3.2.10 Ai). In a second experiment, E_M was found to depolarise in SNAP, hyperpolarize in C-PTIO, and depolarise again in the wash (Figure 3.2.10 Aii). In this example, the very highest resting potentials were recorded in the presence of both SNAP and C-PTIO, suggesting that SNAP is acting to depolarise the cells, where C-PTIO counteracts this effect by causing hyperpolarisation. Statistical significance was shown through the use of a General Linear Model (see Materials and Methods, Chapter 2), but Tukey's *post hoc* did not show significant differences in pair-wise comparisons between periods in SNAP/C-PTIO experiments ($p>0.05$). The period is annotated with a (#), suggesting which period appears to be statistically significant.

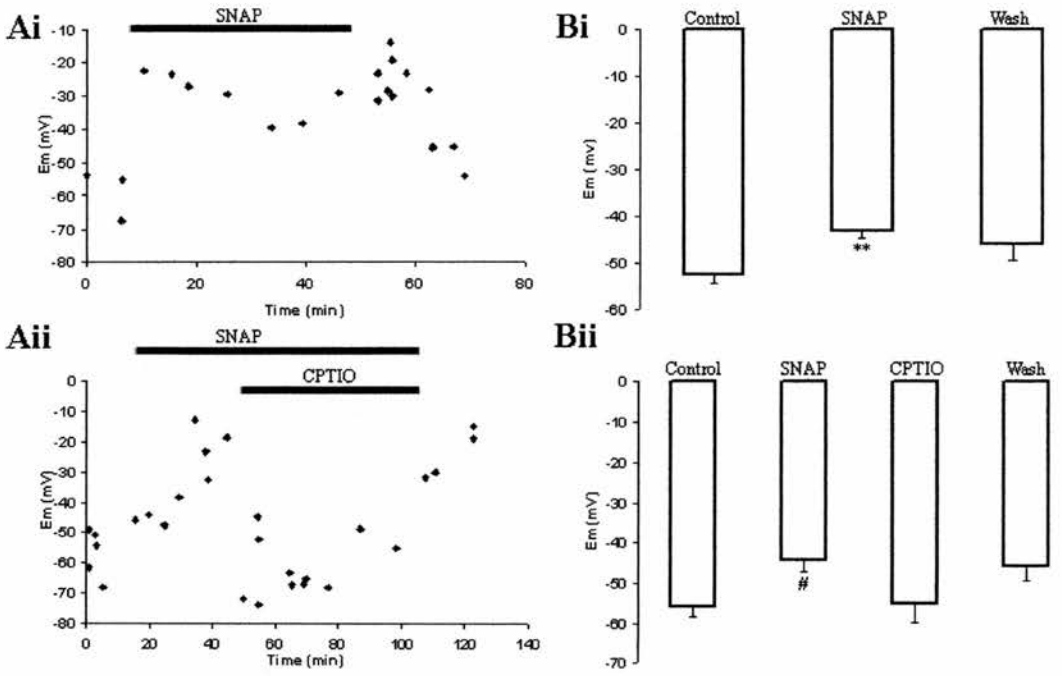

Figure 3.2. 10 Effect of 500 μM SNAP and 500 μM C-PTIO on resting membrane potential (E_M). (A) raw data points showing the change in Em in the presence of SNAP (i) and SNAP with C-PTIO (ii). E_M reversibly increases in the presence of SNAP (black bar, i) and is found to increase in SNAP and decreases in the presence of C-PTIO (black bar, ii). (B) Pooled data from experiments with SNAP (i, n=12) and SNAP with C-PTIO (ii, n=9). E_M significantly and reversibly increases in the presence of SNAP (**$p<0.05$), and is decreased in the presence of C-PTIO (ii). # indicates period purported to show a statistically significant change. Error bars reflect S.E.M.

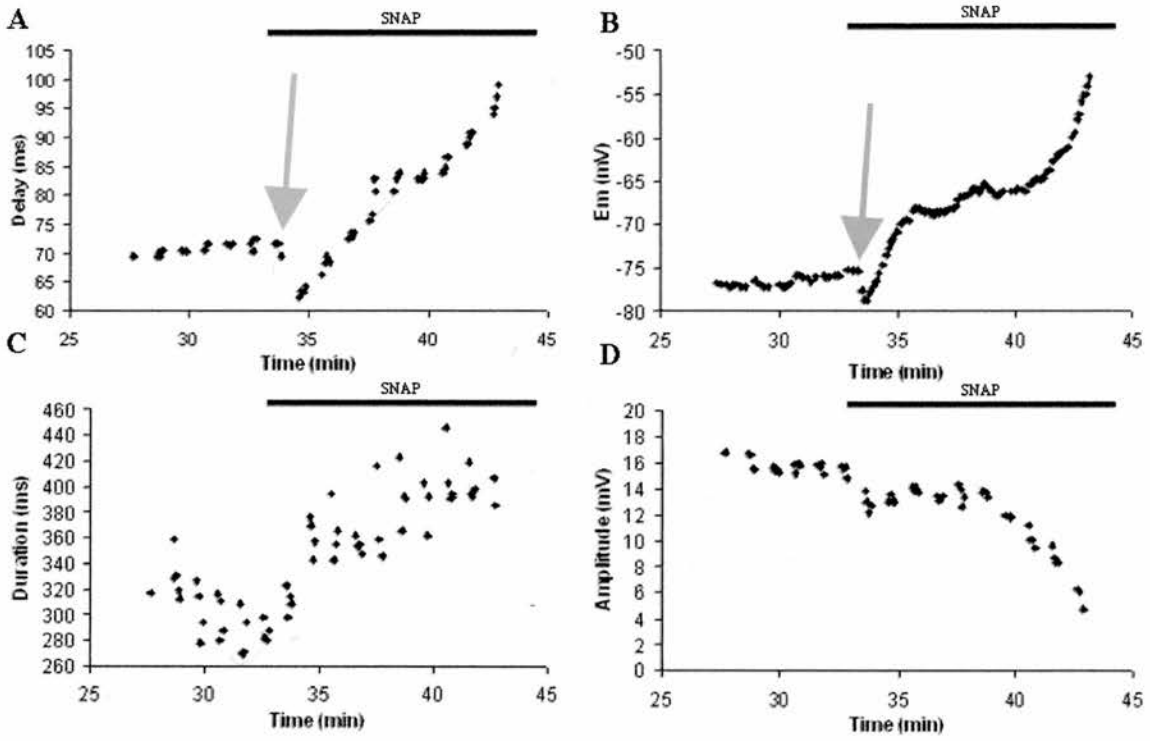

Figure 3.2. 11 SNAP-induced (500μM, black bar) changes recorded simultaneously in a single cell from one stage 37/38 *Xenopus* embryo. (A) Conduction delay (ms); (B) Resting membrane potential (E_M; mV); (C) Impulse duration (ms); (D) Maximum impulse amplitude (mV). Grey arrows point to sharp reversal in trend for delay (A) and duration (B) as evidence of a biphasic response to NO (see figure 3.2.5 Ai).

In one experiment, a recording from a single cell has held throughout the application of SNAP (Figure 3.2.11). In addition to increases in both delay and duration, the resting membrane potential (E_M) increases, while the maximum amplitude relative decreases. Also noticeable in Figure 3.2.11 is evidence for a biphasic response to SNAP-induced NO. Immediately after SNAP is applied, the initial trend in delay is to decrease, after which it rapidly changes course and begins to increase (Figure 3.2.11 A), with E_M following a similar pattern.

In summary, these data suggest that SNAP, in addition to modulating conduction delay and impulse duration, concurrently produces a change in skin cell resting membrane potential. SNAP also shows evidence of a biphasic response: decreasing delay at low concentrations of NO (i.e. immediately after SNAP is added to the bath) and increasing delay at higher concentrations (nearly 5 minutes after SNAP is added). In addition, the biphasic response may be consistent with E_M as well (see Discussion, Chapter 4). However, the only concentration of SNAP used in all experiments was 500 μM, and thus there is no evidence at sustained lower bath concentrations.

Spermine NONOate

Next, an investigation was aimed to explore whether the SNAP-induced change in delay and duration could me mimicked by annother NO donor, spermine NONOate (150 μM). In pooled data from presumed deep cells, however, there were no significant changes in either the average slope of the delay or average duration (n=3). This finding, however, might reflect the slow release of NO from this donor, which has been designed to give a controlled release of NO into the bath. Conversely, the half-life of spermine NONOate is 37 minutes, indicating that it degrades faster than SNAP, which has a half-life of 36 hours. In either case, the release of NO and subsequent bath concentration (or

concentration of spermine NONOate added) may be insufficient to produce any noticeable effects in this skin preparation.

NOS inhibition

In order to further investigate whether endogenously produced NO was responsible for the gradual rise seen in both delay and duration, as indicated by C-PTIO applications, the enzyme inhibitor, N^G-nitro-*L*-arginine methyl esther (L-NAME; 1 mM, c.f. McLean (2001)), was used to reduce endogenous NO levels. L-NAME is a non-specific enzyme inhibitor which acts by irreversibly binding to NOS isozymes, inactivating the further production of NO. In pooled data (n=3) for presumed deep cells, no change is found in either the average slope of the delay or the average duration (Figure 4.14 B). These data suggest that endogenous NO is not responsible for the characteristic rise in both delay and duration. However, enzyme inhibition by L-NAME has been reported take approximately one hour (Torres et al., 1997), which may be too slow to show a significant change within the course of the experiment. Additionally, the evidence from C-PTIO experiments suggest that intracellular washout of NO is sufficient to counter the intrinsic rise in delay and duration. Furthermore, because L-NAME is much larger compared to NO (molecular weights equal to approximately 270 to 30, respectively), it may have been prevented from sufficient tissue access, and thus unable to effectively inhibit NOS enzymes on a large enough scale.

Investigation into the mechanism of SNAP-induced modulation

Inhibition of soluble guanylyl cyclase

The most likely intracellular target for NO is the enzyme soluble guanylyl cyclase (sGC), which converts guanosine triphosphate (GTP) into 3'-5'-guanosine cyclic monophasphate (cGMP; Blute et al., 1998). NO acts by diffusing across cell membranes to bind to sGC, raising endogenous levels of cGMP. Bath-application of 1H-[1,2,4]oxadiazolo[4,3-a]quinoxalin-1-one (ODQ, 10-50 μM), an inhibitor of NO-sensitive sGC, was used to reduce both the endogenous concentration of cGMP, and prevent SNAP-induced activation of sGC by NO *in vivo*. This experiment was designed to test the hypothesis that the NO effect on skin impulse delay and duration is cGMP-dependent.

A consistent effect in all animals (n=11), was the incidence of spontaneous impulses observed within 30 s after application of ODQ (40 μM; Figure 3.2.12). Several impulses were recorded, along with a skin impulse-induced activation of fictive swimming. The impulses were followed by a slow depolarisation of the resting membrane potential, which overshoots 0 mV, and repolarizes to the original resting membrane potential in approximately 1 minute (Figure 3.2.12).

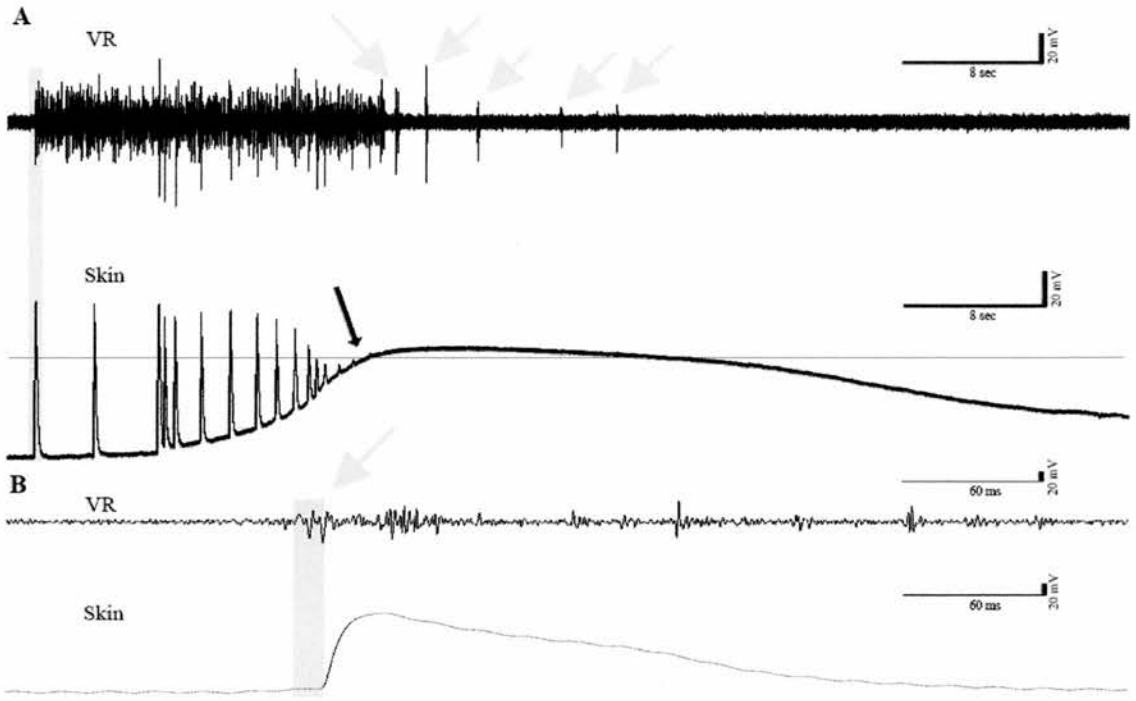

Figure 3.2. 12 40 μM ODQ triggers spontaneous impulses and swimming in stage 37/38 *Xenopus* embryos. (A) Extracellular trace recording from the VR (top) and intracellular trace (bottom) recording from a single skin cell on the head. The trace begins 30 s after the drug application, showing the a nearly immediate generation of spontaneous skin impulses (grey box, bottom; triggering an episode of swimming (top), which are also recorded in the VR trace after the skin cell being recorded intracellularly becomes depolarised (grey arrows). (Bottom) Skin impulse amplitude decreases as resting membrane potential depolarises to above 0 mV (grey line, black arrow) and then returns toward the original value. (B) Enlargement of grey box in (A), showing the extracellular recording of the impulse from within the VR trace (grey arrow) approximately 10 ms before the intracellular skin impulse (grey box, B). Scale bars show 8 sec and 20 mV (A), 60 ms and 20 mV (B).

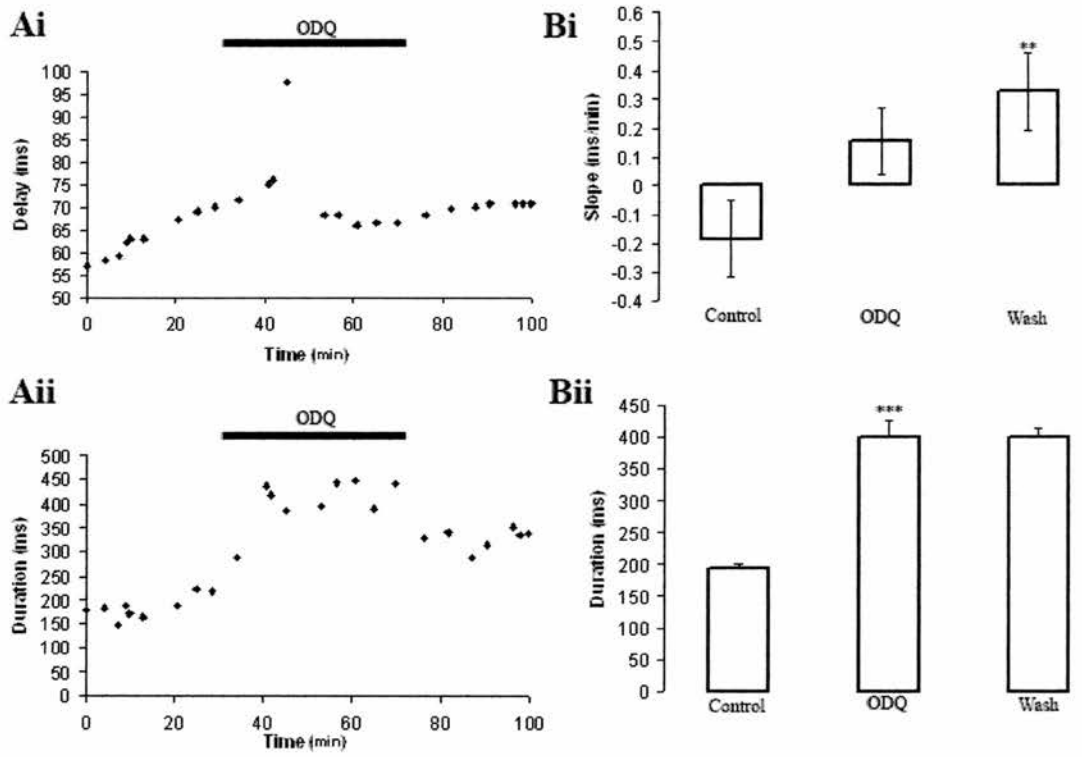

Figure 3.2. 13 Effect of 40 μM ODQ on skin impulse delay and duration in stage 37/38 *Xenopus* embryos. (A) Graphs show raw data for delay (i) and duration (ii) vs. time for one animal. In the presence of ODQ (black bar), the trend in delay (i) begins to decrease and duration (ii) increases reversibly. (B) Pooled data from 11 animals showing the average delay slope (i) and average duration (ii) for control, ODQ, and wash periods. In the presence of ODQ, delay is significantly different from control (i; **, $p<0.01$), and duration (ii) increased irreversibly (***, $p<0.01$). Error bars reflect S.E.M.

In pooled data (n=11), during the presence of ODQ there is no significant change in the average slope of the delay. However, the wash period shows a significant increase in the slope ($p<0.05$; n=11), possibly indicating the prevention of the intrinsic increase in delay. The average duration increased irreversibly with high significance ($p<0.01$; n=11) in the presence of ODQ, which is different from control experiments insofar as control either showed no significant change between periods with a continual rise, or only a significant increase to a lesser degree (Figure 3.2.13 B). The effect on duration may not have washed off consistently due to a considerable lag time in the re-amplification of cGMP. In one experiment (Figure 3.2.13 A), delay continues an upward trend for the first 20 minutes after application of ODQ, and then decreases for the rest of the drug period, where it begins to increase again in wash. Duration is found to increase in the presence of ODQ, and decrease in the wash.

In 5 experiments, embryos were pre-treated with ODQ in order to overcome this transient excitatory effect and presumably completely inhibit sGC. Subsequent application of SNAP was then used to determine if the effects of SNAP on delay and duration (refer back to Figure 3.2.5) are cGMP-dependent. In pooled data (n=5), the average slope of the delay decreased in ODQ, increased again in SNAP, and reversed in the wash. The average duration was found to significantly and reversibly increase when SNAP was applied in the presence of ODQ ($p<0.01$; n=5). In one experiment (Figure 3.2.14 A), the delay continues an increasing trend from control to ODQ periods, which is then rapidly increased in the presence of SNAP, and follows a decreasing trend in the wash. The duration increases in ODQ, increases further in SNAP, and decreases in the wash.

In summary, these data suggest that ODQ may be acting to prevent the natural increase in conduction delay and duration, but it is impossible to conclude from these

data. Instead, it appears to slightly elevate duration. Additionally, ODQ-induced intracellular washout of sGC-dependent cGMP is insufficient to prevent either the SNAP-induced increase in delay or duration. Again, duration appears to be increased by ODQ, and further increased by SNAP, suggesting that SNAP-released NO and inhibition of sGC-dependent cGMP production exert effects in a similar direction.

cGMP analogue

To explore further if the SNAP-induced effect on delay and duration occurs by a cGMP-dependent mechanism, a cell-permeable analogue of cGMP was used. Bath-application 8-Br-cGMP (100 μM) was used in order to elevate intracellular levels of physiologically active cGMP. In pooled data (n=8), no significant change was found in the average slope of the delay, whereas the average duration was found to increase irreversibly in the presence of 8-Br-cGMP with high significance, consistent with control experiments ($p<0.01$; Figure 3.2.15 B). In one experiment (Figure 3.2.15 A), delay was found to be highly variable in control and 8-Br-cGMP periods, with large fluctuations as it increased in trend. The duration showed a gradual increase from control into 8-Br-cGMp periods, and increasing variability in the wash. From these results it is unclear if there were any significant effects from 8-Br-cGMP on delay and duration. Instead, these results suggest that SNAP-induced NO is working through a different mechanism than the sGC/cGMP pathway. However, it is possible that higher concentrations of 8-Br-cGMP are needed in this preparation to produce reliable and significant effects.

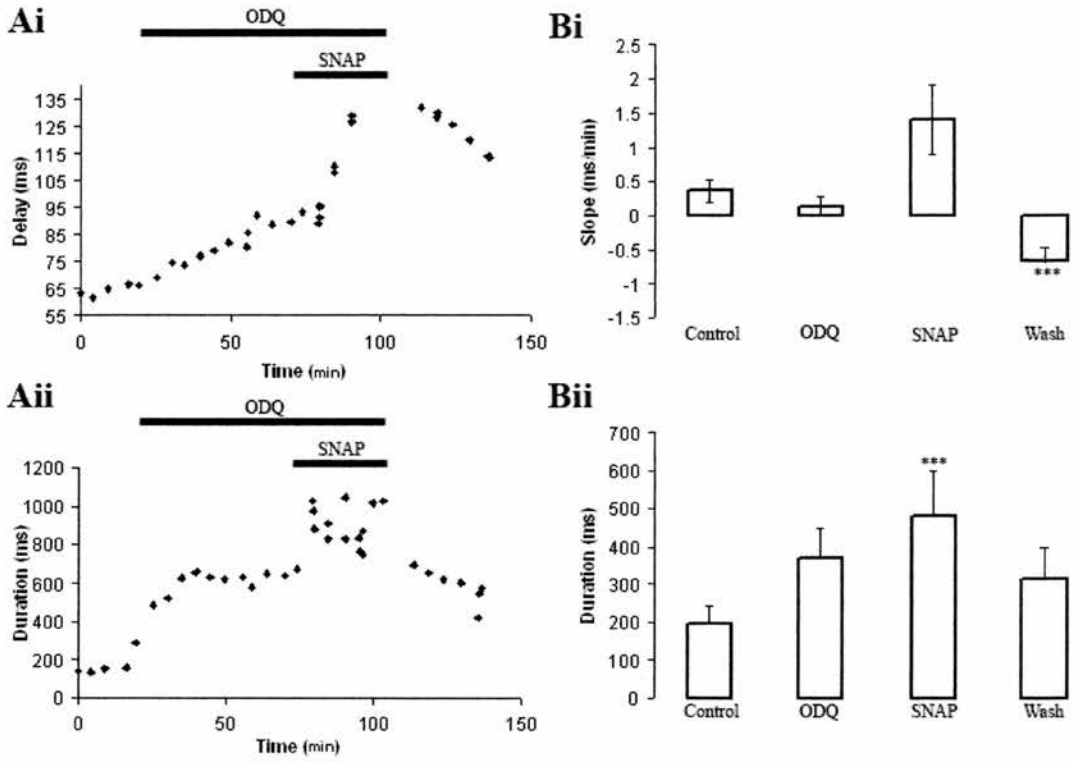

Figure 3.2. 14 Effect of 40 μM ODQ and 500 μM SNAP on skin impulse delay and duration on stage 37/38 *Xenopus* embryos. (A) Graphs of raw data showing delay (i) and duration (ii) vs. time in one animal. In the presence of ODQ (black bar), delay (i) continues an increasing trend and duration (ii) increases. When SNAP is added in the presence of ODQ, delay (i) and duration (ii) increase reversibly. (B) Pooled data from 4 animals showing the average delay slope (i) and duration (ii) for control, ODQ, ODQ + SNAP, and wash periods. The wash slope is significantly different from SNAP-induced slope (***, $p<0.01$). In the presence of ODQ and SNAP duration increases reversibly (***, $p<0.01$). Error bars reflect S.E.M.

The following table summarises the pharmacological effects on skin impulse delay and duration for presumed deep cells:

DRUG	DELAY	DURATION
18-β-GA	–	–
5-HT	–	–
forskolin	↑	–
SP	–	–
L-732,138	–	–
SNAP	↑	↑
C-PTIO	↓	↓
spermine NONOate	–	–
L-NAME	–	–
ODQ	↓ (?)	↑
8-Br-cGMP	–	–

Taken together, these results suggest that neither 5-HT nor SP exert a consistent effect on the skin impulse. The clear SNAP-induced effects on delay and duration and the reversal of this effect by C-PTIO suggest that NO produces profound, modulatory changes on the skin impulse. Therefore, a histological and immunocytochemical investigation was performed to determine if there is an endogenous source for the production of NO within the epithelium of the *Xenopus* embryos.

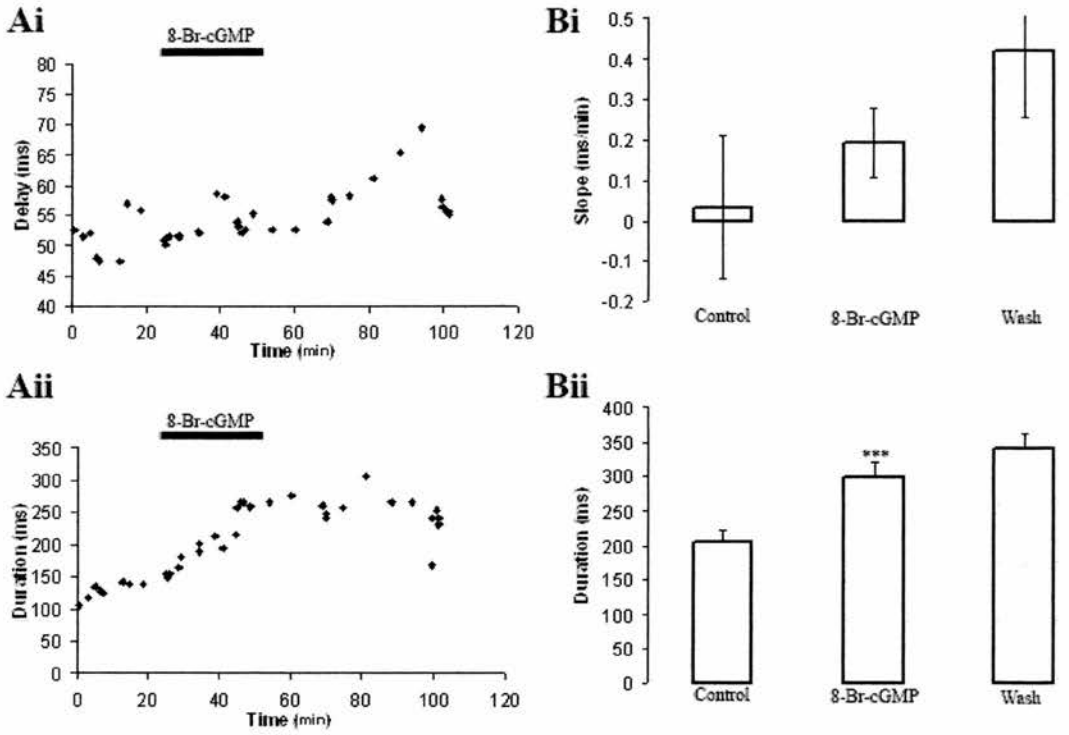

Figure 3.2. 15 Effect of 100 μM 8-Br-cGMP on skin impulse delay and duration in stage 37/38 *Xenopus* embryos. (A) Graphs of raw data points showing delay (i) and duration (ii) vs. time in one animal. In the presence of 8-Br-cGMP (black bar), delay (i) was not found to increase and duration (ii) maintained an increasing trend. (B) Pooled data from 8 animals showing average delay slope (i) and average duration (ii) for control, 8-Br-cGMP, and wash periods. In the presence of 8-Br-cGMP, duration (ii) is found to increase irreversibly (***, $p<0.01$). Error bars reflect S.E.M.

Section 3 – Anatomy of the skin and histology of nitrergic activity

Based on the preceeding pharmacological evidence for modulation of the skin impulse by NO, the anatomy of the skin was examined followed by the search for a potential source of NO. *Xenopus* tadpoles, along with several other tadpole species were imaged using a scanning electron microscope (SEM) in order to characterize the features of the skin surface, and their potential similarities between species. Next, both the NADPHd technique and nNOS immunocytochemistry were used to examine the potential localisation of NOS-positive skin cells as was initially shown by McLean and Sillar (2001) in a stage 42 larva (see General Introduction, Chapter 1). Finally, DAF fluorescence was performed to explore the distribution of NO in the skin. The histological findings below support the pharmacological results shown with SNAP, suggesting that NO is produced by skin cells and can act as an endogenous modulator of the *Xenopus* skin impulse.

Scanning Electron Microscopy

Xenopus laevis

SEM images of *Xenopus laevis* tadpoles between developmental stages 37/38 and 42 revealed that at all stages examined, the skin comprises a heterogeneous mixture of ciliated and non-ciliated cells. Cells viewed in the images were between 10-30 μm in diameter, and had between 4-7 sides of varying length (4-10 μm). Extremely high-powered images show the cell surface of non-ciliated cells to display a textured pattern (see Figure 3.3.2 A-B). Several presumed mucus-secreting pores are visible on the surface, either between cells, or directly on the cell surface. There were also points on the surface at which it appeared that secretions had been captured in the fixation technique (Figure 3.2.1 Aiv), but these are not necessarily distinguishable from other debris that

could have contaminated the sample. Other cells show a webbed pattern on their surface (Figure 3.3.2 E). The surface of ciliated cells appeared as a dense mixture of long and thin hairs, generally covering the entire outer membrane of the cell (Figure 3.3.2 C). The membranous surface on some ciliated cells is visible, with a sparse covering of cilia, but this may be a result of the fixation and dehydration process which could have damaged the tissue (Figure 3.3.2 E). In lower powered images of the skin where the entire epidermis is visible, a punctate pattern of ciliated cells relative to non-ciliated cells can be seen with a ration of 1:6, respectively (Figure 3.3.2 D). The ciliated cells are found over the entire epidermis, albeit with variable densities on different regions of the body.

Rana temporaria

Stages 18-21 of *Rana temporaria* were also examined under the SEM. The surface of the skin appears similar to that of *Xenopus* embryos at equivalent developmental stages (37/38-42). The punctate pattern of ciliated cells (appearing relatively lighter) stands out amongst the darker, cuboidal cells (Figure 3.3.3). Ciliated cells are found over the entire epidermis, including the immature gills of stage 18-19, and the more developed gills found at stages 20-21 (Figure 3.3.4). Images showed cells that are also comparable in size and shape to those of *Xenopus*, ranging between 10-30 μm, and having 4-6 sides of varying length (7-15 μm). In high powered images, ciliated cells appear as a dense covering of long, hair-like structures (Figure 3.3.3 Aiii; 3.3.4 Aiii).

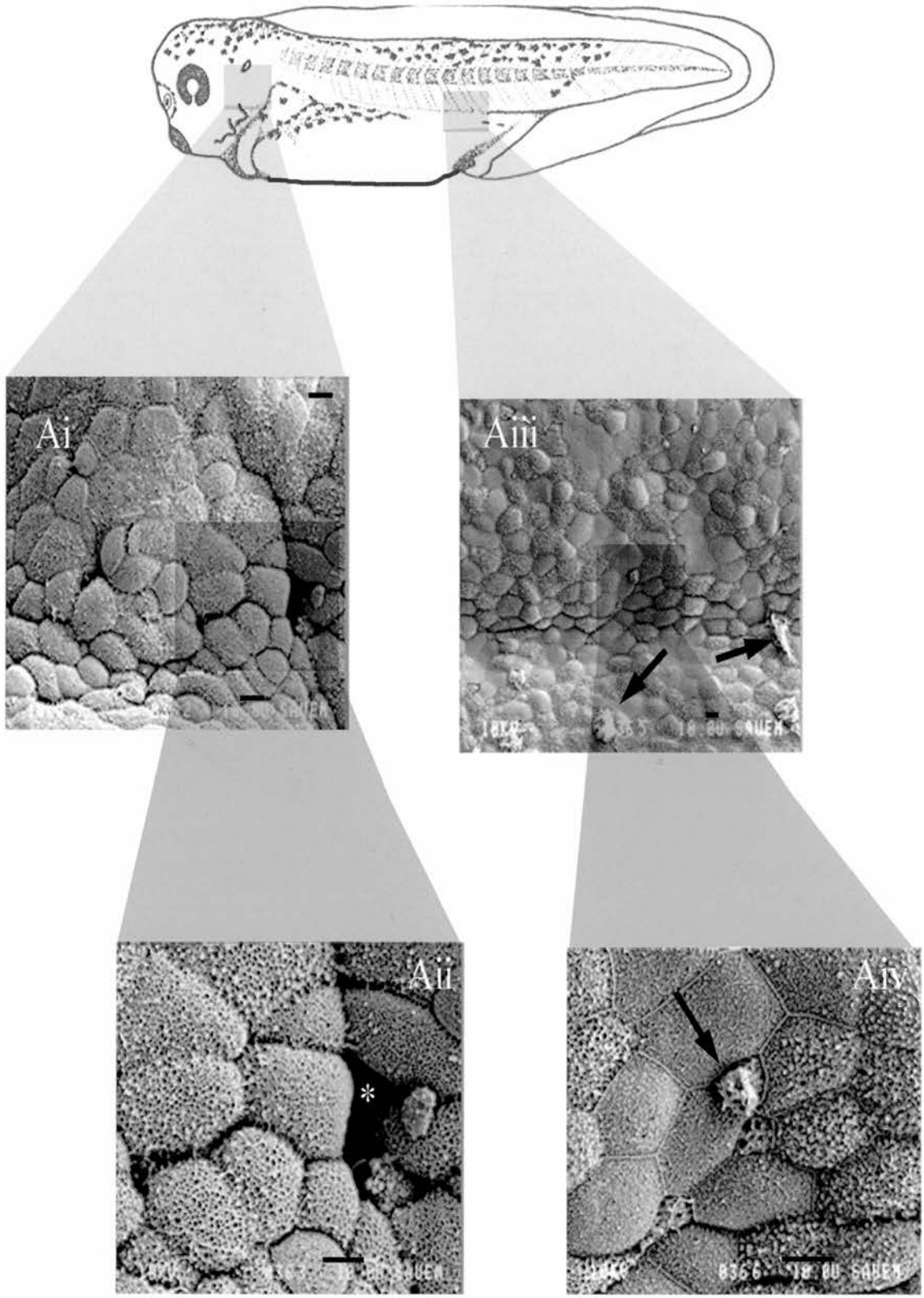

Figure 3.3. 1 Drawing of a stage 37/38 tadpole (Nieuwkoop and Faber, 1956). (Ai-iv) SEM photographs of a stage 37/38 *Xenopus* embryo. Skin cells on the head (i, x860) and torso (iii, x440) show a variety of different sizes and shapes. Black arrows point to hair cells (iii). (ii, x2000 and iv, x1800) are enlarged images of the shaded box in (i and iii), respectively. White star indicates a crater in the skin (ii). Black arrow points to a presumed secretion captured in the fixation process (iv). Scale bar =10 μm.

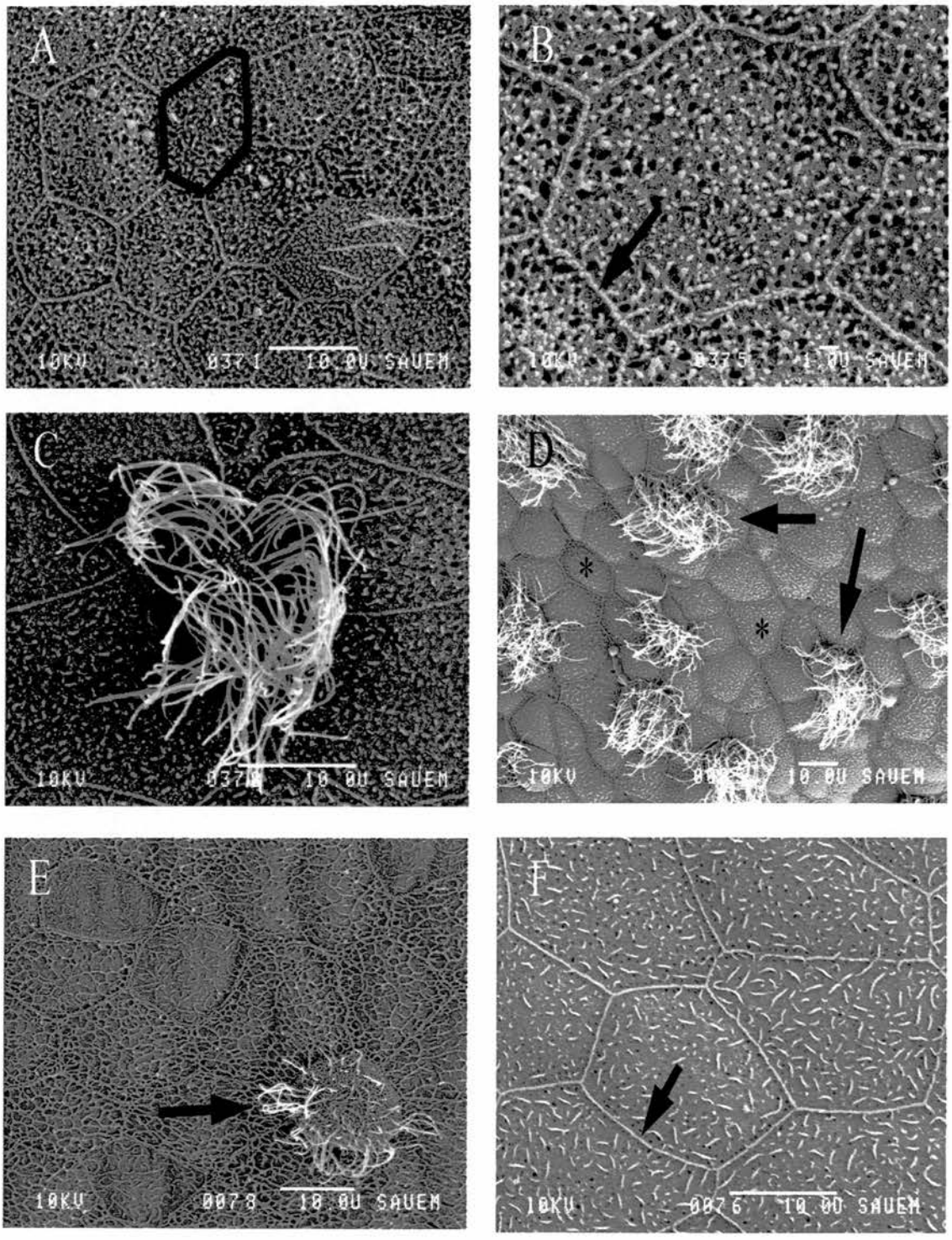

Figure 3.3. 2 (A-F) SEM images of *Xenopus* tadpole skin at various developmental stages. (A) Stage 39 embryo showing several non-ciliated cells on the tail at x2400. Black outline indicates the boundary of one skin cell. (B) is an individual skin cell at x5400 on the tail of (A). Black arrow indicates the divisional boundary between adjacent skin cells. (C) Individual ciliated cell at x3200 on the torso of a stage 40 larva. (D) Punctate pattern of ciliated cells (arrows) among non-ciliated cells (stars) of a stage 42 larva (1:6, respectively). (E) One ciliated cell (arrow) among several non-ciliated cells (star) on the fin of a stage 42 larva. (F) Several individual skin cells on the tail of a 42 larva. Arrow indicates the divisional boundary between cells. Scale bar = 10 μm.

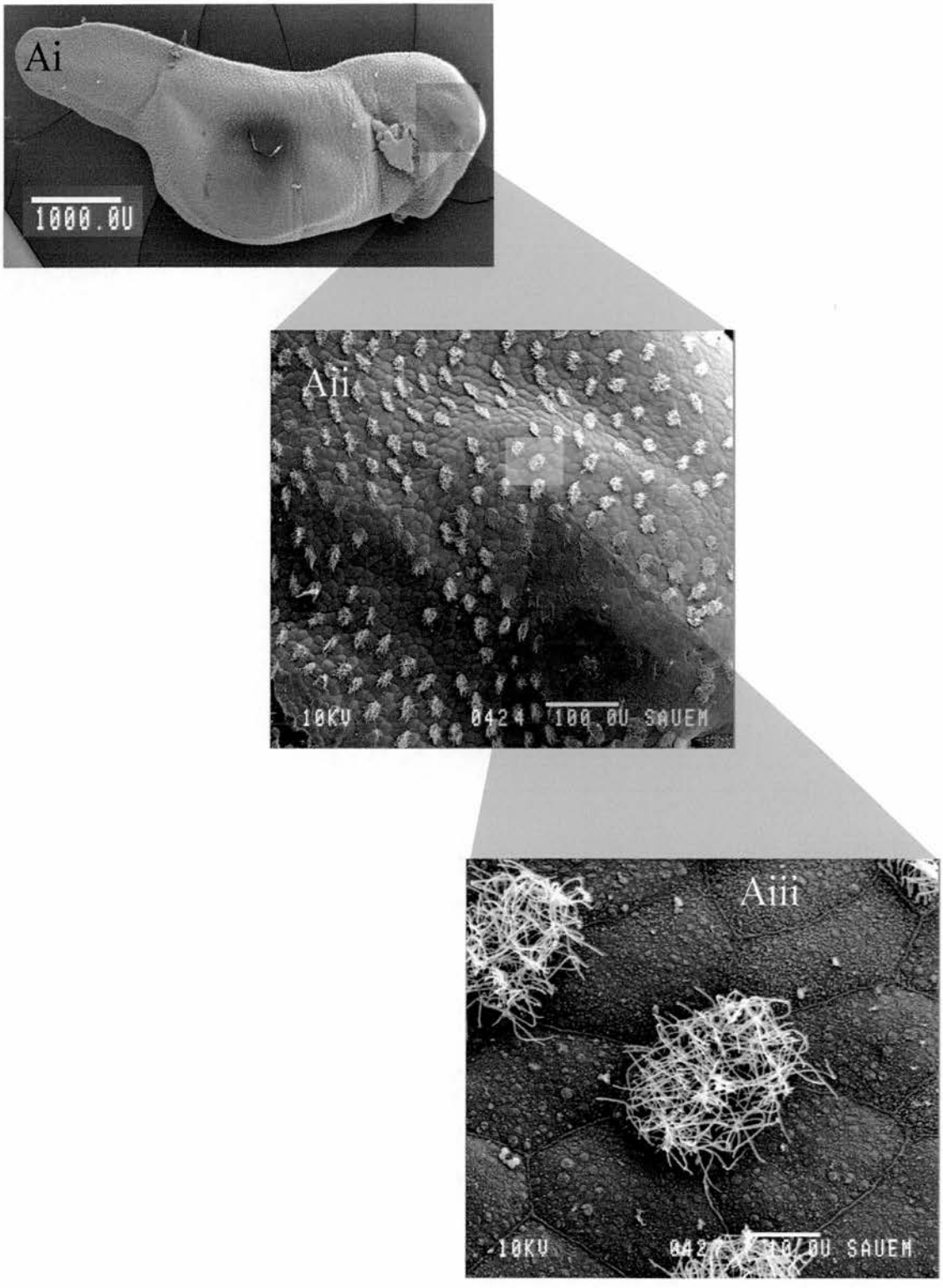

Figure 3.3. 3 (Ai-iii) SEM images of a stage 19 *Rana* embryo. (i) Entire whole embryo at x22. (ii) Enlarged image of area over a premature eye in Ai at x200 with a punctate pattern of ciliated cells (lighter) amongst non-ciliated cells (darker). (iii) Enlarged image of individual cells of Aii at x2000. Scale bars show 1 mm (i), 100 μm (ii), and 10 μm (iii).

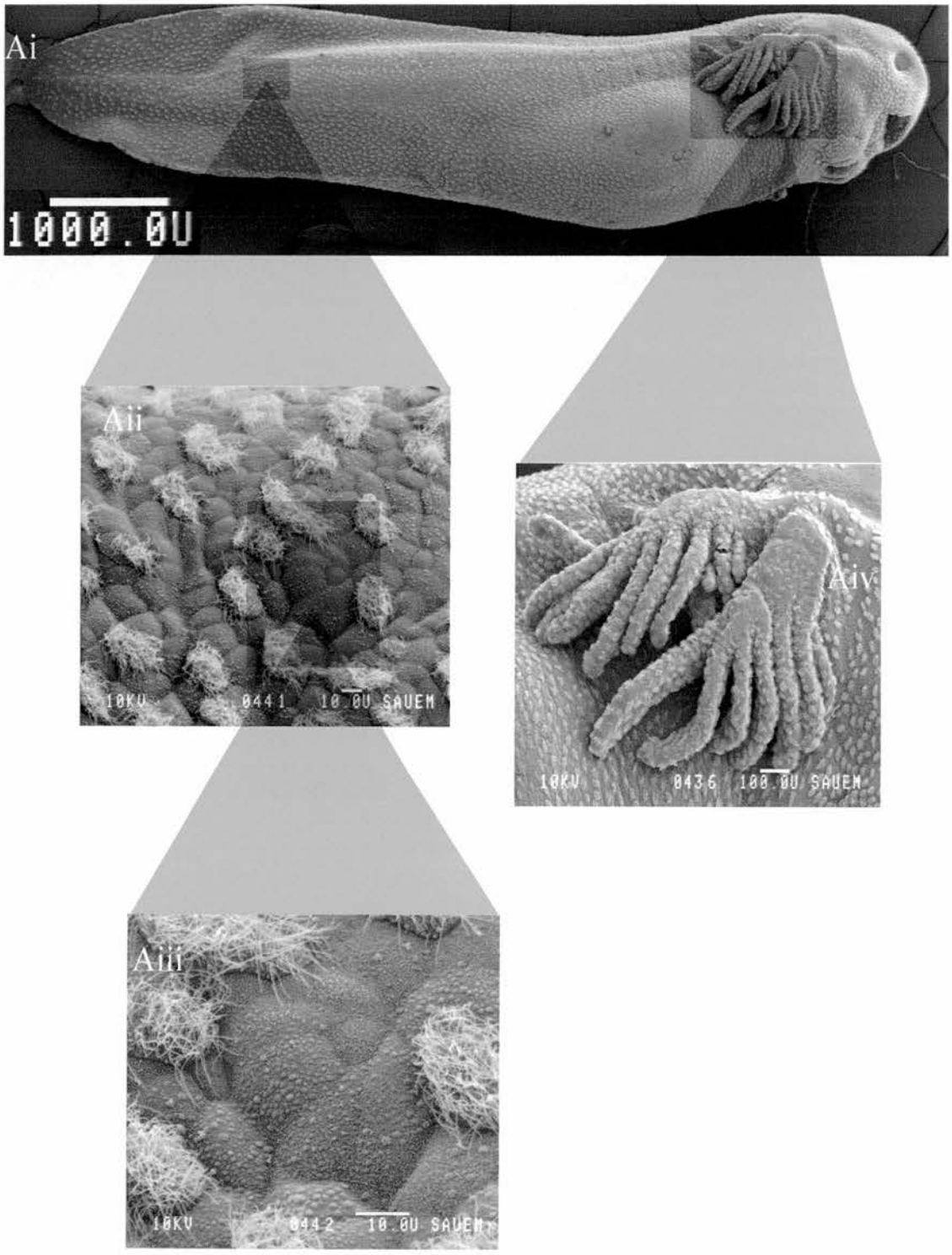

Figure 3.3. 4 (Ai-iv) SEM images of a Stage 21 *Rana* embryo. (i) Entire embryo. (ii) Enlarged area of the skin from (i) at x660. (ii) Enlarged area of (ii) at x1800. (iv) Enlarged area from (i) of the ciliated and non-ciliated skin cells covering the gills at x100. Scale bars = 1 mm (i), 10 μm (ii-iii), and 100 μm (iv).

Bufo bufo

Images of the epidermis of *Bufo bufo* were also taken with a SEM at stages ranging from 18-21 (Figure 3.3.5). The epidermis as a whole closely resembles *Rana* in its punctate pattern of lighter ciliated cells amongst darker, cuboidal cells. Skin cells appeared very similar to *Rana* and *Xenopus*, having similar shapes and dimensions. As in *Xenopus*, porous cells were found. In *Bufo*, the pores were found to protrude upwards out from mounds on the cell's surface (Figure 3.3.5 Biv).

Triturus vulgaris

In SEM images of hatchling *Triturus vulgaris* embryos (Figure 3.3.6), The epidermis was found to be composed of sparsely populated ciliated cells, cuboidal cells in the head region and gills and flattened cells on the torso. The skin cells on the gills are very rounded, and sometimes form arrays surrounding a porous region (Figure 3.3.6 Aii). In other areas, pores can be found between cell boundaries, lying at the intersection of several cell membranes (3.3.6 Aiv). Cell size and dimensions are consistent with *Bufo, Rana*, and *Xenopus*, except in the torso, where cells are generally larger, having diameters up to 40 μm (Figure 3.3.6 Avi).

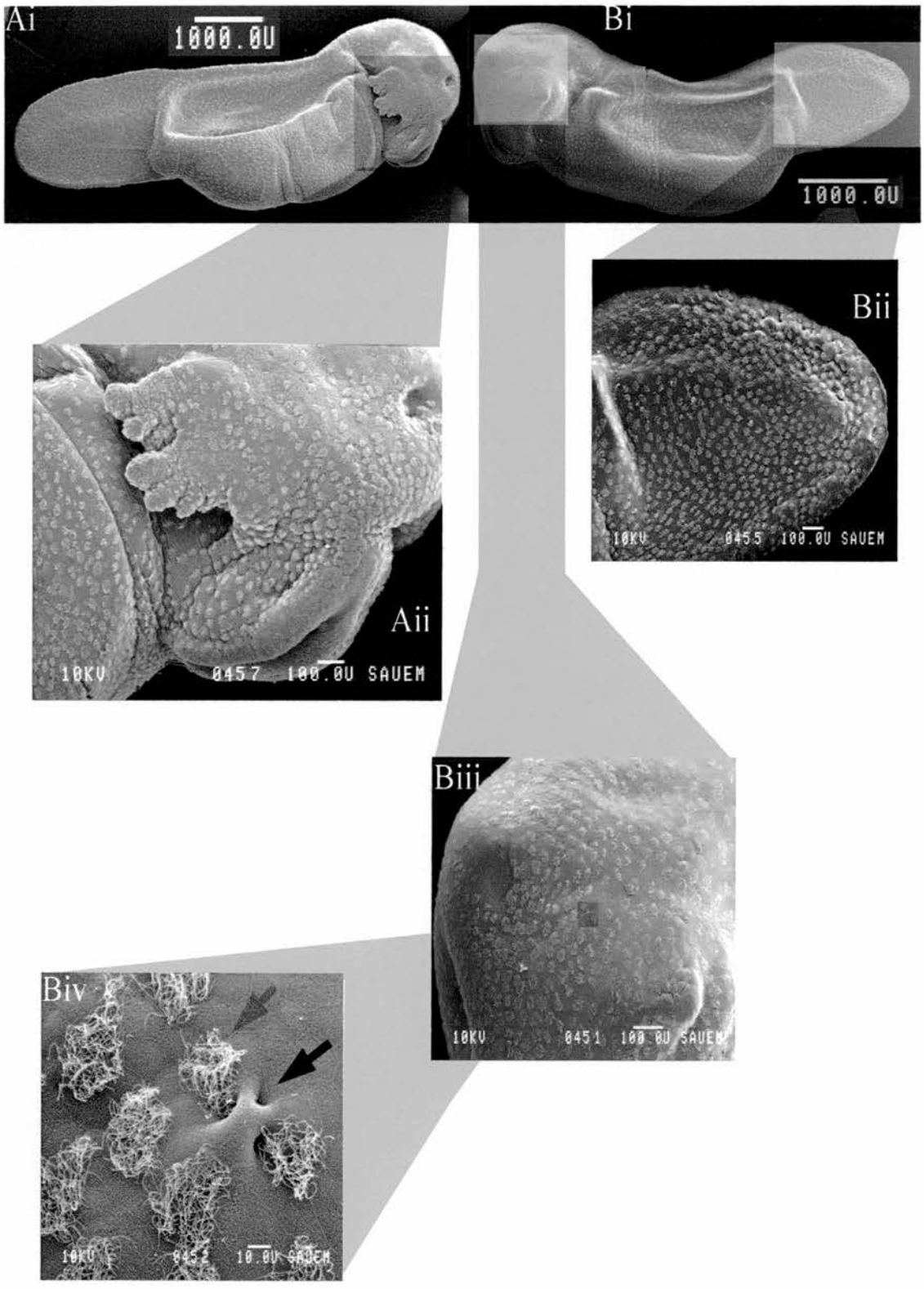

Figure 3.3. 5 (A-B) SEM images of stage 19 (B) and 20 (A) *Bufo* embryos. (Ai) Entire embryo at x16 and (Aii) is an enlargement of the skin on the head and gills at x80. (Bi) shows an entire tadpole at x22. (Bii) Enlargement of the tail and fin at x86. (Biii) Enlargement of the head at x120 and (Biv) is an enlargment of Biii at x940. (Biv) shows pores (black arrow) and ciliated cells (grey arrow). Scale bar = 1 mm (Ai, Bi), 100 μm (Aii, Bii-Biii), and 10 μm (Biv).

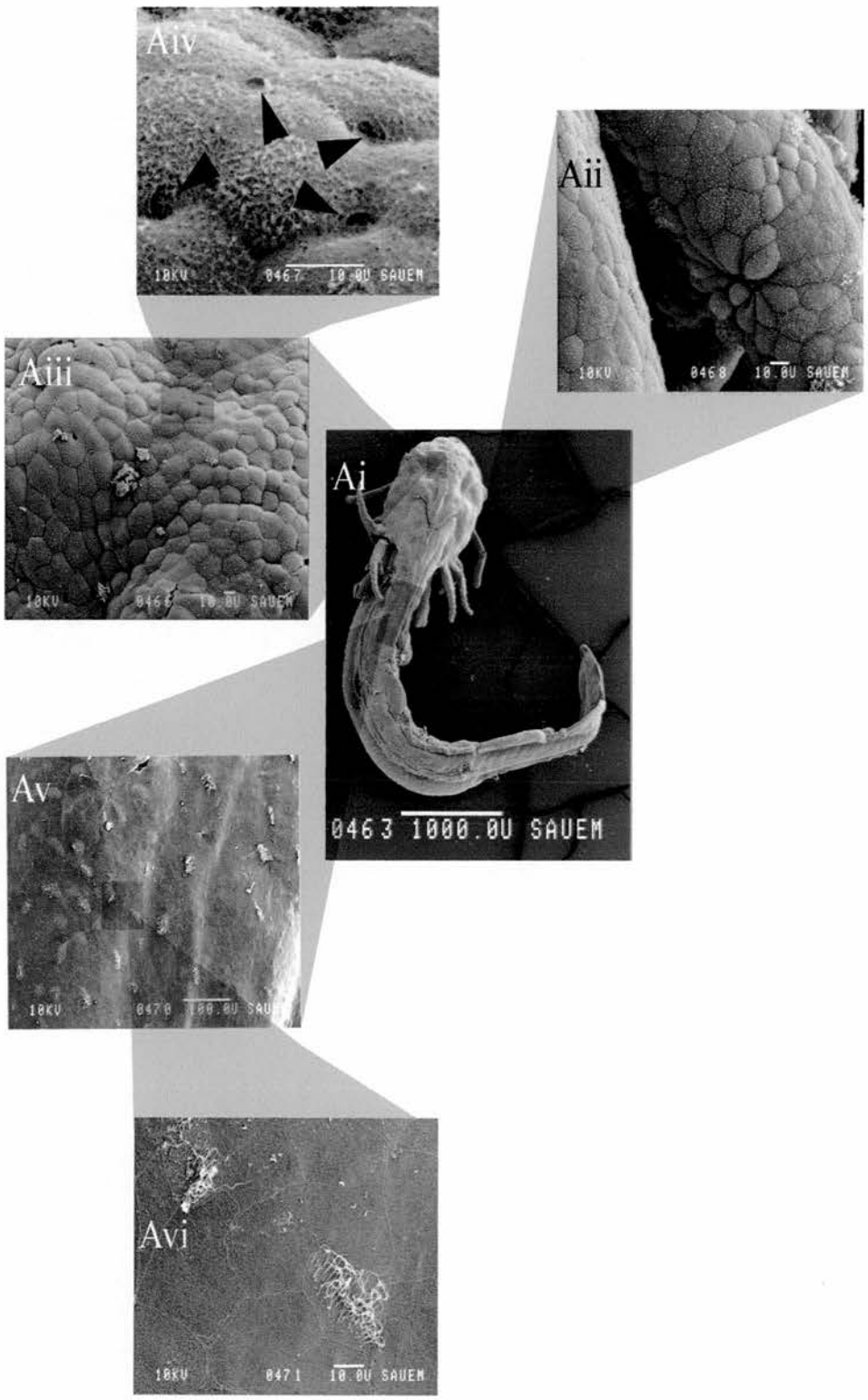

Figure 3.3. 6 (A) SEM images of a hatchling *Triturus* embryo. (Ai) Entire animal. (Aii) Enlargement of gill skin from (Ai) at x780. Aiii and Aiv are enlargements of skin on the head from (Ai) at x400 and (Aiii) at x3200, respectively. Arrow heads indicate 4 pores surrounding a single skin cell. Av and Avi are enlargements of the dorsal skin from (Ai) at x200 and (Av) at x1200, respectively. Scale bars show 1 mm (Ai), 100 μm (Av), and 10 μm (Aii, iii, iv, vi).

Investigation into an endogenous source of NO in the skin

NADPH Diaphorase histochemistry

The preceding pharmcalogical data using the NO donor, SNAP, raises the possibility that endogenously released NO could modulated the excitability of the skin. In addition, a previous study using the NADPHd technique provided preliminary evidence for NOS expression in the epithelium of both *Xenopus* (McLean and Sillar, 2001) and *Rana* (McLean et al., 2000). Therefore, the following experiments were conducted in part to replicate previous findings and further extend knowledge on the location of NOS and NO production in the skin. Initially, using the NADPHd technique in *Xenopus* embryos, specimens were both cross-sectioned and prepared in wholemount including excised skin patches. The pattern of NADPHd staining found in cross-sections at stage 42 replicated the findings of McLean and Sillar (2001, data not illustrated) and in addition revealed strong labelling in only a few cells in the skin, interspersed with many cells that displayed either weak staining or not staining at all.

Thus, cross-sections suggested only a sporadic occurrence of NADPHd-positive skin cells in the epithelium. To confirm this finding, excised skin patched were isolated from both wild-type and albino stage 37/38 *Xenopus* embryos and stained with the NADPHd technique. In both wild-type (n=2; Figure 3.3.7) and albino embryos (n=9, Figure 3.3.8), a population of skin cells stained positively. This punctate pattern of staining was observed over the entire surface of the epidermis. The proportion of labelled cells was approximated by counting the stained cells in a given area taken from 2 wild-type and 2-albino embryos, and this suggest an average of approximately 18 % (± 2.4%, S.E.M.) staining. Areas around the edge of the skin patch usually stained completely blue, which was attributed to tissue curling and overlap. However, this could be evidence that potential NOS-positive cells are involved in wound healing (see Discussion, Chapter 4).

Although not investigate in detail, preliminary experiments using the NADPHd technique were performed on *Triturus vulgaris*, a related amphibian species, to determine whether the cells of the skin might also act as an endogenous source of NO. In relation to *Xenopus*, far fewer cells stained positive, but evidence of staining was still present. Skin cells of *Triturus* showed relatively lighter staining throughout the epidermis. Unlike the punctate patterning of *Xenopus,* dark staining was found around the edges of several cells that shared common divisional boundaries, creating an intercellular density. Additionally, but to a different extent than *Xenopus*, several large densities within cells were found, showing a halo of staining around the cells, bleeding out concentrically. This suggests that another related amphibian species has a skin-specific source for NO. Since the pattern of expression observed is less defined, it is unclear as to what its function might be in relation to skin excitability, as *Triturus* were not found to exhibit a skin impulse (see Results, Section 1).

nNOS immunocytochemistry

Although it is generally accepted that the NADPHd technique labels NOS, a more direct method using NOS immunocytochemistry was performed to provide additional evidence. In addition, NADPHd is a non-specific marker of NOS isozymes, whereas immunocytochemistry can be used to more specifically identify the NOS isozyme present in skin cells. Due to the embryological origins of the epidermal germ layer (and availability of antibodies in the laboratory) an nNOS antibody was used on excised pieces of skin from 3 animals. The fluorescent marking (red) indicative of positive staining for the nNOS enzyme was found in stage 37/38 embryos (n=3; Figure 3.3.9). An

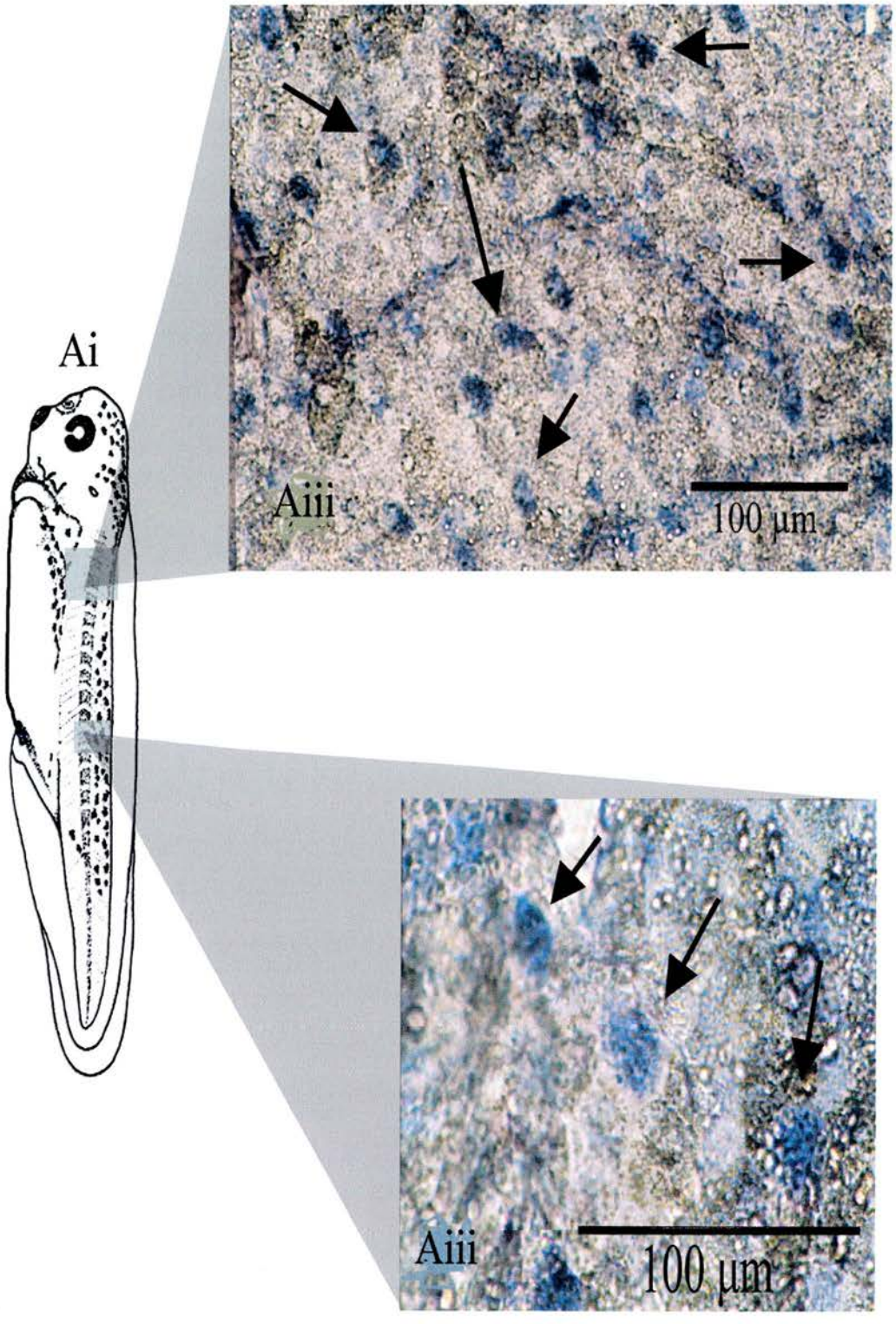

Figure 3.3. 7 Drawing of a stage 37/38 *Xenopus* embryo (i; Nieuwkoop and Faber, 1956). (ii-iii) Excised skin patch of a stage 37/38 wild-type *Xenopus* embryo stained using the NADPHd technique. Punctate pattern of staining (dark blue) viewed at x40 (ii) and x100 (iii). Arrows indicated examples of labelled cells. Scale bars show 100 µm.

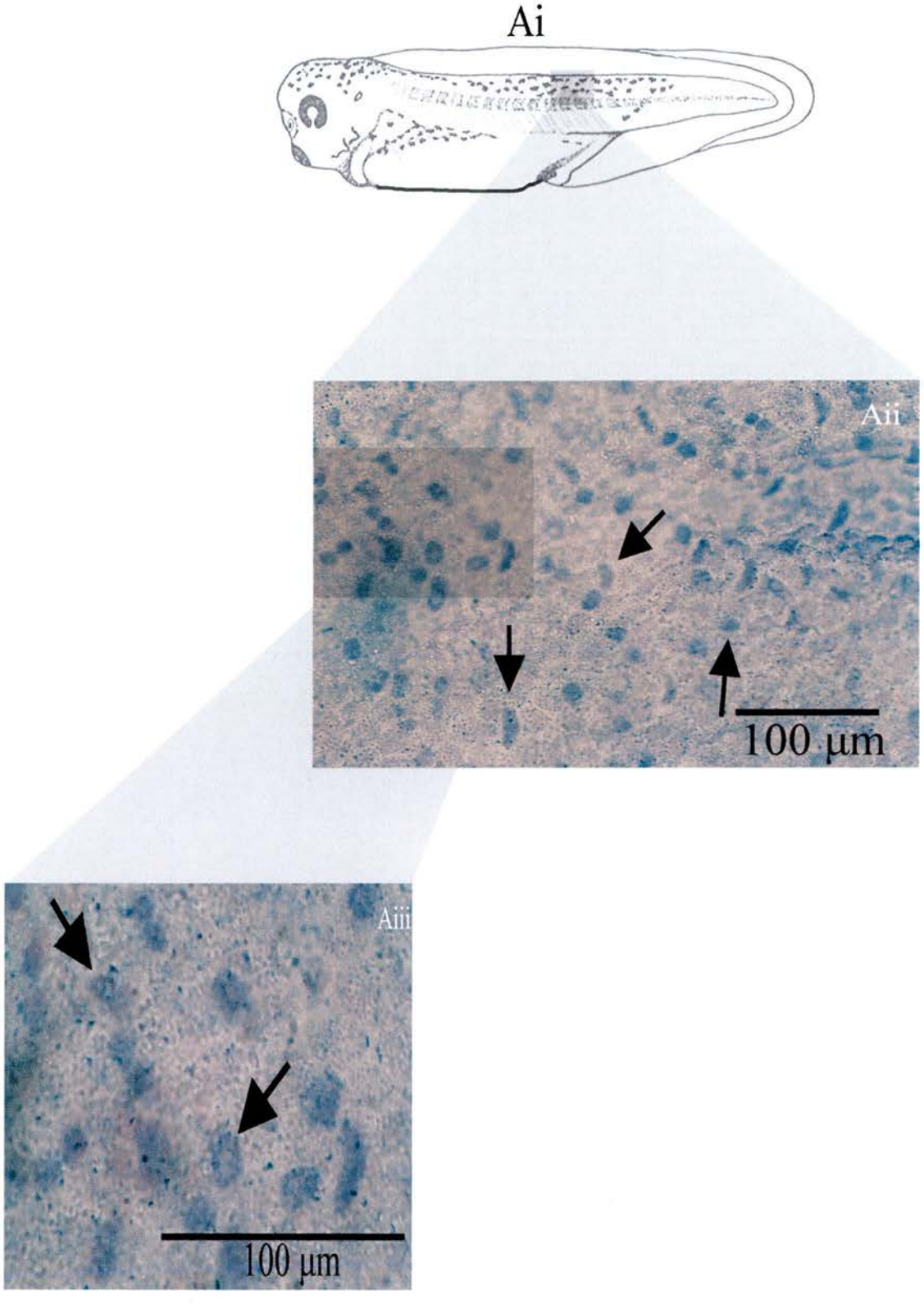

Figure 3.3. 8 Drawing of a stage 37/38 *Xenopus* embryo (i; Nieuwkoop and Faber, 1956). (ii-iii) Skin patch of a stage 37/38 albino *Xenopus* embryo stained using the NADPHd technique. Punctate pattern of staining (dark blue) viewed at x40 (ii) and x100 (iii). Arrows point to stained cells. Scale bars show 100 µm.

irregular patterning was observed in all skin patches and this distribution was very similar to that found using the NADPHd technique. Individual cells fluorescing red also show localized intracellular densities of staining, suggesting a production of NOS enzyme which is specific to subcellular organelles (Figure 3.3.9 Av). In one control preparation, where the primary antibody was excluded, but the fluorescent secondary antibody was included, no fluorescence was observed. This suggests that the staining observed in the skin is specific to nNOS.

DAF Fluorescence

The preceding experiments using NADPH and nNOS immunochemistry strongly suggest that a sub-population of skin cells is capable of generating NO which, in turn, is capable of modulating skin cell excitability. To investigate further whether NO is produced by cells in the skin, stage 37/38 *Xenopus* embryos were treated with the fluorescent probe DAF-2 DA, a cell-permeable analogue of DAF-2. Within the cell, NO binds DAF-2 to form DAF-2 T, which can be viewed using a fluorescent microscope. Confocal microscopy was used to obtain images of wholemount embryos displaying fluorescence in the skin. Green fluorescence, indicating the presence of NO, was found in cells dispersed over the entire surface of the animal in wholemount preparations (n=4). The clearest fluorescent signal was found in the skin cells localized to the dorsal fin of the tadpole, where only skin cells are present (Figure 3.3.10 Ai). However, the punctate pattern of green staining in the skin was also observed in other such regions as the ventral fin and yolk sac (Figure 3.3.10 Aii). Excised pieces of skin were also treated with DAF-2 DA, and found to display positive staining (n=6; Figure 3.3.11). As in single cells stained for nNOS, several densities of green fluorescence were localized to particular subcellularcompartments (Figure 3.3.11 A iv, v), which may indicate NO production

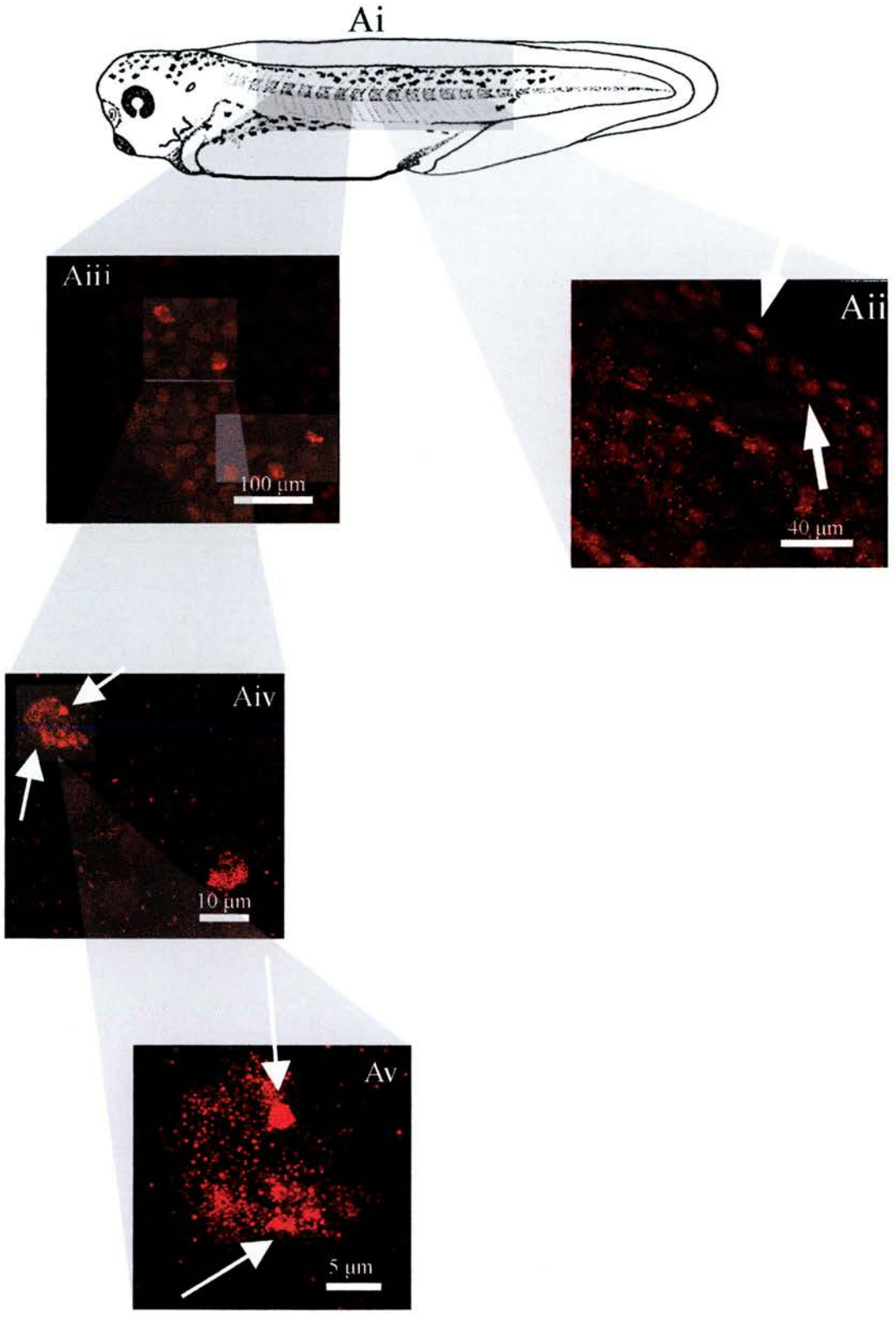

Figure 3.3. 9 (Ai) Drawing of a stage 37/38 *Xenopus* embryo (Nieuwkoop and Faber, 1956). (Aii-v) Confocal images showing nNOS immunofluorescence in an excised skin patch. (ii) arrows point to individual cells exhibiting staining (red). (Aiii-v) Successive enlargements displaying an irregular pattern of NOS-positive (iii, bright red, x10) to a single cell (v, x63 (x10.95 zoom). (iv-v) arrows point toward possible subcellular compartments staining. Scale bars = 40 (ii), 100 (iii), 10 (iv), and 5 (i) µm.

from specific organelles such as mitochondria, for example. Thus, the appearance of DAF fluorescence in the skin suggests that skin cells are capable of producing NO, presumably using the NOS enzyme. It is this NO, localized to the skin, which could be released to alter the excitability of the skin. It is notable that the punctate distribution and proportion of NADPHd-, nNOS-, and DAF-positive cells are all very similar, not just to each other but also relative to the ciliated cells seen under SEM (see Discussion, Chapter 4).

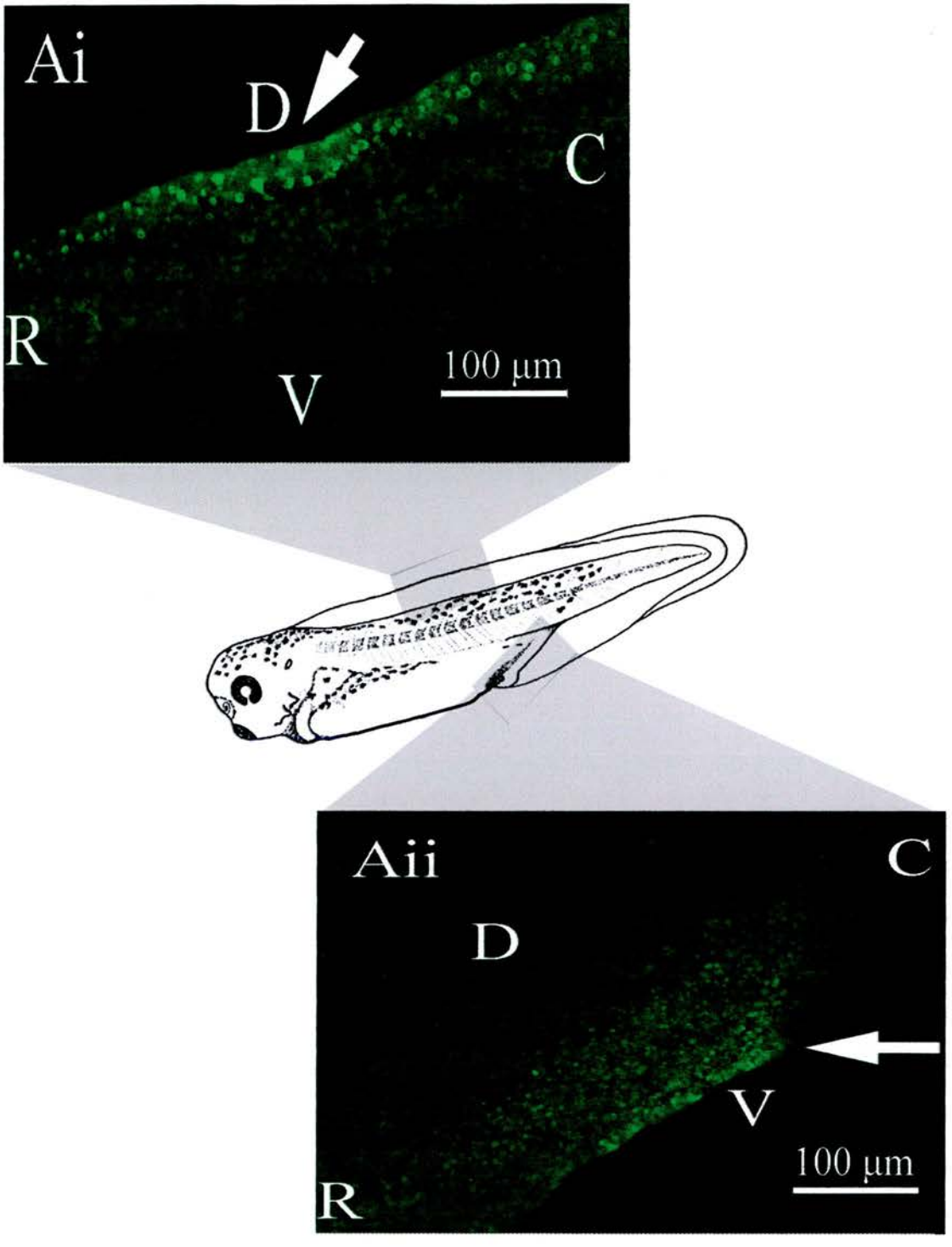

Figure 3.3. 10 Drawing of a stage 37/38 *Xenopus* tadpole (center). (A) Confocal image of a wholemount preparation showing DAF fluorescence in a stage 37/38 *Xenopus* embryo at x10. Green fluorescence indicates positive staining along the dorsal fin (i, arrow) and yolk sac (ii, arrow). R, rostral; C, caudal; D, dorsal; V, ventral. Scale bars = 100 µm.

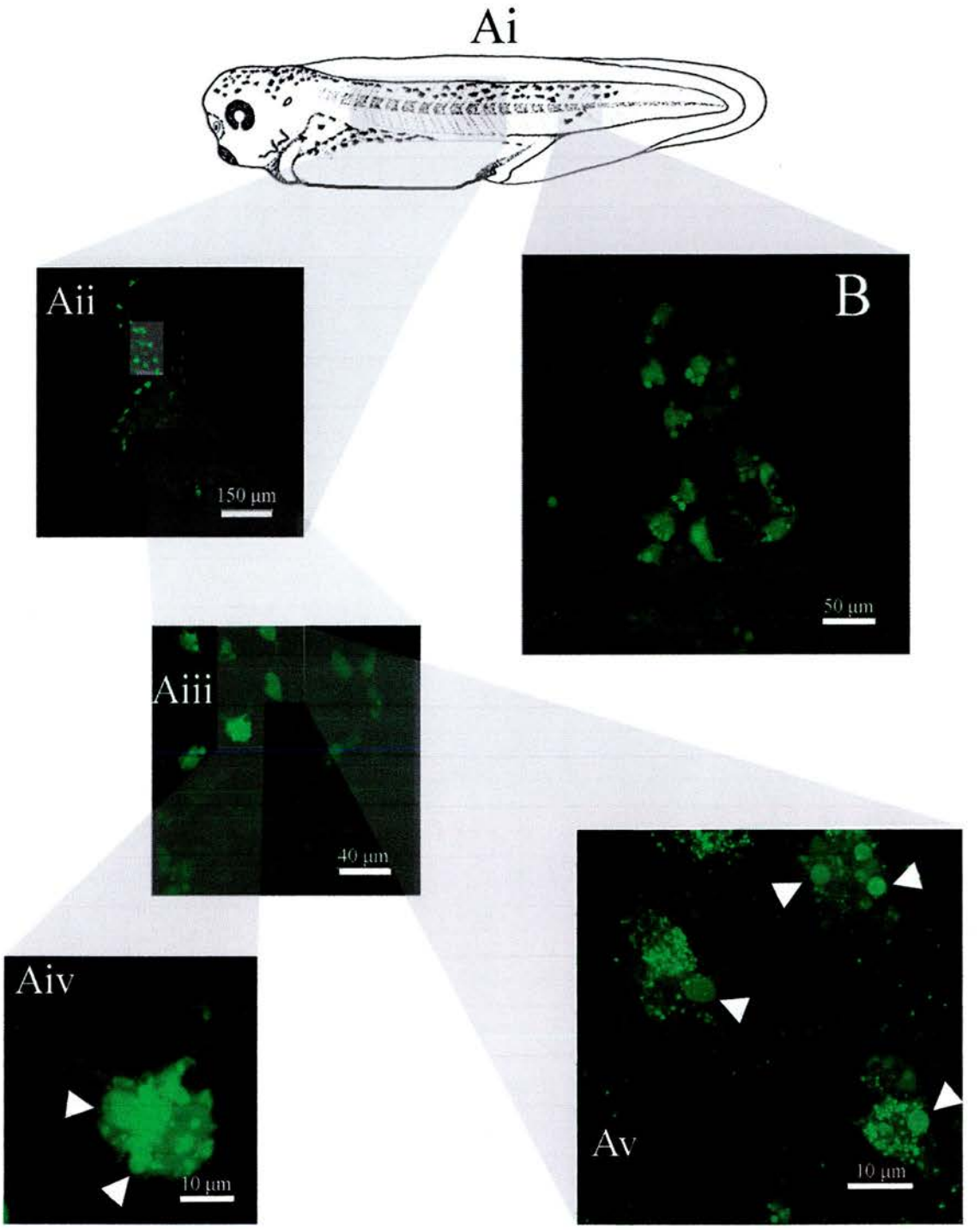

Figure 3.3. 11 (A-B) Confocal images showing DAF fluorescence in two 37/38 *Xenopus* embryos. (Ai) Drawing of a stage 37/38 tadpole (Nieuwkoop and Faber, 1956). (ii-v) Successive enlargements from a skin patch (ii, x10) to single cells (iv, x20 (x16 zoom); v, x63) showingfluorescence (green). (iv) arrow heads point toward potential areas of subcellular localisation of NO. (B) Punctate pattern of fluorescence (green) in another patch of skin at x20. Scale bars = 150 (Aii), 50 (B), 40 (Aiii), and 10 µm (Aiv,v).

Chapter 4 – Discussion

Summary

The aim of thesis was to examine various neuroactive substances localised to the skin of *Xenopus* embryos and determine if they were sufficient or necessary modulators of the skin impulse. In doing so, several previous findings were confirmed and several novel electrophysiological, and immunocytochemical properties of tadpole skin were discovered.

Initial experiments by Roberts (1971) explored the properties and propagation of the skin impulse in *Xenopus*; characterizing both the anatomy of skin cells and the waveform of the impulse, and positing the possibility that it may propagate by direct current flow through low resistance junctions between cells (i.e. GJs). The experiments described in this thesis confirmed that the skin impulse is cardiac-like in appearance, having a fast rise, followed by a sustained shoulder phase that is much longer in duration. In addition, the skin impulse of two other species, namely *Rana* and *Bufo*, was examined and found to exhibit similar properties to that of *Xenopus*. Surprisingly, the tadpole of another related species, *Triturus*, was examined for the existence of a skin impulse, which was not found despite the presence of a negative resting potential in skin cells.

Although Roberts (1971) describes both the superficial and deep layers of *Xenopus* skin as having a negative resting potential, this thesis provides evidence to suggest that each layer exhibits a characteristically different impulse. The waveforms of impulses in the deep layer are typically faster in rise and longer in duration. Impulses are conducted faster across the epidermis in the deep layer than in superficial layers. The waveforms of the skin impulse was shown to be highly sensitive to rapid stimulation, whereby frequencies above 1 Hz dramatically increase the delay while simultaneously

decreasing the duration of the impulse. This reflects the two common properties of the impulse and they exhibited the most distinct changes in all preparations. Surprisingly, experiments with *Rana* showed very little change in the impulse in response to high frequency stimulation. The main parameters of the skin impulse, conduction delay and impulse duration, typically were found to increase during the course of an experiment. Gradual changes in pH or temperature was ruled out as the underlying cause, as was the possibility of increasing suction from the stimulating electrode. However, the irreversibility of this upward trend provided an essential marker for differentiating endogenous increases in either parameter from bath-applied drug effects.

Several pharmacological agents were used in order to examine the possible modulation of the skin impulse. Experiments with the gap junction blocker 18-β-GA, were intended to quantify effects that would be seen due to GJs uncoupling between skin cells, but no consistent effects were seen. The time course of its action, or possibly the efficacy of its access to the skin cells are possible reasons why no effect was detected. The effects of bath-applied 5-HT, SP and their related antagonists or potential downstream targets were variable and thus it proved impossible to conclude if these modulators had a role in skin impulse propagation.

In contrast, reliable effects were seen with the NO donor SNAP (i.e. increased delay and duration). Furthermore, these effects were reversed by the NO scavenger, C-PTIO, suggesting that the SNAP-induced effect was due to a release of NO. However, the intracellular mechanisms underlying NO effects have yet to be confirmed. Subsequent experiments sought to find an endogenous source of NO in the skin through the use of the NADPHd technique, nNOS immunocytochemistry, and DAF fluorescence.

All three techniques verified the localisation of NADPHd, nNOS enzyme, and NO, respectively, within certain cells of the epidermis. Taken together, the data presented in this thesis point to NO as a potent modulator of the skin impulse in *Xenopus laevis*.

Time-dependent effects

A persistent hurdle to understanding the basic properties of the skin impulse sensory system, which presented itself through the course of experiments, was the change observed in both conduction delay and impulse duration. Time-dependent changes in delay and duration could involve the response of the skin to lesions which occurred while securing the preparation and dissecting the tadpole (i.e., pinning through the notochord, and removing the flank skin). However, the increase of conduction delay and duration also occurred in preparations in which skin lesions were minimized (see Introduction Chapter 1), although the notochord was pinned in both preparations types. This suggests that the changes in both of these impulse properties were not related to the skin lesion, but could reflect a general property in the continual growth and development of skin at this stage. However, two findings point to alternative mechanisms underlying this change: (1) rapid wound healing in *Xenopus* at this stage (Yoshii et al., 2005a; Yoshii et al., 2005b), and (2) the very dense staining of NADPHd found in excised skin preparations. Each could provide an additional explanation for the effects seen in delay and duration. The likelihood and validity of each of these possibilities is discussed below.

The conduction of the skin impulse depends upon a pathway established by the syncytium of skin cells in the epidermis. Once initiated, the skin impulse radiates in all

directions from the point of stimulation. The impulse recorded either extracellularly or intracellularly, ought to reflect the impulse that travels the most direct path across the skin from the point of stimulus on the tail to the point of recording on the head. It was assumed that this pathway length was constant throughout each experiment. However, pathway length may have been a variable parameter, subject to a number of influences including normal growth, skin lesioning and subsequent wound healing. By this logic, the pathway could change in two paradoxical ways, ultimately producing a gradual increase in the distance between stimulating and recording electrodes: (1) by formation of *de novo* skin cells, or in contrast, (2) by the lesion-induced triggering of apoptosis in the skin during the course of the preparation. The former (1) would result in a predictable increase in the number of cells through which the impulse must propagate and a corresponding increase in conduction delay. The latter (2) could lead to a gradual disruption of the pathway over the skin, insofar as the skin impulse would take a longer, less direct route, with subsequently greater time for the impulse to travel. There is reason to suggest that at this stage of development, there are many growth-related changes occurring. Gross structural changes occur within hours during the embryonic stage, particularly an increase in cell size (see Introduction, Chapter 1). Gradual changes in the rate of either cell death or growth could manifest as an increased conduction delay across the epidermis.

Wound healing

The wound healing response in the skin of *Xenopus* has been closely studied during the first 8 hours after bisecting an embryo at stage 22 (Yoshii et al., 2005a; Yoshii et al., 2005b). The resulting half embryos were found to display very rapid wound healing whereby the epidermis had covered nearly 80% of the wound area in the first 30 minutes post-wounding, and the wound had completely healed in the next 3-6 hours. The resulting healed half embryos continued to develop into half-tadpoles By applying either inhibitors of actin polymerisation (the process by which cytoskeletal proteins are elongated) or myosin-ATPase (the enzyme which catalyses the hydrolysis of actin to form myosin), wound healing progress was severely retarded, supporting an actin 'purse-string' method of wound closure (Davidson et al., 2002). Using SEM, the response of the epidermal tissue was monitored immediately after bisection revealing a pattern of changes: (1) a retraction of the epidermis and roughening of the individual cells in the wound zone, with both deep and superficial layers increasing in roundness or height, and (2) the initiation of wound closure beginning after 3 minutes, indicated by a reversion of cells to a smooth shape, reducing in thickness as they flatten and spread over the wound region. Ultrastructural observation indicated that the epidermis moved as a sheet of tissue, as opposed to the migration of individual cells. This type of cell movement is likened to epiboly, the morphogenetic movement of the epidermis over the mesoderm during gastrulation (Gilbert, 2003). This confirmed that the wound closure is mediated by cytoskeletal motility, and that the epidermal tissue undergoes a mass movement of cells in a short time span. There is reason to suggest that both the purse-string and protrusive method of wound healing act in a synergistic manner (Davidson et al., 2002;

Yoshii et al., 2005a; Yoshii et al., 2005b). These types of changes are indicative of a very large-scale mechanism underlying wound healing, and presumably involve the incorporation of intercellular signaling in order to coordinate the movement of an entire germ layer.

Changes similar to those catalogued at stage 22 could conceivably occur at the later stage of 37/38. Cuts made in the skin of the dorsal and ventral fins before immobilisation (see Materials and Methods, Chapter 2) were observed to repair completely within 30 minutes. The rapid time scale of this wound closure is very similar to what was reported by Yoshi, et al. (2005a; 2005b). However, in none of the preparations was the skin found to repair itself after removal of both skin layers over the mytomal region. Aside from the pins which remained piercing the notochord, the lesion in the preparation involved only the removal of skin. Without damaging the other tissue layers, this might not be sufficient to induce the coordination of large scale wound healing. In fact, at stage 9 ½, Davidson et al. (2002) suggests that wound enclosure would only occur if the deeper layer of the ectoderm is left intact. Even though embryos used in experiments were always 1-2 days older, this could explain why no wound healing was observed. However, in preparations of excised skin patches (see Materials and Methods, Chapter 2), staining for NADPHd showed heavy labelling all along the edges of the skin. The density in colour relative to the internal, flatter areas of skin could have been caused by a curling of the skin at the edges. Nonetheless, if the NADPHd activity is indicative of increased levels of NOS activation in wound areas, it may imply a role for NO in wound healing or by contrast, indicate a pathological response to cuts and abrasions.

In confluent monolayers of both bovine pulmonary endothelial cells and mouse mammary epithelial cells, mechanical wounding can induce a rapid increase in intracellular free Ca^{2+}($[Ca^{2+}]_i$) in vitro (Sammak et al., 1997). The rise in $[Ca^{2+}]_i$ took the form of a propagated $[Ca^{2+}]_i$ wave which spread decrementally with constant velocity away from cells at the wound margin at a rate of 20-28 μm/sec, extending between 10 and 12 cell rows. In endothelial cells, Ca^{2+} influx from the extracellular medium was almost exclusively responsible for the rise in $[Ca^{2+}]_i$, and provides a model for a cell-to-cell-independent mechanism for the propagation of the $[Ca^{2+}]_i$ wave. It was demonstrated, however, that in epithelial cells connected by gap junctions, intercellular signaling of the $[Ca^{2+}]_i$ wave proceeded through direct flow between cells, and was mediated through the diffusion of soluble factors, like ATP, as seen in other preparations using mammary epithelial cells (Enomoto et al., 1994). The $[Ca^{2+}]_i$ wave is thought to play a role in cell motility and proliferation (reviewed in Sammak et al., 1997).

In mammals, cuts or abrasions are often associated with a subsequent inflammatory response initiated by the immune system (reviewed in Witte and Barbul, 2002): the recruitment of platelets, fibroblasts (Schwentker et al., 2002), and the movement of epithelial cells, as in *Xenopus* (Davidson et al., 2002; Yoshii et al., 2005a). Macrophages, among other cells in the humoral response, have been found to express iNOS, but evidence suggests the expression of endothelial NOS (eNOS) is just as important in wound healing. Subsequent production and release of NO by NOS affects many processes such as collagen formation (Shi et al., 2000; Shi et al., 2001), cell proliferation and wound contraction. Deletions of the iNOS gene, as seen in knock-out mice (reviewed in Butler and Nicholson, 2003), retards the wound healing response,

whereas exogenous application of NO and arginine (a metabolic precursor essential to the production of NO via NOS; Shi et al., 2000) enhances healing (reviewed in Witte and Barbul, 2002). However, even though it is stated that qualitative differences in the healing of incision-induced wounds in wild-type compared to iNOS knock-out mice are unapparent (Most et al., 2002), exogenous arginine can still enhance wound healing (Shi et al., 2000). This suggests that wound healing in mice can be iNOS-independent, and constitutive isoforms (i.e. eNOS and nNOS) may play a role.

Given the variety of effects triggered by skin lesioning, it seems plausible that a wound inflicted on a stage 37/38 *Xenopus* embryo could trigger a rise in $[Ca^{2+}]_i$, propagated in the form of a wave, that is simultaneously facilitated by the skin impulse (which is the response to noxious stimuli; see Introduction, Chapter 1), in the epithelial cells of the epidermis from the wound margin (Sammak et al., 1997). Increases in cytoplasmic Ca^{2+} itself in moderate levels can cause GJs to uncouple (reviewed in Evans et al., 2006). In addition, the wave can flow directly from cell to cell via GJs in addition to soluble, paracrine 2nd messengers. Ciliated epithelial cells in lungs have been shown to exhibit inositol 1,4,5-trisphosphate ($InsP_3$)-induced Ca^{2+} release from intracellular stores in response to mechanical stimulation (Sanderson et al., 1990). This suggests that $InsP_3$ acts as an intercellular messenger, mediating communication through GJCs in ciliated epithelial cells, and thus could parallel the response to mechanical stimulation or injury in *Xenopus* skin cells. Additionally, a paracrine messenger such as ATP released from epithelial cells (Enomoto et al., 1994; Sammak et al., 1997), has been shown to regulate both CxHcs and GJs through a Ca^{2+}-induced ATP activation of membrane-bound, G-coupled receptors to further activate an $InsP_3$-dependent mechanism (reviewed in Evans

et al., 2006; see Figure 1.11). Also, mechanical stimulation can release ATP which triggers Ca^{2+} release via P_2 purinoreceptors in mammary epithelial cells (Enomoto et al., 1994). Within this very diverse and comprehensive intercellular signalling cascade, Ca^{2+} via a calmodulin (CaM)-dependent mechanism could activate NOS, elevating levels of NO (Newman et al., 2004; Gribovskaja et al., 2005; Shirran et al., 2005; Spratt et al., 2006). The propagation of Ca^{2+} waves at several points within the epidermis could potentially lead to a global increase in NO concentration. I turn, NO through either the cGMP or cAMP pathway, could induce gap junction uncoupling.

Certainly, experiments with SNAP have shown that NO can increase the conduction delay for impulse propagation (discussed below). Evidence for GJ regulation via NO/cGMP-dependent and –independent pathways is numerous, and is found to involve different effects depending on the system and cell-type (Fessenden and Schacht, 1998), with increasing importance being placed on connexin specificity (Kameritsch et al., 2003; Kameritsch et al., 2005; Yao et al., 2005; Patel et al., 2006). NO has been shown to produce coupling effects on Cx43 in mesangial cells (MC; Yao et al., 2005), uncoupling effects on Cx35 in HeLa cells (epithelial cells from a cervical carcinoma expressing transfected human umbilical vein endothelial cell (HUVEC) Cxs; Patel et al., 2006), *de novo* formation of HeLa cell Cx40 (Hoffmann et al., 2003), and concurrent *de novo* formation of Cx40 proteins, with uncoupling of Cx37, in HeLa cells (Kameritsch et al., 2003). Other systems in which the NO/cGMP pathway exhibits GJ uncoupling effects are found in the developing rat sensorimotor cortex (Rorig et al., 1996) and the H_2 horizontal cells of the bass retina (Lu and McMahon, 1997). Functional localisation of sGC was also found in the amacrine cells of the turtle retina using cGMP-like

immunoreactivity (cGMP-LI) after exposing cells to SNAP or spermine adduct (nitric oxide; Blute et al., 1998). As supported by Mills and Massey (1995), the cGMP-LI which was observed is indicative of the regulated integration of cone bipolar cells (BPs) by rods. In the retinal system, rods are directly coupled to BPs via AII-type amacrine cells, which are also coupled to other amacrine cells in series. Pharmacological evidence suggested the presence of two 2nd messenger pathways responsible for uncoupling, working in parallel on two different junctional connections within the same cell: (1) a dopamine (DA)-dependent uncoupling via cAMP between adjacent AII amacrine cells, and (2) a NO/cGMP-dependent uncoupling between AII amacrine cells and BPs. This clearly shows the diverse nature of 2nd messenger-related effects on gap junctional coupling. The only immediate similarity in the aforementioned systems known to display NO-mediated effects on connexins, is that NO is not regulating GJs directly, but indirectly via 2nd messenger cascades, in a connexin-, cell-, and species-specific manner. However, both the variety of possible pathways for regulating gap junctions, and the presence of NOS, and NO in the skin of *Xenopus*, strongly suggests that through one of these mechanisms, NO could be uncoupling GJs. A possible method by which this uncoupling effect could then manifest itself is through an increase in the conduction delay of the skin impulse across the epidermis. A complex and far-reaching signaling cascade via wound-induced release of NO from within the skin could then potentially result in a rapid and progressive closure of GJCs, appearing in experimental preparations as a continual and irreversible increase in conduction delay of the skin impulse.

NO and apoptosis

As mentioned above, the wound-induced activation of NOS, and subsequent release of NO in *Xenopus* embryos, could also be responsible for programmed cell death (apoptosis). This pathogenic response would be fundamentally different from the thyroxine-induced NOS activation and apoptosis seen during metamorphosis (Kashiwagi et al., 1999; discussed below). As reviewed in Choi et al. (2002) and Weller (1997), the effect of NO production is biphasic and entirely concentration-dependent, having (1) anti-apoptotic consequences at low levels and (2) pro-apoptotic consequences at higher levels (e.g. in response to an NO donor). The latter (2) is found to occur in several cell types including macrophages, thymocytes (T cell precursors derived from the thymus), pancreatic islets, some neurones, and tumor cells. The induction of apoptosis in these cells involves a complex integration of several factors including the mitochondrial membrane protein, cytochrome C, whose NO-induced release from mitochondria leads to a caspase (a cysteine protease)-dependent apoptotic signalling cascade. NO combines with mitochondrial superoxide to form cytotoxic peroxynitrite (Tsikas, 2004), which can lead to increased expression of the tumor suppressor gene, p53, inducing cell cycle arrest. Pro-apoptotic responses to NO can be inhibited with either ODQ or a protein kinase G (PKG) inhibitor, demonstrating the dependence on the sGC/cGMP/PKG pathway in the induction of cell death. The former (1) is purported to act via both cGMP-dependent (i.e. to decrease $[Ca^{2+}]_i$) and –independent pathways in several cell types including hepatocytes, lymphocytes, and endothelial cells (reviewed in Choi et al., 2002). There is also evidence that in the presence of NO, S-nitrosylation can modulate the cysteine in the active zone of the caspase catalytic site. S-nitrosylation is a mechanism in which proteins

(e.g. caspase) are regulated through modification of sulfhyrdyl groups, and by which NO can directly inhibit apoptosis by preventing the caspase-induced apoptosis cascade.

Additionally, NO-induced apoptosis can be initiated via intracellular Ca^{2+} increase through T-type Ca^{2+} channels (Liao et al., 2003). In hypertensive episodes occurring in cardiomyocytes, NO is generated via stretch-induced influx of Ca^{2+}. L-NAME (non-specific NOS isozyme inhibitor) blocked the activation of iNOS, but not eNOS, and elimination of intracellular Ca^{2+} prevented increases in both iNOS and NO elevation (Liao et al., 2006). In this system, the stretch-induced Ca^{2+} response leads to eNOS activation, possibly through a CaM-dependent mechanism (Shirran et al., 2005). iNOS is then activated in response to the rise in eNOS-induced NO production, ultimately leading to cardiomyocyte apoptosis through one of the possible mechanisms mentioned above. Interestingly, GJ coupling can be linked to apoptosis in granulosa cells (a slowly developing tumor cell that usually affects the ovaries; Ngezahayo et al., 2005). Through application of ODQ, the induction of apoptotic reactions ensued, including DNA-strand breaks and chromatin condensation. This suggests a cGMP-dependent uncoupling, although it was never verified. Instead, it was suggested that GJ uncoupling inhibits the transport of NAD^+ between cells, which when depleted within cells, can disrupt the mitochondrial membrane, triggering a caspase-dependent or -independent pathway for induction of apoptosis. The validity of this apoptotic mechanism, and its role in *Xenopus* skin could further elucidate the mechanism by which an endogenous increase in conduction delay is related to NO and programmed cell death. However, treatment of tadpoles with L-NAME (1mM) had no effect on the continual increase in either conduction delay or duration (as discussed below). Further research will be

necessary to better understand how the technique of the experimental preparation is affecting the propagation of the skin impulse.

Skin impulse waveform

Initial experiments by Roberts (1971) showed that the skin impulse is Na^+-dependent, as it is abolished in the presence of TTX. In cardiac action potentials, Ca^{2+} influx acts as the single channel conductance responsible for the prolonged repolarisation phase of the impulse (Silverthorn, 1998). Additionally, the cardiac action potential and skin impulse exhibit similarities in waveform and subsequently, an underlying fundamental function (Roberts, 1971). The long duration resulting from the influx of Ca^{2+}, greatly increases the length of the refractory period. The behavioural implication is that the cells will exhibit refractoriness at higher frequencies, which serves to regulate beating in the heart and escape responses in the tadpole (i.e. flexion or swimming), avoiding "useless flutter" (Roberts, 1971). However, despite the latter similarity and very similar waveforms, Ca^{2+} is thought not to be responsible for the repolarisation phase of the *Xenopus* skin impulse. Bath-applied 10mM Mn^{2+} (an inhibitor of Ca^{2+} currents), would be expected to reduce the duration of the skin impulse. After the cell becomes depolarised in response to Na^+ influx, an outward, voltage-sensitive cation channel is likely responsible for repolarising the cell back towards its negative resting potential. Generally, depolarisation-activated K^+ currents act to quickly repolarise the cell during this phase of an impulse (Kandel et al., 2000). In cardiac cells, a slow, inward Ca^{2+} current acts to sustain the depolarisation by combating the K^+ current, thereby greatly increasing the duration of the action potential. Instead, Mn^{2+} was reported by Roberts (1971) to have "produced only a slight change in the skin impulse," with the example

provided only displaying a slight increase in duration, the opposite of the predicted effect. Three possibilities are apparent which could explain these findings: (1) Mn^{2+} does not inhibit the specific type of Ca^{2+} channel found in tadpole skin, (2) a different conductance could be responsible or (3) the drug was unable to achieve sufficient access to the inner membrane of the skin cells where the current generating the impulse is thought to flow (Roberts, 1971). In increasing concentrations of Mn^{2+} between 2 -10 mM, the expected change to an impulse as seen in the frog ventricular muscle fibre, is the gradual decrease in the rate of rise, a decrease in the overshoot above 0 mV, and a decrease in the plateau (repolarisation) phase. However, there is evidence that extracellular Ca^{2+} is required for impulses generated in isolated frog skin (Finkelstein, 1964). Decreasing the concentration of Ca^{2+} in the bathing solution to 0 greatly increased the threshold for impulse activation, whereas greater concentrations lead to a reversible increase in the duration of the repolarisation phase, and a shortened refractory period. Nevertheless, various concentrations of Mn^{2+} were also reported to have no effect on the impulse (Hagiwara and Nakajima, 1966).

There are several channels identified in oocytes of related amphibian species which, if paralleled in *Xenopus*, could explain the basis for the waveform of the skin impulse. The toad oocyte is reported to have a Cl^- conductance which contribute to the impulse generated across its membrane (reviewed in Shepherd, 1981). Theoretically, a depolarisation-activated outward Cl^- conductance could produce the same waveform as a depolarisation-activated inward Ca^{2+}conductance, if the intracellular Cl^- concentration were large enough. A similar effect could be produced by the outward rectifying voltage-dependent K^+ channel in *Bufo bufo* and *Rana esculenta* oocytes (Peres et al., 1985; Yao

et al., 1992). In *Xenopus* oocytes, both a voltage-gated Ca^{2+} channel (Molotkovskaia and Skoblina, 1999) and a Ca^{2+}-inactivated Cl^- channel (Amasheh and Weber, 1999) could account for the repolarisation phase in embryos The latter could explain why Mn^{2+} have little effect on both the embryonic (Roberts, 1971) and adult skin impulse (Finkelstein, 1964). In this case, an inhibition of the Ca^{2+} current could relieve the inhibition on an outward Cl- current which could then act to retain cell depolarisation. However, this would presumably cause a change from the normal ionic properties of the impulse, and possibly lead to an even longer impulse, which was not seen by either Roberts (1971) or Finkelstein (1964). Given the ineffectiveness of Mn^{2+}, the ionic properties of the *Rana* pipiens oocyte points to a more plausible sequential combination of currents. These oocytes are found to have an action potential generated by Na^+, and outwardly rectified by a K^+ followed by Cl^- conductance (Schlichter, 1989). The fundamental properties of this impulse could provide evidence for the nature of the other underlying ionic properties of the *Xenopus* embryonic skin impulse, although clearly this requires further investigation.

Pharmacological Investigations

The present hypothesis is that neuroactive substances produced in the skin (i.e. amines, peptides, and NO) might act to modulate the skin impulse, either by acting on the biophysical properties of single cell membranes or on the propagation of the impulse from cell to cell via direct current flow through gap junction intercellular communication (GJIC). Previous studies have shown that the GJ blocker carbenoxolone (CBX) produced an increase in conduction delay (K.T. Sillar and W.J. Heitler, personal communication). However, CBX is notoriously non-specific. Therefore experiments were performed with

18- β-GA (75-100 μM), a more specific GJ blocker, but no change was found in the skin impulse delay or duration. Higher concentrations of 18- β-GA (up to 150 μM) caused physical deterioration and shedding of skin. If skin cells in *Xenopus* embryos form a syncytium through GJIC, then a GJ uncoupler would be predicted to show a dramatic increase in the conduction delay of the impulse across the skin. Decreasing the opening probability of a GJC ought to effectively increase the distance over which the skin impulse must travel from an initiation point on the tail to a rostral recording point. Assuming that all GJs would not be simultaneously closed, an increase in the proportion of GJCs closed at any given time would create a less direct pathway over the skin and cause an increase in delay.

The absence of a significant increase in the rate of delay under 18-β-GA, could be due to the time-course of 18-β-GA action. It has been reported that in a spinal cord preparation of *Xenopus* embryos, 18-β-GA may require 45-60 minutes to exert an effect (H. Zhang, personal communication). Due to this relatively slow time-course of action, the drug may have been unsuitable to display significant changes in the slope of the impulse delay. Furthermore, the irreversible binding of 18-β-GA also makes any effect difficult to discern, as a slow increase in delay which does not reverse also occurs in control conditions. Previous extracellular experiments have shown an increase in delay by approximately 40 ms in the presence of carbenoxolone (Sillar, 2005; personal communication). Due to the faster time course of CBX (20-40 minutes), and its reversibility at 100 μM concentrations (Winmill and Hedrick, 2003), it is more likely that its effect on delay in the skin impulse is due to the uncoupling of epidermal GJCs.

Prompted by a report of 5-HT immunoreactivity displayed in *Xenopus* skin cells at larval stage 42 (Blades, 1993; see Introduction, Chapter 1), the effects of serotonin (5-HT) on the skin impulse were examined. Monoamines such as 5-HT and DA are widely known as intercellular modulators of GJIC in several systems, including but not limited to, H1 horizontal cells of the turtle and bass retina (Piccolino et al., 1984; Lasater and Dowling, 1985), and rat somatosensory cortex (Rorig and Sutor, 1996). In the retina, GJs play a significant role in light adaptation, facilitating horizontal cell center-surround antagonism in variable levels of light (reviewed in Katz, 1999). In response to daylight, $_{L}$-glutamate release is reduced from photoreceptors, causing cells to hyperpolarize. This inhibitory signal spreads laterally for long distances through GJs. In order to avoid redundant signals in visual processing, the lateral inhibition develops around the center region of the receptive field. By contrast, in low level light, the lateral inhibition and subsequent center-surround antagonism are relieved as an adaptive mechanism though the release of DA (Lasater and Dowling, 1985). Here, DA acts through the activation of AC, increasing intracellular cAMP, which activates protein kinase A (PKA) to uncouple gap junction channels via phosphorylation (Lasater, 1987). This effect manifests in the reduction in both the duration and the frequency of channel openings (reviewed in Katz, 1999).

In the developing rat neocortex, thalamocortical neurones are pruned during a short period of raphe-mediated serotonergic up-regulation in primary sensory areas (reviewed in Rorig and Sutor, 1996). It has been shown that pyramidal neurones are extensively coupled by GJs and are modulated by 5-HT. In contrast to DA in the retina, 5-HT acts via the activation of a 5-HT_2 metabotropic receptor, initiating a rise in

intracellular Ca^{2+} via its release from intracellular stores through the 2nd messenger $InsP^3$ (Rorig and Sutor, 1996). Ca^{2+} bound to protein kinase C (PKC) then acts to phosphorylate GJs, causing their closure (Rorig and Sutor, 1996). Like DA, 5-HT also acts to uncouple cells in the nervous system. With this understanding, it seemed plausible that 5-HT localised to certain skin cells of *Xenopus* embryos, could also be released in a similar fashion to produce a change in GJ coupling. However, the investigation of serotonergic modulation of the impulse showed no significant change in the delay or duration from the characteristic rise seen in control animals. Even though, 5-HT is thought to be produced in larval skin cells (Blades, 1993), and has been demonstrated to be produced and secreted from adult *Xenopus* skin (van der Veerdonk, 1960; Mueller et al., 1980; Bennett et al., 1981; Seki et al., 1989), exogenous application did not appear to induce any changes.

However, certain anticipated serotonergic changes in the CNS were also not observed in my experiments. For example, it has been shown that the threshold for activation of swimming via the skin sensory pathway dramatically increases in the presence of 2 μM 5-HT (Sillar and Simmers, 1994). In control, stimulation of the skin excites not only skin cells but also primary afferent R-B sensory neurones, which release excitatory amino acids (EAA; i.e. glutamate) onto dorsolateral interneurones (dLi) (reviewed in Sillar and Simmers, 1994). Application of 5-HT is believed to mimic the effects of descending medullary raphe neurones, which presynaptically inhibit the release of EAA transmitters from R-B terminals at the R-B – dLi interface (Sillar and Simmers, 1994). The fact that no significant effect of 5-HT was found on swimming threshold even at 100 μM may indicate that the stock of 5-HT used in the present experiments was

inactivated, possibly due to its sensitivity to light. Additionally, Blades (1993) found that 25 minutes after bath-application of 100 μM 5-HT, the threshold for skin impulse initiation increases from 1 to 4 V, and by 30 minutes, reached 15 V. He also noted an increase in the impulse failure following high frequency trains of stimuli, which could be overcome to an extent by increasing the stimulus voltage. These observations are suggestive of a similar effect of 5-HT on both the skin impulse and R-B neurones, although presumably by different mechanisms. In the skin, 5-HT is most likely secreted as an autocrine or paracrine messenger, which still could modulate GJs through one of the various 2nd messenger pathways (described below).

However, even though effects with 5-HT were not found, it does not eliminate the possibility that 5-HT affects GJ coupling. Using the uncoupling of GJ by monoamines as a model, whereby DA uncouples horizontal bipolar cells in the retina (Lasater, 1987), a cell- permeable activator of AC, forskolin (100 μM), was used in order to activate a potential 2nd messenger cascade to uncouple purported GJs in the skin. The addition of forskolin is intended to increase intracellular levels of cAMP, increasing PKA activation to directly gate potential GJs via phosphorylation (Rorig and Sutor, 1996). In the present experiments, significant increases in the slope of the delay in the presence of forskolin suggest that the skin impulse may be modulated by cAMP, insofar as the activation of AC could lead to decreased coupling between skin cells. However, the two other findings with forskolin, namely the irreversible and significant increase in the average delay and duration, detract from the possibility of forskolin exhibiting an effect (see Figure 3.2.1). Both of these factors display similar trends to what is observed in control animals (see Results, Chapter 3). Whereas impulse duration may not necessarily be

modulated by increased cAMP levels, the average delay would be expected to increase in the presence of forskolin and decrease after the return to control saline. However, an increase in delay would not reverse if AC activation could be responsible for long-term changes to intercellular coupling, namely the internalisation of connexin proteins, and ultimately GJCs (Evans et al., 2006; see Figure 1.10). The reduction in the number of GJs between cells could account for an irreversible increase in delay, however, as can be seen in Figure 3.2.1 A, the delay does begin a notable decrease approximately 25 minutes into the wash. More experiments are clearly necessary in order to reconcile these rather ambiguous results, but at this stage it remains possible that 5-HT modulates junctional coupling via a cAMP-dependent pathway.

Substance P (SP)-like immunoreactivity is present in the unmyelinated neurites and free nerve endings of R-B neurones (Clarke et al., 1984), but the function of SP release both within the CNS, and peripherally within the skin is still unknown in *Xenopus* embryos. In the retina of several vertebrate species, SP is expressed by amacrine, interplexiform, and ganglion cells (Casini et al., 2002). In the fish retina, Djamgoz (1996) showed that inhibition of SP by SP antibodies causes increased coupling in horizontal cell somas. In this system, SP is purported to facilitate the release of DA (Laufer et al., 1981), which uncouples retinal horizontal cells (Djamgoz et al., 1996). Additionally, as SP is the natural agonist for neurokinin 1 (NK1) receptors, NK1 immunoreactivity was performed in the rabbit retina, showing localisation to both a population of ON-type cone bipolar cells (a type of bipolar cell which is excited when stimulated in the center of its receptive field; Kandel et al., 2000), and dopaminergic amacrine cells (Casini et al., 2002). The proximal localisation supports a functional

interplay between both messengers. A model of the system suggests that light-induced release of SP binds NK1 receptors to release DA from tyrosine hydroxylase (TH; a subtype of amacrine cells) amacrine cells, either via direct synaptic transmission, or as a paracrine messenger. TH amacrine cells are then thought to directly modulate AII (type II) amacrine cells, which are electrically coupled to ganglion cells. As SP stimulates DA release, and since DA is known to be involved in light-adaptation in other retinal systems (Lasater, 1987), SP is then possibly involved in the modulation of light adaptation in the rabbit (Casini et al., 2002). The retinal spatial properties provide a model in which a monoamine (i.e. DA) is acting to directly uncouple gap junctions through stimulation by SP. Given the cutaneous location and potential release of SP in peripheral tissues of *Xenopus* embryos, SP could stimulate the release of 5-HT from skin cells, to lead to GJ uncoupling, or act directly on non-serotonergic skin cells.

However, in the presence of SP, no significant changes in any of the parameters measured were seen. In fact, opposing trends were at times seen between animals, leading to the large error bars during SP applications (see Figure 3.2.2), and suggesting that there was no consistent drug effect. Swimming episode duration and cycle period were also monitored in SP experiments as there is one report that SP (2-5 μM) leads to a reversible decrease in swimming cycle period (Lebofsky, 2002). However, repeated experiments showed conflicting results with increases, decreases and no changes observed. It was also suggested by Merrywest and Sillar (2003) that SP at this concentration can increase sensitivity of the skin to electrical shocks; a single shock typically elicits one skin impulse, but multiple impulses were seen to be generated in the presence of SP. Additionally, SP was reported to increase the occurrence of spontaneous

skin impulses (i.e. impulses with no preceding electrical stimulus). While the occurrence of both multiple stimulated and spontaneous impulses was not consistently observed, spontaneous episodes of swimming did appear to increase in frequency in the presence of SP. However, due to the prevalence of spontaneous episodes in control periods, and the irreversibility of the effect, it was difficult to discern if this could be attributed to an effect of SP, or an intrinsic excitability of the animal within the context of the preparation.

The NK_1 receptor antagonist, L-732,138 was applied both on its own to inhibit the effects of any endogenously released SP (see Materials and Methods, Chapter 2), and in the presence of SP to establish if this caused an opposing effect in the trends of delay and duration between agonist and antagonist periods. However, the increasing trend in delay and the reversible decrease in duration found in the presence of L-732,138 dissolved in 1% (v/v) ethanol were the same as effects observed in the presence of 1% ethanol alone. This suggests that effects observed were vehicle-related, and not caused by L-732,138. Thus, no evidence was found to suggest that SP was acting to affect either GJIC or impulse waveform.

In pursuit of an endogenous modulator of the skin impulse, experiments with NO donor, SNAP, provided the most consistent and reliable results. Thus, four important findings have emerged, showing that SNAP: (1) reversibly increases the conduction delay of the propagating skin impulse across the epidermis, (2) produces a fast, large and reversible increase in the duration of the skin impulse, (3) causes a reversible membrane depolarisation, and (4) that SNAP-induced release of NO and its subsequent effects on delay, duration, and resting membrane potential are reversed by C-PTIO. Some SNAP

experiments were performed while cells in each of the two presumed skin layers were being recorded. The results showed that the cells of the superficial layer are modulated in the same manner as deep cells. Superficial cells were recorded as having longer delays relative to deep, whereas deep cells exhibited a much larger increase in duration. It is not yet clear whether cells of the different layers of skin exhibit different impulses, or if it is simply dependent upon which type of skin cell from the superficial or deep layer is being recorded. However, by virtue of the fact that deep cells are found below superficial cells, and two jumps in resting potential are recorded by the electrode as it travels through the skin, a difference between layers seems likely. In fact, Mackie (1970) found that neuroid impulses of the *Hydromedusae* may conduct independently between ectodermal and endodermal layers. However, neuroid impulses in *Xenopus* are only found in the ectoderm, and within this germ layer, exist the two layers of epithelial cells. Thus, it is yet to be proven conclusively whether the differences in impulses were solely related to the two layers in *Xenopus* skin.

The SNAP effects on delay suggest that elevation of bath NO concentration is sufficient to cause a widespread uncoupling effect on the GJs between the cells of the skin. If the cells are indeed coupled by GJs (Roberts, 1971), then it is plausible that NO may either be directly or indirectly gating the opening probability of GJCs. Beginning in the oocyte, many connexins are expressed in *Xenopus* (Levin and Mercola, 2000; Landesman et al., 2003; see General Introduction, Chapter 1). During amphibian development, cells of the developing spinal cord (neuroblasts) and ectodermal cells are extensively coupled to each other, before losing coupling between germ layers after the closing of the neural tube (reviewed in Kandler and Katz, 1995). Still, neuroblasts do

retain GJIC, establishing the first form of neuronal communication. They remain coupled until development of the early spinal cord (stage 42), when uncoupling is thought to be responsible for the development of asynchronous bursts involved in the synaptic drive for swimming (Makino, 2005). However, at the embryonic stage, it is unknown if tadpoles retain connexins from before neurulation, within the cells of the skin. It is conceivable that if GJIC is found in the spinal cord at this stage, then the skin may remain coupled as well. Given the potential for NO to uncouple GJs in other system (Fessenden and Schacht, 1998; described above; Kameritsch et al., 2003; Kameritsch et al., 2005; Yao et al., 2005; Patel et al., 2006; described above), it remains possible that the SNAP-induced release of NO leads to an uncoupling effect in the skin at stage 37/38. Additionally, there is reason to believe that SNAP at lower concentrations, hence a lower NO bath concentration, might produce a coupling effect. While monitoring the skin impulse delay in SNAP experiments, the rapid increase (uncoupling) was always preceded by an initial decrease (coupling) in delay, perhaps as NO concentration begin to increase (see Figure 3.2.11), which is supported by the biphasic effect of NO in cultured keratinocytes (reviewed in Butler and Nicholson, 2003; discussed below). However, further experiments at lower concentrations of SNAP (e.g. 100 μM) are still necessary to better characterize the biphasic response to NO in *Xenopus* skin cells.

Furthermore, evidence for long-term plasticity emerged during experiments whereby the delay did not decrease after washing off the drug. Instead, delay stopped from an accelerated rate of ascent, and remained at a heightened level. In other systems for example, where synaptic plasticity occurs in the form of long-term potentiation and depression (LTP and LTD, respectively; Lev-Ram et al., 1997; Kimura et al., 1998;

reviewed in Kandel et al., 2000; Jacoby et al., 2001; Smith and Otis, 2003; discussed below), NO plays an important role as an intercellular messenger as it is rapidly produced and released to diffuse through cell membranes. As discussed before, NO could be involved in an injury response, ultimately leading to a degradation of GJs through CxHc phosphorylation (Laird, 2005). As reviewed by Sáex et al. (2005), CxHcs are gated by both the formation of disulfide bonds of cysteine residues and phosphorylation. In the normal state, disulfide bonds between adjacent cysteine residues and phosphorylated cysteine residues are reduced, which act to gate the CxHc by decreasing the opening probability (P_o). In *Xenopus* oocytes, phosphorylation of Cx46 may act to decrease P_o via protein kinase C (PKC) activation, a CaM-dependent protein kinase (Ngezahayo et al., 1998). As NO is known to activate various 2^{nd} messenger cascades responsible for phosphorylation (as discussed above), here is a possible example of how NO might act to decrease P_o of certain CxHcs, and thus GJs, thereby either temporarily, or permanently altering the propagation of the skin impulse through GJIC.

In the presence of SNAP, duration was seen to rapidly increase. The duration of the skin impulse, with its resulting waveform, is created by an underlying voltage-gated membrane fluctuation. As discussed above, the initiation of the spike is Na^+-dependent and the plateau phase is probably Ca^{2+}-independent (Roberts, 1971). The increase in duration is likely affecting the latter of the two phases of the impulse, because an alteration in influx of Na^+ ions would primarily affect the rise time. However, a delayed inactivation of the Na^+ current, while another cation is acting to repolarise the cell, could keep the cell depolarised resulting in a prolonged plateau phase. Additionally, SNAP-released NO could be responsible for blocking the conductance which is responsible for

the repolarisation phase. If, for instance, a K^+ conductance acted to repolarise the cell, a delayed activation, or partial inhibition could result in a lengthening of the duration. Another possibility is that NO, via a 2nd messenger such as cGMP or cAMP, could be acting indirectly to modulate a cyclic nucleotide-gated channel (CNG; Hofmann et al., 2005). As the possibility of NO directly gating an ion channel is unlikely, an intracellular amplification of cGMP or cAMP could be responsible for the rapid increase in duration (ca. 5 minutes after adding the drug) found in the presence of SNAP. These channels, including CNAGA1[1-3], CNAGA2[1-3] and CNAGA3[1-5] are all possible channels with high affinity especially for cGMP and cAMP. All can pass Ca^{2+}, K^+ and Na^+, with selectivity decreasing in that order. Even though selectivity is higher for Ca^{2+}, it does not negate the efficacy of a CNG channel, even though Mn^{2+} had no effect on the impulse duration (Roberts, 1971), as Mn^{2+} may not block CNG channels. Lastly, a Cl^- conductance could be responsible for the increased duration during the presence of SNAP; however, there is no evidence that the intracellular Cl^- concentration is high enough to generate a current large enough to overcome a voltage-gated depolarising conductance, like K^+. Further studies using various ion channel blockers will be necessary to further characterize the mechanism involved.

Evidence has been provided both in individual experiments and from pooled data that SNAP causes a depolarisation of the resting membrane potential (E_M). This finding is supported by findings in presumed motor neurones (pMNs) in the *Xenopus* spinal cord at stage 37/38 (McLean and Sillar, 2002). In the presence of 1 mM SNAP, pMNs were found to depolarise 5-10 mV, an effect which reversed when the drug was washed off. This depolarisation was associated with an increase in the input resistance (R_i) of the

neurones and is consistent with a decrease in a resting conductance of a K^+ "leak" channel, although no direct evidence confirming this has been reported. Similarly, the decrease in membrane potential in skin cells could also be caused by a reduction in a K^+ conductance, leading to a significant depolarisation of the E_M. Data for SNAP experiments showed statistical significance. However, SNAP– C-PTIO experiments did not explicitly identify a significant depolarisation within the SNAP period, but modulations in between SNAP and C-PTIO periods show decreased and increased resting potentials relative to control, respectively. Furthermore, results from a single skin cell held throughout the SNAP application support the conclusion that NO depolarises skin cells.

The experiments with SNAP show that an exogenous increase in bath NO concentration is sufficient to modulate the skin impulse, by increasing the delay and duration and depolarising the cell. The NO scavenger, C-PTIO, was used to confirm that the SNAP-induced effect was due to the release of NO. C-PTIO was also applied on its own to determine if endogenously released NO was responsible for the intrinsic increase of both delay and duration found during control experiments. The results of these experiments suggest that the SNAP-induced increase in delay and duration and the corresponding depolarisation in E_M are indeed the result of an increase in bath NO concentration. The SNAP-induced effect on delay, duration, and E_M always reversed in the presence of C-PTIO. Additionally, experiments with C-PTIO alone showed the removal of endogenous NO could have partially reversed the characteristic increase in delay and duration, suggesting that a slow release of NO from skin cells could be responsible for changes seen in control experiments. Further experiments attempting

both to confirm an NO-induced SNAP effect, and to explore the possible cellular mechanism of the SNAP effect are described below.

The NO donor spermine NONOate was used after observed effects on delay and duration in the presence of SNAP to act as a positive control. Ideally, in the presence of another NO donor, a similar change should occur whereby an increase in delay follows a fast increase in duration. However, this was not the case for either parameter. Delay showed a continually decreasing slope, nearly the opposite of SNAP, and duration showed a significant and irreversible increase that is indistinguishable from control experiments. There are three ways to reconcile this discrepancy between drugs effects: (1) the SNAP effect is not NO-dependent, (2) the concentration of spermine NONOate was too low or (3) the fast release of NO by spermine NONOate compared to SNAP was insufficient to generate a stable and effective concentration in the experimental period. (1) The first is unlikely because the DMSO vehicle was controlled for, and McLean (2000) showed that $_N$-acetylpenicillamine (NAP, an inactive analogue of SNAP) did not mimic the SNAP effect in relation to swimming, E_M, or conductance. (2) The second can only be reconciled through further experimentation as the EC_{50} = 6.2 mM, the half-maximal effective concentration for relaxation of rabbit aorta, at 37°C, pH 7.4 (TOCRIS) is much higher than the concentration which was used (i.e. 150 μM). (3) The third is harder to discern, as spermine NONOate is designed for a controlled release of NO with a half-life of 39 minutes, whereas SNAP is a stable analogue of endogenous S-nitroso compounds with a half-life of 37 hours. Perhaps too low a concentration of NO was released from the spermine NONOate compared to SNAP in these experiments.

Therefore, even though spermine NONOate did not mimic the SNAP effect, this is not reason enough to suggest that the SNAP effect is NO-independent.

Experiments with the non-specific NOS-inhibitor, L-NAME (1mM), were performed to test if the characteristic rise in delay and duration were caused by the production of NO from endogenous NOS in the skin or other underlying tissues. However, the results of experiments with L-NAME (1 mM) did not differ from control experiments. This suggests that neither constitutive nor inducible NOS isozymes are responsible for this time-dependent change. However, L-NAME may have been unable to reach the desired targets, especially within the skin. Additionally, since L-NAME irreversibly binds to NOS enzymes (reviewed in McLean, 2001), it cannot be tested whether removal of the inhibitor would cause an acceleration in the increase of both parameters. Thus, analogous to experiments with 18-β-GA, a reversible NOS inhibitor would be more useful in this type of experiment due to the continuing and underlying temporal change in delay and duration.

ODQ (40 μM) was applied to test the hypothesis that the SNAP-induced release of NO activated the sGC/cGMP 2nd messenger pathway to produce changes in delay and duration. ODQ triggers a train of skin impulses directly after the onset of the drug followed by a slow and long depolarisation, suggesting that ODQ does have an effect on the excitability of the skin (see Figure 3.2.13). However, it is unclear by what mechanism of action this occurs, nor why it might be a transient response, directly affecting impulse propagation. ODQ acts to inhibit intracellular production of cGMP by reversibly blocking sGC. The expected response of the tadpole in the presence of ODQ was a prevention of the increase in delay and/or duration. While delay effects were variable,

duration was observed to significantly and irreversibly increase. This change could be argued to be different from the characteristic increase found in control animals. Since the pooled data shows very little increase between ODQ and wash periods, this reflects that the duration increased during the ODQ period, and remained at a heightened value. Secondly, the increase in delay is not gradual, and repeatability of a coordinated increase suggests that it is an effect of ODQ (see Figure 3.2.12).

In animals pre-treated with ODQ, delay increases seemed to be partially inhibited, whereas duration showed prominent increases. Although not statistically significant, delay showed a small decrease in slope during ODQ periods, and very large increase in slope after the application of SNAP. This appears to indicate that ODQ is causing a slight retardation of the characteristic delay increase, but the SNAP effect can occur independently of sGC. Further evidence negating the possibility that NO is working via sGC is the highly significant and reversible increase in SNAP in the presence of ODQ. Paradoxically, however, ODQ also appears to produce a nearly stepwise increase in duration, which is smaller in magnitude than that of the SNAP-induced effect (see Figure 3.2.14). Increases in duration following application of ODQ suggest that sGC and subsequently produced cGMP are affecting the duration of the skin impulse, but it is unclear how this may be working. It is possible, as discussed above, that NO is acting through a CNG-cGMP-dependent channel, but results indicate similar effects between SNAP and ODQ, when the effects ought to be in opposition. It is difficult to reconcile the effects observed, as these data simultaneously negate the possibility that SNAP-released NO acts on sGC to produce cGMP, while supporting a role for sGC in the regulation of both delay and duration, producing a decrease and increase, respectively.

8-Br-cGMP (100-300 μM) was also applied to determine if the SNAP-induced release of NO was acting via a sGC/cGMP pathway. If this were the mechanism by which NO was acting to increase both delay and duration, then exogenously applied 8-Br-cGMP (a cell permeable cGMP analogue) ought to mimic this response. However, no significant increase in delay was found, and a highly significant and irreversible increase in duration suggests that it is no different from control experiments. It is possible that bath-applied concentrations were too low to produce a significant effect, as the large amplification of the 2nd messenger, cGMP, produced in the activation of sGC may have been grossly underestimated. Nevertheless, these data further indicate that the purported SNAP-induced increase in NO, does not act through either sGC, or it subsequent metabolite, cGMP.

Therefore, NO has a distinct effect on the skin by acting to both increase the skin impulse delay, and increase the duration of the waveform. However it is unclear how NO is acting intra- and inter-cellularly to modulate these properties. Further investigation is necessary, as there are many aspects of intracellular signalling that could fit with the present hypothesis that NO induces GJ uncoupling and affects transmembrane ion fluctuations. With this clear effect of NO in mind, studies were then turned towards finding an anatomical confirmation that NO might be released from the skin cells as an autocrine and paracrine messenger.

NO is found in the skin

The SEM study confirmed previous findings which described the ultra-structural surface of the skin. The majority of skin cells found in *Xenopus* at stages 37/38 to 42 are

roughly cuboidal to hexagonal in shape. Cells that contain and potentially secrete mucus from vesicles cannot be seen using SEM, but are reported to constitute the majority of the skin surface at the embryonic stage (Roberts, 1971). Ciliated (hair) cells sparsely cover the skin in *Xenopus*, with the highest concentration in the torso, whereas in *Rana* and *Bufo* embryos, they can be found at a much higher concentration, densely covering the entire epidermis including the finger-like gills at all embryonic stages. The heterogeneous mixture of cells in *Xenopus* skin is found to have high mucus content, suggesting that the skin may secrete the mucus. The hair cells could then act to waft the mucus over the epidermis, possibly providing a protective covering. Nevertheless, distribution of hair cells is visible as a punctate patterning over the epidermis. This type of irregular patterning is also observed in immunological studies using the PAP technique to label 5-HT-positive cells (Blades, 1993), and has now been found when cells are labelled for NO or NOS. This raises the possibility that the ciliated cells contain both 5-HT and NO.

NADPHd histochemistry is a technique used to localize putative NOS-containing cells. It was found to label a sub-population of skin cells, but its specificity for NOS can be unreliable (reviewed in McLean, 2001). The NADPHd technique relies on the fact that the NOS enzyme is uniquely resistant to formaldehyde fixation. However, there is some evidence that NADPHd and NOS immunocytochemical staining do not overlap completely in the rat pituitary (Wang et al., 1997). Thus, care must be taken in attributing NADPHd staining to the localisation of NOS. This notwithstanding, the NADPHd reactivity found in cross sections of skin by McLean (2001) and the further identification of labelling in excised skin patches presented in this thesis, support the

possibility that NOS is localised to a sub-population of skin cells. Staining was found in both wild-type and albino patches of excised skin, with staining being much clearer in the latter; due to absence of skin pigmentation in albino skin, any coloration in the skin is a direct result of the NADPHd technique

The appearance of nNOS immunofluorescence in excised skin patches confirmed the presence of NOS in skin cells of *Xenopus* embryos at stage 37/38, with the pattern of staining being similar to the punctate staining of NADPHd. Furthermore, the findings using DAF fluorescence (discussed below) suggest that the NOS present in these cells is biologically active, confirming an endogenous source of NO. Because the patterning of nNOS immunofluorescence is also similar to the punctate staining of the DAF fluorescence, this indicates that NO may be produced in the same cells as nNOS. Furthermore, in vertebrates, the skin is derived from the ectodermal tissue. This earlier germ layer also differentiates into nervous tissue. Thus, nNOS present in skin cells at stage 37/38, may be retained from synthesis at earlier stages in development. During the time of gastrulation, cells could be primed with the NOS enzyme before eventually diverging to become part of the spinal cord where NOS is expressed at early embryonic stages (McLean and Sillar, 2001), or part of the epidermis as represented by the nNOS immunofluorescence. The possible retention of nNOS from an earlier stage in development suggests that other cellular characteristics like connexins and their resulting intercellular GJs also present in the early embryo (reviewed in Mackie, 1970; Warner, 1985; Kandler and Katz, 1995; Levin and Mercola, 2000; Landesman et al., 2003) could be retained through the late embryo stage. This is of great consequence, as the presence of gap junctions beginning at stage 22 when the skin impulse is first found (Roberts,

1971), would support Roberts' theory that the impulse propagates through the skin by direct current flow through low-resistance junctions.

Of particular appeal in the pattern of staining observed in both wild-type and albino preparations using NADPHd and nNOS immunocytochemistry is the punctate pattern and widespread distribution. This bears a striking resemblance to the pattern of ciliated cells found on the skin using the SEM. As of yet, there is no evidence linking NADPHd reactivity to hair cells, as hair cells could not be resolved under a light microscope. However, the colocalisation of ciliary and NADPHd staining could provide evidence for a potential function of ciliary cells, or a role for NOS in ciliary function. In either case, the widespread distribution of NADPHd reactivity throughout the skin provides an important clue that NOS might be produced by certain cells, and thus serve as an endogenous source for the production of NO.

In light of the presence of NOS in skin cells, DAF fluorescent marking was used to visualize the endogenous production of NO in skin cells. Cellular staining observed using confocal imaging showed similar result to the staining observed using NADPHd and nNOS immunocytochemistry. In patches of excised skin, a punctate pattern of staining was found, suggesting that NO is present in some, but not all skin cells. This is consistent with the distribution of NADPHd and nNOS staining, and suggests that the two may colocalize in the skin. DAF fluorescence has previously been found in *Xenopus* tadpoles at the hatchling stage, also displaying a punctate pattern of staining in wholemount preparations (Waddington, 2005). However, the staining that is observed cannot be distinguished from cells staining in other tissue layers below the skin. The excised preparation used in this present thesis confirms that cells of the skin specifically

contain NO, further supporting that NOS may be present and physiologically active in the epidermis at this stage in development. Again, the pattern of DAF fluorescence resembles the pattern of ciliated cells, suggesting that they may also be co-localised. Moreover, the exact location of reputed sources of NO in the skin are yet to be confirmed.

Several DAF fluorescent images of individual *Xenopus* skin cells are consistent with previous findings showing possible subcellular compartmentalisation of NO (Saini et al., 2006). In rat polymorphonuclear neutrophrils (PMNs; a common type of phagocytotic granulocyte with 3 to 5 nuclear lobes involved in the immune response), subcellular areas such as the nucleus, perinuclear region, and cytoplasm showed segregated DAF fluorescence. Although PMNs are much larger than *Xenopus* skin cells, approximately 40 and 10 μm, respectively, their granular makeup may suggest similarities in cell infrastructure. The punctate pattern of DAF fluorescence described by Saini et al. (2006) was reported to diffuse from regional densities within 20-30 minutes, but still exhibited defined areas of cell staining. After both PMNs and *Xenopus* skin cells are fixed (Saini et al., 2006; see Materials and Methods, Chapter 2), DAF-2DA loading is confined to the cells in which it enters, permanently marking these cells, and thus preserving the DAF-labelled NO topography. As DAF fluorescence is believed to be a sufficient marker for the presence of intracellular NO, its presence in cells further supports findings using nNOS and iNOS immunocytochemistry, whereby colocalisation of both isoforms was found in PMNs (Saini et al., 2006), and localisation of solely nNOS immunofluorescence in *Xenopus* skin cells. The identification of endogenous NO through DAF labelling suggests that NO is being released as an autocrine or paracrine

messenger. Its distribution across the epidermis is consistent with the diffusion properties of NO as a gaseous molecule through tissue layers. NO can be responsible for a variety of changes in the cells it reaches before becoming inactivated, with ranges reported at 150 μm in parallel fibres of the cerebellum (Jacoby et al., 2001), equating approximately to 15 cell diameters in *Xenopus* embryonic skin. NOS-derived NO can be simultaneously produced along with O_2^- (superoxide), thus forming peroxynitrite ($ONOO^-$), which subsequently degrades into nitrite and nitrate (Tsikas, 2004). In other tissues such as the vertebrate hippocampus and cerebellum, NO is known to act as a retrograde messenger, responsible for producing large-scale effects on synaptic plasticity such as long-term potentiation or long-term depression (LTD; Lev-Ram et al., 1997; Kimura et al., 1998; Jacoby et al., 2001; Smith and Otis, 2003), respectively. The former has implications for long-term spatial learning, whereas the latter is implicated in motor learning (reviewed in Kandel et al., 2000). Following a tetanus (a train of action potentials), both models of LTP and LTD have been proposed to involve the release of NO. In LTP, retrograde release of NO from post-synaptic terminals in CA1 pyramidal neurones leads to a sustained increase in post-synaptic response, whereas in LTD, as found in Purkinje neurones of the cerebellum, NO facilitates a sustained decrease in post-synaptic response. In the cerebellum, NO-stimulated modulations in neuronal firing are associated with differing mechanisms and involvement of 2nd messenger signaling cascades. Neuronal firing rate has been shown to increase in response to NO via a cGMP-dependent pathway, whereby NO activates the enzyme soluble guanylyl cyclase (GC) to convert guanosine triphosphate (GTP) into cGMP (Smith and Otis, 2003). Similarly, but in a reverse manner, NO released from parallel fibers and Purkinje

neurones can trigger LTP through a cAMP-dependent pathway (Kimura et al., 1998; Jacoby et al., 2001). The LTP response was induced through the addition of forskolin, a cell-permeable activator of adenylyl cyclase (AC), which converts ATP into cAMP, and prevented through the use of the NO scavenger C-PTIO. These findings bear a striking similarity to pharmacological investigations in skin impulse modulation using the NO donor SNAP and the NO scavenger, C-PTIO.

The presence of NO is found widespread across the vertebrates. In humans, the presence of NO in the skin has numerous implications for protection against infection and disease pathology (reviewed in Butler and Nicholson, 2003). Keratinocytes, which are the most common cell in the epidermis, produce NO and hydrogen peroxide when stimulated by cytokines. This response could be a possible defense mechanism against bacteria or fungi that could penetrate the epidermal barrier if cut. In the pathological condition, psoriasis (a chronic disease of the skin marked by red patches with white scales), stimulation of iNOS leads to elevated levels of NO. However, it is unclear whether this activation of iNOS is a symptom of the diseased condition, or an attempt of the immune system to combat the distress. In cultured keratinocytes, a biphasic response to NO is observed; low concentrations lead to enhancement of cell proliferation and high concentrations increase cell differentiation, a possibility that may occur in *Xenopus* (see above). However, fibroblasts, which are found in the dermis (inner layer of skin), respond differently to NO (reviewed in Weller, 1997). This suggests that a delicate balance in NO concentration and the subsequent location of NO in the epidermis is necessary for homeostasis.

Ultraviolet B (UVB) irradiation is found to stimulate iNOS in keratinocytes, with prolonged activation even after exposure has ceased. The exact mechanism of how UVB light stimulates NO production is unknown, but NO has several roles in response to UV-induced tumours, including vasodilatation to provide increased blood flow (Bruch-Gerharz et al., 1998). UVB irradiation is known to be a major stimulus in the production of skin pigmentation. Radiation activates a paracrine pathway, whereby NO-stimulated keratinocytes produce cGMP, which triggers the release of melanin from melanocytes (another common cell type in the epidermis). This identifies the NO/cGMP as a cross-species mechanism underlying epidermal cell intracellular signaling, as possibly exists in *Xenopus*.

Furthermore, NO has been implicated in wound healing in mice (reviewed in Butler and Nicholson, 2003). Knock-out mice that lack a copy of the gene which is responsible for synthesising iNOS experience severe impairment in wound healing. As part of the biphasic response to NO, new keratinocytes are important in forming new tissue to replace that which is damaged in the wound. In addition, new blood vessels are formed, suggesting a functional role for iNOS in both cell proliferation and angiogenesis. Wound healing has been investigated in *Xenopus* embryos (Davidson et al., 2002; Yoshii et al., 2005b, I & II), but not specifically linked to NO. Surprisingly, a NOS-independent source of NO exists in the sweat secreted from skin cells. Certain bacteria which possess the enzyme nitrate reductase, can act to convert secreted nitrates into NO. Additionally, the acid content of the skin can act to protonate nitrite to form NO and H_2O. Both of these methods of NO generation, in addition to NO released from keratinocytes, can act as a protective mechanism against pathogenic bacteria (Butler and Nicholson, 2003).

In a related species to *Xenopus*, *Triturus italicus*, the endothelial isoform of NOS (eNOS) is reported to stain heavily in the larval epidermis (Brunelli et al., 2005). The observed immunofluorescence for eNOS begins to disappear in pre-metamorphic and metamorphic periods with a simultaneous rise in staining of the inducible isoform of NOS (iNOS). This suggests that in *T. italicus*, a switch occurs in the developmental cycle, and NOS-derived NO may be responsible for the remodelling of skin cells during the metamorphic period. The developing tadpole synthesizes thyroid hormone, thyroxine (T^4), in the thyroid gland. T^4 is then released into the circulatory system to reach peripheral tissues where type II iodothyronine deiodinase (D2) converts thyroxine (T^4) to the active hormone 3,5,3'-triiodothyronine (T^3) (Cai and Brown, 2004). An increase in thyroid hormone levels is known to precede the onset of metamorphosis, and exogenous exposure to T^4 can trigger premature metamorphosis through the elevation of D2 levels. T^4 increased NOS activity in cells of the tail of the pre-metamorphic *Rana japonica* tadpole, leading to premature degradation (Kashiwagi et al., 1999). In tadpoles treated with N-monomethyl-L-arginine (NMMA), a NOS-inhibitor, the tail degradation effects enhanced by T^4 were suppressed. An NO donor had a similar effect to T^4, suggesting that thyroxine enhances NO production via NOS, leading to apoptosis in the tail. In *Xenopus*, transgenic tadpoles expressing a dominant negative thyroid hormone specifically in their skin, develop normally with the exception of their larval skin which is arrested in development and retained over the developing adult epidermis (Schreiber and Brown, 2003). Therefore, the activation of NOS in peripheral tissues (i.e. the tail) shows clear links to apoptosis of skin cells and metamorphosis. This suggests a distinct functional role for NOS presence in the skin of larval *Xenopus* tadpoles.

To a different extent, pre-metamorphic and metamorphic roles for NOS and the production of NO have been suggested in the CNS of *Xenopus*. The pattern of staining found by NADPHd and nNOS immunofluorescence in the developing nervous system is spatiotemporal, with progressive staining found in the brainstem and in the spinal cord until the forelimbs appear (McLean and Sillar, 2001; Ramanathan et al., 2006). The progressive appearance of different clusters of NADPHd-positive neurones in the brainstem suggests that from embryonic to pre-metamorphic periods, NO plays a persistent role in larval development (McLean and Sillar, 2001). Subsequent experiments provided evidence for nitrergic modulation of both GABAergic and glycinergic inhibitory neurones which influence the rhythms of fictive swimming in larval tadpoles (McLean and Sillar, 2002). Bath-application of SNAP (100 – 500 μM) was found to inhibit swimming through facilitation of both γ-aminobutyric acid (GABA) and glycine release. This produced a reversible depolarisation in E_M and decreased membrane conductance (1 mM). Additionally, bands of NOS-positive neurones in the spinal cord of pre-metamorphic tadpoles are localised to areas excluded from future limb development, possibly implicating that NO may inhibit differentiation in the inter-limb areas (Ramanathan et al., 2006).

Various developmental roles for NOS and the production of NO could be simultaneously active in different regions of the *Xenopus* embryos. Therefore, because putative NOS-containing cells have previously been found (McLean and Sillar, 2001), and several new markers have localised nitrergic activity in the skin of developing embryos (i.e. DAF and nNOS immunofluorescence), NOS and the production of NO may be affecting development of the skin directly at embryological stages. The

pharmacological findings of this thesis provide new evidence for NO-induced modulation of the skin impulse and neuroid sensory pathway of the skin.

Future directions

Given the plethora of apparent changes in the developing *Xenopus* embryo, there are many possible avenues for future studies, including but not limited to:

(1) The localisation of GJ in skin cells would provide useful information to have regarding the propagation of the skin impulse and could support the present theory of how NO is affecting the skin cells. With the use of gap junction specific antibodies, immunocytochemistry could be used to mark the occurrence or absence of these proteins. Especially since GJs occupy intercellular space, fluorescence in such a location would avoid mistaking them for other intercellular proteins that might label. Furthermore, isolation of specific connexin sub-types could be achieved in a similar way, and would be useful since different connexins are known to have different properties of regulation.

(2) A simple dissection separating the two layers of the epidermis would provide conclusive evidence showing that the superficial and deep cells do in fact produce different impulses. With the layers anatomically separated, each individual layer would be easily identifiable, and subsequent intracellular recordings could be matched to either deep or superficial cells.

(3) Given the wide variety of changes that occur after skin lesions in *Xenopus* embryos, apoptosis and wound healing would be important areas to investigate. Especially because the experimental preparation relies upon lesioning the skin for immobilisation, the recording of swimming, and drug access, it is important to

know the consequences of any activated signalling cascades that have physiological consequences.

(5) Computer modelling could be useful to show how GJs work to coordinate resting potential and other homeostatic properties within a syncytium. Through simulations whereby different drugs added to the system modulate individual cells accordingly, it can then be estimated how the system will be affected when GJ are blocked, for instance.

(6) A valuable exercise would be to design a very stable experiment *in vivo* where the tadpole is monitored over several days of embryonic and larval life. This would certainly show how the skin impulse might evolve and act to regulate sensory signals of the tadpole until it disappears after stage 42. By this preparation, intrinsic changes in delay and duration could be monitored more completely to better assess the nature of these particular properties of the skin impulse. Factors such as cell growth could then better be identified as effectors on the propagation of the impulse across the epidermis.

(7) Important to the present thesis however is the colocalisation of the various fluorescent markers used to provide evidence for an endogenous source of NO in the skin. Similarly, NADPHd and 5-HT immunohistochemistry could be used to show that the cells of the skin producing 5-HT also contained the nNOS isozyme. Finally, anatomical evidence should be sought to test the hypothesis that the ciliated "hair" cells in the skin match those cells that also produce NO and, potentially 5-HT as well.

Literature Cited

Amasheh, S. and Weber, W. (1999) Further characteristics of the Ca^{2+}-inactivated Cl^- channel in *Xenopus laevis* oocytes. *J. Membr. Biol.*, **172**, 169-179.

Bennett, G. W., Balls, M., Clothier, R. H., Marsden, C. A., Robinson, G. and Wemyss-Holden, G. D. (1981) Location and release of TRH and 5-HT from amphibian skin. *Cell Biol. Int. Rep.*, **5**, 151-158.

Blades, K., J. (1993) The role of 5-HT in the generation and propagation of the cardiac-like action potentials in the skin of *Xenopus* tadpoles. BSc Honours. University of St. Andrews.

Blute, T. A., Velasco, P. and Eldred, W. D. (1998) Functional localization of soluble guanylate cyclase in turtle retina: modulation of cGMP by nitric oxide donors. *Vis. Neurosci.*, **15**, 485-498.

Bruch-Gerharz, D., Ruzicka, T. and Kolb-Bachofen, V. (1998) Nitric oxide and its implications in skin homeostasis and disease - a review. *Arch. Dermatol. Res.*, **290**, 643-651.

Brunelli, E., Perrotta, I., Talarico, E. and Tripepi, S. (2005) Localization of two nitric oxide synthase isoforms, eNOS and iNOS, in the skin of *Triturus italicus* (Amphibia, Urodela) during development. *Comp. Biochem. Physiol. A Mol. Integr. Physiol.*, **142**, 249-255.

Butler, A. and Nicholson, R. (2003) *Life, Death and Nitric Oxide*. Cambridge, The Royal Society of Chemistry.

Cai, L. and Brown, D. D. (2004) Expression of type II iodothyronine deiodinase marks the time that a tissue responds to thyroid hormone-induced metamorphosis in *Xenopus laevis*. *Dev. Biol.*, **266**, 87-95.

Casini, G., Sabatini, A., Catalani, E., Willems, D., Bosco, L. and Brecha, N. C. (2002) Expression of the neurokinin 1 receptor in the rabbit retina. *Neuroscience*, **115**, 1309-1321.

Choi, B. M., Pae, H. O., Jang, S. I., Kim, Y. M. and Chung, H. T. (2002) Nitric oxide as a pro-apoptotic as well as anti-apoptotic modulator. *J. Biochem. Mol. Biol.*, **35**, 116-126.

Clarke, J. D., Hayes, B. P., Hunt, S. P. and Roberts, A. (1984) Sensory physiology, anatomy and immunohistochemistry of Rohon-Beard neurones in embryos of *Xenopus laevis*. *J. Physiol.*, **348**, 511-525.

Coghill, G. E. (1924) Correlated anatomical and physiological studies of the growth of the nervous system in Amphibia. III. The floor plate of *Amblystoma*. *J. Comp. Neurol.*, **37**, 37-69.

Davidson, L. A., Ezin, A. M. and Keller, R. (2002) Embryonic wound healing by apical contraction and ingression in *Xenopus laevis*. *Cell Motil. Cytoskel.*, **53**, 163-176.

Djamgoz, M. B., Evans-Capp, A. J. and Wagner, H. J. (1996) Intra-vitreal injection of substance P antibodies as an antagonist in the vertebrate (fish) retina. *J. Neurosci. Methods*, **64**, 237-243.

Dushane, G. P. (1938) Neural fold derivates in the Amphibia: Pigment, spinal ganglia and Rohon-Beard cells. *J. Exp. Zool.*, **78**, 485-503.

Enomoto, K., Furuya, K., Yamagishi, S., Oka, T. and Maeno, T. (1994) The increase in the intracellular Ca^{2+} concentration induced by mechanical stimulation is propagated via release of pyrophosphorylated nucleotides in mammary epithelial cells. *Pflugers Arch.*, **427**, 533-542.

Evans, W. H., De Vuyst, E. and Leybaert, L. (2006) The gap junction cellular internet: connexin hemichannels enter the signalling limelight. *Biochem. J.*, **397**, 1-14.

Fessenden, J. D. and Schacht, J. (1998) The nitric oxide/cyclic GMP pathway: a potential major regulator of cochlear physiology. *Heart Res.*, **118**, 168-176.

Finkelstein, A. (1964) Electrical excitability of esolated frog skin and toad bladder. *J. Gen. Physiol.*, **47**, 545-565.

Fox, H. (1988) Riesenzellen, goblet cells, Leydig cells and the large clear cells of Xenopus, in the amphibian larval epidermis: fine structure and a consideration of their homology. *J. Submicrosc. Cytol. Pathol.*, **20**, 437-451.

Furshpan, E. J. and Potter, D. D. (1968) Low-resistance junctions between cells in embryos and tissue culture. *Curr. Top. Dev. Biol.*, **3**, 95-127.

Gilbert, S. F. (2003) *Developmental Biology*. Sunderland, Sinauer Associates, Inc.

Gosner, K. L. (1960) A simplified table for staging anuran embryos and larvae with notes on identification. *Herpetologica*, **16**, 183-190.

Gribovskaja, I., Brownlow, K. C., Dennis, S. J., Rosko, A. J., Marletta, M. A. and Stevens-Truss, R. (2005) Calcium-binding sites of calmodulin and electron transfer by inducible nitric oxide synthase. *Biochemistry*, **44**, 7593-7601.

Hagiwara, S. and Nakajima, S. (1966) Differences in Na and Ca spikes as examined by application of tetrodotoxin, procaine, and manganese ions. *J. Gen. Physiol.*, **49**, 793-806.

Hoffmann, A., Gloe, T., Pohl, U. and Zahler, S. (2003) Nitric oxide enhances *de novo* formation of endothelial gap junctions. *Cardiovasc. Res.*, **60**, 421-430.

Hofmann, F., Biel, M. and Kaupp, U. B. (2005) International Union of Pharmacology. LI. Nomenclature and structure-function relationships of cyclic nucleotide-regulated channels. *Pharmacol Rev*, **57**, 455-462.

Hooker, D. (1911) The development and function of voluntary and cardiac muscle in embryos without nerves. *J. of Exp. Zool.*, **11**, 159-186.

Hughes, A. (1957) The development of the primary sensory system in *Xenopus laevis* (Daudin). *J. Anat.*, **91**, 323-338.

Jacoby, S., Sims, R. E. and Hartell, N. A. (2001) Nitric oxide is required for the induction and heterosynaptic spread of long-term potentiation in rat cerebellar slices. *J. Physiol.*, **535**, 825-839.

Kameritsch, P., Hoffmann, A. and Pohl, U. (2003) Opposing effects of nitric oxide on different connexins expressed in the vascular system. *Cell Commun. Adhes.*, **10**, 305-309.

Kameritsch, P., Khandoga, N., Nagel, W., Hundhausen, C., Lidington, D. and Pohl, U. (2005) Nitric oxide specifically reduces the permeability of Cx37-containing gap junctions to small molecules. *J. Cell. Physiol.*, **203**, 233-242.

Kandel, E. R., Schwartz, J. H. and Jessell, T. M. (2000) *Principles of Neural Science*. New York, McGraw-Hill.

Kandler, K. and Katz, L. C. (1995) Neuronal coupling and uncoupling in the developing nervous system. *Curr. Opin. Neurobiol.*, **5**, 98-105.

Kashiwagi, A., Hanada, H., Yabuki, M., Kanno, T., Ishisaka, R., Sasaki, J., Inoue, M. and Utsumi, K. (1999) Thyroxine enhancement and the role of reactive oxygen species in tadpole tail apoptosis. *Free Radic. Biol. Med.*, **26**, 1001-1009.

Katz, P. S. (1999) *Beyond Neurotransmission*. New York, Oxford University Press.

Kimura, S., Uchiyama, S., Takahashi, H. E. and Shibuki, K. (1998) cAMP-dependent long-term potentiation of nitric oxide release from cerebellar parallel fibers in rats. *J. Neurosci.*, **18**, 8551-8558.

Laird, D. W. (2005) Connexin phosphorylation as a regulatory event linked to gap junction internalization and degradation. *Biochim. Biophys. Acta*, **1711**, 172-182.

Landesman, Y., Postma, F. R., Goodenough, D. A. and Paul, D. L. (2003) Multiple connexins contribute to intercellular communication in the *Xenopus* embryo. *J. Cell Sci.*, **116**, 29-38.

Lasater, E. M. (1987) Retinal horizontal cell gap junctional conductance is modulated by dopamine through a cyclic AMP-dependent protein kinase. *Proc. Natl. Acad. Sci. U S A*, **84**, 7319-7323.

Lasater, E. M. and Dowling, J. E. (1985) Dopamine decreases conductance of the electrical junctions between cultured retinal horizontal cells. *Proc. Natl. Acad. Sci. U S A*, **82**, 3025-3029.

Laufer, M., Negishi, K. and Drujan, B. D. (1981) Pharmacological manipulation of spatial properties of S-potentials. *Vision Res.*, **21**, 1657-1660.

Lebofsky, R. (2002) Substance P neuromodulatory effect on motor activity. BSc Honours University of St. Andrews.

Lev-Ram, V., Nebyelul, Z., Ellisman, M. H., Huang, P. L. and Tsien, R. Y. (1997) Absence of cerebellar long-term depression in mice lacking neuronal nitric oxide synthase. *Learn. Mem.*, **4**, 169-177.

Levin, M. and Mercola, M. (2000) Expression of connexin 30 in *Xenopus* embryos and its involvement in hatching gland function. *Dev. Dyn.*, **219**, 96-101.

Liao, X., Liu, J. M., Du, L., Tang, A., Shang, Y., Wang, S. Q., Chen, L. Y. and Chen, Q. (2006) Nitric oxide signaling in stretch-induced apoptosis of neonatal rat cardiomyocytes. *FASEB J.*, **20**, 1883-1885.

Liao, X. D., Tang, A. H., Chen, Q., Jin, H. J., Wu, C. H., Chen, L. Y. and Wang, S. Q. (2003) Role of Ca^{2+} signaling in initiation of stretch-induced apoptosis in neonatal heart cells. *Biochem. Biophys. Res. Commun.*, **310**, 405-411.

Lu, C. and McMahon, D. G. (1997) Modulation of hybrid bass retinal gap junctional channel gating by nitric oxide. *J Physiol*, **499** 689-699.

Mackie, G. O. (1970) Neuroid conduction and the evolution of conducting tissues. *Quart. Rev. Biol.*, **45**, 319-332.

Mackie, G. O. and Passano, L. M. (1968) Epithelial conduction in *Hydromedusae*. *J. Gen. Physiol.*, **52**, 600-621.

Makino, H. (2005) Gap junction-mediated spike synchronization of spinal locomotor activity in *Xenopus laevis* tadpoles. BSc Honours. University of St. Andrews.

McLean, D. L. (2001) The gaseous messenger molecule, nitric oxide: a modulator of locomotor movements during early amphibian development. PhD. University of St. Andrews.

McLean, D. L., McDearmid, J. R. and Sillar, K. T. (2001) Induction of a non-rhythmic motor pattern by nitric oxide in hatchling *Rana temporaria* embryos. *J. Exp. Biol.*, **204**, 1307-1317.

McLean, D. L., Merrywest, S. D. and Sillar, K. T. (2000) The development of neuromodulatory systems and the maturation of motor patterns in amphibian tadpoles. *Brain Res. Bull.*, **53**, 595-603.

McLean, D. L. and Sillar, K. T. (2000) The distribution of NADPH-diaphorase-labelled interneurons and the role of nitric oxide in the swimming system of *Xenopus laevis* larvae. *J. Exp. Biol.*, **203** 705-713.

McLean, D. L. and Sillar, K. T. (2001) Spatiotemporal pattern of nicotinamide adenine dinucleotide phosphate-diaphorase reactivity in the developing central nervous system of premetamorphic *Xenopus laevis* tadpoles. *J. Comp. Neurol.*, **437**, 350-362.

McLean, D. L. and Sillar, K. T. (2002) Nitric oxide selectively tunes inhibitory synapses to modulate vertebrate locomotion. *J. Neurosci.*, **22**, 4175-4184.

Mills, S. L. and Massey, S. C. (1995) Differential properties of two gap junctional pathways made by AII amacrine cells. *Nature*, **377**, 734-737.

Molotkovskaia, I. M. and Skoblina, M. N. (1999) The effect of the composition of the medium on the concentration of free calcium ions in the cells of the follicular wall in the common frog and in the clawed toad. *Ontogenez.*, **30**, 229-233.

Most, D., Efron, D. T., Shi, H. P., Tantry, U. S. and Barbul, A. (2002) Characterization of incisional wound healing in inducible nitric oxide synthase knockout mice. *Surgery*, **132**, 866-876.

Mueller, G. P., Alpert, L., Reichlin, S. and Jackson, I. M. (1980) Thyrotropin-releasing hormone and serotonin secretion from frog skin are stimulated by norepinephrine. *Endocrinology*, **106**, 1-4.

Muntz, L. (1964) Neuro-muscular foundations of behaviour in embryonic and larval stages of the Anuran, *Xenopus laevis*. PhD. University of Bristol.

Newman, E., Spratt, D. E., Mosher, J., Cheyne, B., Montgomery, H. J., Wilson, D. L., Weinberg, J. B., Smith, S. M., Salerno, J. C., Ghosh, D. K. and Guillemette, J. G. (2004) Differential activation of nitric-oxide synthase isozymes by calmodulin-troponin C chimeras. *J. Biol. Chem.*, **279**, 33547-33557.

Ngezahayo, A., Altmann, B., Steffens, M. and Kolb, H. A. (2005) Gap junction coupling and apoptosis in GFSHR-17 granulosa cells. *J. Membr. Biol.*, **204**, 137-144.

Ngezahayo, A., Zeilinger, C., Todt, I. I., Marten, I. I. and Kolb, H. (1998) Inactivation of expressed and conducting rCx46 hemichannels by phosphorylation. *Pflugers Arch.*, **436**, 627-629.

Nieuwkoop, R. D. and Faber, J. (1956) *Normal table of Xenopus laevis (Daudin).* Amsterdam, North Holland Publishing Company.

Parker, G. H. (1919) *The Elementary Nervous System*. Philadelphia, Lippincott.

Patel, L. S., Mitchell, C. K., Dubinsky, W. P. and O'Brien, J. (2006) Regulation of gap junction coupling through the neuronal connexin Cx35 by nitric oxide and cGMP. *Cell Commun. Adhes.*, **13**, 41-54.

Peres, A., Bernardini, G., Mancinelli, E. and Ferroni, A. (1985) A voltage-dependent K^+ channel controlling the membrane potential in frog oocytes. *Pflugers Arch.*, **403**, 41-46.

Piccolino, M., Neyton, J. and Gerschenfeld, H. M. (1984) Decrease of gap junction permeability induced by dopamine and cyclic adenosine 3'-5'-monophosphate in horizontal cells of turtle retina. *J. Neurosci.*, **4**, 2477-2488.

Ramanathan, S., Combes, D., Molinari, M., Simmers, J. and Sillar, K. T. (2006). Developmental and regional expression of NADPH-diaphorase/nitric oxide synthase in spinal cord neurons correlates with the emergence of limb motor networks in metamorphosing *Xenopus laevis*. University of St. Andrews; Universités Bordeaux

Roberts, A. (1971) The role of propagated skin impulses in the sensory system of young tadpoles. *Z. vergl. Physiologie*, **75**, 388-401.

Roberts, A. (1996) Trigeminal pathway for the skin impulse to initiate swimming in hatchling *Xenopus* embryos. *J. Physiol.*, **493.P**, 40-41P.

Roberts, A. (1998) Amphibian Biology: Sensory Perception. *Skin Sensory Systems of Amphibian Embryos and Young Larvae*. Surrey Beatty & Sons, Chipping Norton

Roberts, A. and Smyth, D. (1974) The development of a dual touch sensory system in embryos of the amphibian *Xenopus laevis*. *J. Comp. Physiol.*, **88**, 31-42.

Roberts, A. a. S., C. A. (1971) The properties and propagation of a cardiac-like impulse in the skin of young tadpoles. *Z. vergl. Physiologie*, **71**, 295-310.

Rorig, B., Klausa, G. and Sutor, B. (1996) Intracellular acidification reduced gap junction coupling between immature rat neocortical pyramidal neurones. *J. Physiol.*, **490** 31-49.

Rorig, B. and Sutor, B. (1996) Regulation of gap junction coupling in the developing neocortex. *Mol. Neurobiol.*, **12**, 225-249.

Rorig, B. and Sutor, B. (1996) Serotonin regulates gap junction coupling in the developing rat somatosensory cortex. *Eur. J. Neurosci.*, **8**, 1685-1695.

Rozental, R., Srinivas, M. and Pray, D. (1985) How to Close a Gap Junction Channel. *Methods in Molecular Biology*. Humana Press. Inc., Totowa.

Saez, J. C., Retamal, M. A., Basilio, D., Bukauskas, F. F. and Bennett, M. V. (2005) Connexin-based gap junction hemichannels: gating mechanisms. *Biochim. Biophys. Acta*, **1711**, 215-224.

Saini, R., Patel, S., Saluja, R., Sahasrabuddhe, A. A., Singh, M. P., Habib, S., Bajpai, V. K. and Dikshit, M. (2006) Nitric oxide synthase localization in the rat neutrophils: immunocytochemical, molecular, and biochemical studies. *J. Leukoc. Biol.*, **79**, 519-528.

Sammak, P. J., Hinman, L. E., Tran, P. O., Sjaastad, M. D. and Machen, T. E. (1997) How do injured cells communicate with the surviving cell monolayer? *J. Cell. Sci.*, **110** 465-745.

Sanderson, M. J., Charles, A. C. and Dirksen, E. R. (1990) Mechanical stimulation and intercellular communication increases intracellular Ca^{2+} in epithelial cells. *Cell Regul.*, **1**, 585-596.

Satake, H. and Kawada, T. (2006) Overview of the primary structure, tissue-distribution, and functions of tachykinins and their receptors. *Curr. Drug Targets*, **7**, 963-574.

Schlichter, L. C. (1989) Ionic currents underlying the action potential of *Rana pipiens* oocytes. *Dev. Biol.*, **134**, 59-71.

Schreiber, A. M. and Brown, D. D. (2003) Tadpole skin dies autonomously in response to thyroid hormone at metamorphosis. *Proc. Natl. Acad. Sci. USA*, **100**, 1769-1774.

Schwentker, A., Vodovotz, Y., Weller, R. and Billiar, T. R. (2002) Nitric oxide and wound repair: role of cytokines? *Nitric Oxide*, **7**, 1-10.

Seki, T., Kikuyama, S. and Yanaihara, N. (1989) Development of *Xenopus laevis* skin glands producing 5-hydroxytryptamine and caerulein. *Cell Tissue Res.*, **258**, 483-489.

Seki, T., Kikuyama, S. and Yanaihara, N. (1995) *In vitro* development of *Xenopus* skin glands producing 5-hydroxytryptamine and caerulein. *Experientia*, **51**, 1040-1044.

Shepherd, G. M. (1981) Neurons without Impulses. *Introduction: the nerve impulse and the nature of nervous function.* Cambridge, Cambridge University Press.

Shi, H. P., Efron, D. T., Most, D., Tantry, U. S. and Barbul, A. (2000) Supplemental dietary arginine enhances wound healing in normal but not inducible nitric oxide synthase knockout mice. *Surgery*, **128**, 374-378.

Shi, H. P., Most, D., Efron, D. T., Tantry, U., Fischel, M. H. and Barbul, A. (2001) The role of iNOS in wound healing. *Surgery*, **130**, 225-229.

Shirran, S., Garnaud, P., Daff, S., McMillan, D. and Barran, P. (2005) The formation of a complex between calmodulin and neuronal nitric oxide synthase is determined by ESI-MS. *J. R. Soc. Interface*, **2**, 465-476.

Sillar, K. T. and Roberts, A. (1988) A neuronal mechanism for sensory gating during locomotion in a vertebrate. *Nature*, **331**, 262-265.

Sillar, K. T. and Simmers, A. J. (1994) Presynaptic inhibition of primary afferent transmitter release by 5-hydroxytryptamine at a mechanosensory synapse in the vertebrate spinal cord. *J. Neurosci.*, **14**, 2636-2647.

Sillar, K. T., Wedderburn, J. F. and Simmers, A. J. (1992) Modulation of swimming rhythmicity by 5-hydroxytryptamine during post-embryonic development in *Xenopus laevis*. *Proc. Biol. Sci.*, **250**, 107-114.

Silverthorn, D. U. (1998) *Human Physiology: An integrated approach.* Upper Saddle River, Prentice-Hall, Inc.

Slayman, C. L., Long, W. S. and Gradmann, D. (1976) Action potentials in neurospora crassa, a mycelial fungus. *Biochim. Biophys. Acta*, **426**, 732-744.

Smith, S. L. and Otis, T. S. (2003) Persistent changes in spontaneous firing of Purkinje neurons triggered by the nitric oxide signaling cascade. *J. Neurosci.*, **23**, 367-372.

Spratt, D. E., Newman, E., Mosher, J., Ghosh, D. K., Salerno, J. C. and Guillemette, J. G. (2006) Binding and activation of nitric oxide synthase isozymes by calmodulin EF hand pairs. *FEBS J.*, **273**, 1759-1771.

Torres, J. E., Kreisman, N. R. and Gozal, D. (1997) Nitric oxide modulates in vitro intrinsic optical signal and neural activity in the nucleus tractus solitarius of the rat. *Neurosci. Lett.*, **232**, 175-178.

Tsikas, D. (2004) Measurement of nitric oxide synthase activity *in vivo* and *in vitro* by gas chromatography-mass spectrometry. *Methods Mol. Biol.*, **279**, 81-103.

van der Veerdonk, F. C. G. (1960) Serotonin, a melanocyte-stimulating component in the dorsal skin secretion of *Xenopus laevis*. *Nature*, **187**, 948-949.

Waddington, R. (2005) The effects of glucose and homocysteine upon the embryonic development of *Xenopus laevis*. BSc Honours. University of St. Andrews.

Wang, H., Christian, H. C. and Morris, J. F. (1997) Dissociation of nitric oxide synthase immunoreactivity and NADPH-diaphorase enzyme activity in rat pituitary. *J. Endocrinol.*, **154**, R7-11.

Warner, A. E. (1985) The role of gap junctions in amphibian development. *J. Embryol. Exp. Morphol.*, **89 Suppl.**, 365-380.

Weller, R. (1997) Nitric oxide - a newly discovered chemical transmitter in human skin. *Br. J. Dermatol.*, **137**, 665-672.

Winmill, R. E. and Hedrick, M. S. (2003) Gap junction blockade with carbenoxolone differentially affects fictive breathing in larval and adult bullfrogs. *Respir. Physiol. Neurobiol.*, **138**, 239-251.

Wintrebert, P. (1904) Sur l'existence d'une irritabilité excito-motrice primitive indépedante voies nerveuses chez les embryons ciliés batraciens. *C. R. Soc. Biol. (Paris)*, **57**, 645-647.

Witte, M. B. and Barbul, A. (2002) Role of nitric oxide in wound repair. *Am. J. Surg.*, **183**, 406-412.

Yao, J., Hiramatsu, N., Zhu, Y., Morioka, T., Takeda, M., Oite, T. and Kitamura, M. (2005) Nitric oxide-mediated regulation of connexin43 expression and gap junctional intercellular communication in mesangial cells. *J. Am. Soc. Nephrol.*, **16**, 58-67.

Yao, Y., Gu, Q. B., Zhu, H., Bao, Y. D. and Tso, J. K. (1992) [A voltage-dependent potassium channel of outward rectifier type in plasma membrane of oocyte from toad, *Bufo bufo* gargarizans]. *Sheng Li Xue Bao*, **44**, 461-469.

Yoshii, Y., Matsuzaki, T., Ishida, H. and Ihara, S. (2005b) Wound healing ability of *Xenopus laevis* embryos. II. Morphological analysis of wound marginal epidermis. *Dev. Growth Differ.*, **47**, 563-572.

Yoshii, Y., Noda, M., Matsuzaki, T. and Ihara, S. (2005a) Wound healing ability of *Xenopus laevis* embryos. I. Rapid wound closure achieved by bisectional half embryos. *Dev. Growth Differ.*, **47**, 553-561.